Space Radiation-Induced Bystander Signaling in 2D and 3D Skin Tissue Models

By

Sarah B. Lumpkins

B.S. Engineering Physics
The University of Oklahoma, 2007

SUBMITTED TO THE HARVARD-MIT DIVISION OF HEALTH SCIENCES AND TECHNOLOGY
IN PARTIAL FULFULLMENT OF THE REQUIREMENTS FOR THE DEGREE OF

DOCTOR OF SCIENCE IN MEDICAL PHYSICS AND BIOASTRONAUTICS
AT THE
MASSACHUSETTS INSTITUTE OF TECHNOLOGY

February 2012

© 2012 Massachusetts Institute of Technology. All rights reserved.

ARCHIVES
MASSACHUSETTS INSTITUTE OF TECHNOLOGY
MAR 13 2012
LIBRARIES

Author .....
Harvard-MIT Division of Health Sciences and Technology
January 30, 2012

Certified by .....
Kathryn D. Held, Ph.D.
Associate Professor, Harvard Medical School
Associate Radiation Biologist, Massachusetts General Hospital
Thesis Supervisor

Accepted by .....
Ram Sasisekharan, Ph.D.
Director, Harvard-MIT Division of Health Sciences and Technology
Edward Hood Taplin Professor of Health Sciences & Technology and Biological Engineering

Space Radiation-Induced Bystander Signaling in 2D and 3D Skin Tissue Models

by

Sarah B. Lumpkins

Submitted to the Harvard-MIT Division of Health Sciences and Technology
on January 30, 2012, in Partial Fulfillment of the
Requirements for the Degree of

DOCTOR OF SCIENCE IN MEDICAL PHYSICS AND BIOASTRONAUTICS

ABSTRACT

Space radiation poses a significant hazard to astronauts on long-duration missions, and the low fluences of charged particles characteristic of this field suggest that bystander effects, the phenomenon in which a greater number of cells exhibit damage than expected based on the number of cells traversed by radiation, could be significant contributors to overall cell damage. The purpose of this thesis was to investigate bystander effects due to signaling between different cell types cultured within 2D and 3D tissue architectures. 2D bystander signaling was investigated using a transwell insert system in which normal human fibroblasts (A) and keratinocytes (K) were irradiated with 1 GeV/n protons or iron ions at the NASA Space Radiation Laboratory using doses from either 2 Gy (protons) or 1 Gy (iron ions) down to space-relevant low fluences. Medium-mediated bystander responses were investigated using three cell signaling combinations. Bystander signaling was also investigated in a 3D model by developing tissue constructs consisting of fibroblasts embedded in a collagen matrix with a keratinocyte epidermal layer. Bystander experiments were conducted by splitting each construct in half and exposing half to radiation then placing the other half in direct contact with the irradiated tissue on a transwell insert. Cell damage was evaluated primarily as formation of foci of the DNA repair-related protein 53BP1.

In the 2D system, both protons and iron ions yielded a strong dose dependence for the induction of 53BP1 in irradiated cells, while the magnitudes and time courses of bystander responses were dependent on radiation quality. Furthermore, bystander effects were present in all three cell signaling combinations even at the low proton particle fluences used, suggesting the potential importance of including these effects in cancer risk models for low-dose space radiation exposures. Cells cultured in the 3D constructs exhibited a significant reduction in the percentages of both direct and bystander cells positive for 53BP1 foci, although the qualitative kinetics of DNA damage and repair were similar to those observed in 2D. These results provide evidence that the microenvironment significantly influences intercellular signaling and that cells may be more radioresistant in 3D compared to 2D systems.

Thesis supervisor: Kathryn D. Held

Title: Associate Professor, Harvard Medical School

Associate Radiation Biologist, Massachusetts General Hospital

To my family

Acknowledgements

I would like to thank Dr. Kathryn Held for the opportunity to work in her laboratory and for her constant guidance and encouragement throughout my time at MIT. I would also like to thank other members of the Cellular and Molecular Radiation Oncology Laboratory, particularly Dr. Hongying Yang, Chelvi Rajadurai, Dr. Asima Chakraborty, and Nicole Magpayo. I would like to thank Professor Laurence Young for serving as my thesis committee chair and for his guidance and support through the Bioastronautics program. I would also like to thank Dr. Harald Paganetti for serving on my thesis committee and for his advice on this thesis.

Special thanks goes to the excellent support staff at the NASA Space Radiation Laboratory at Brookhaven National Laboratory, including Dr. Adam Rusek and the rest of the physics team as well as Dr. Peter Guida and other personnel in the Medical Department.

The internships I participated in at the NASA Johnson Space Center (JSC) were highlights of my time at MIT. Working in the laboratory of Dr. Francis Cucinotta during my first internship inspired me to pursue this thesis work in the field of space radiation, and I would like to thank my mentors Dr. Janice Huff and Dr. Zarana Patel. My second internship was through the Aerospace Medicine Clerkship through Wyle Laboratories and JSC, and I would like to thank the program coordinator, Elisca Hicks, and my mentor, Kathleen Garcia, for the unique exposure to the operational side of space flight.

I could not have completed this graduate program without the constant support from my parents, Jim and Elizabeth Lumpkins, and my sister Valerie, who have always encouraged me to pursue my dreams.

Words cannot express my deep appreciation and love for my husband, Tatsuya, who weathered the ups and downs of graduate school with me. His constant encouragement and support kept me motivated during my pursuit of this degree. Tatsuya, thank you for sailing with me on this journey through graduate school, and I am excited to continue our journey through life together.

This research was supported by a grant from the National Aeronautics and Space Administration, and additional funding was provided by fellowships through the National Science Foundation, National Space Biomedical Research Institute (Grant # EO01001), and MIT.

Table of Contents

List of Figures

List of Tables

List of Abbreviations

BCC = basal cell carcinoma

BFO = blood forming organ

BNL = Brookhaven National Laboratory

CDKs = cyclin dependent kinases

CNS = central nervous system

DAPI = 4', 6'-diamidimo-2-phenylindole

DNA-PK = DNA dependent protein kinase complex

DSBs = double strand breaks

GCRs = galactic cosmic rays

GJIC = gap junction intercellular communication

HR = homologous recombination

HZE = high atomic number and energy

ICRP = International Commission on Radiation Protection

IL-8 = interleukin 8

LEO = low Earth orbit

LET = linear energy transfer

MN = micronuclei

NCRP = National Council on Radiation Protection

NHEJ = nonhomologous end joining

NO = nitric oxide

NSRL = NASA Space Radiation Laboratory

PTIO = 2-phenyl-4,4,5,5-tetramethylimidazolineoxyl-1-oxyl-3-oxide

RBE = relative biological effectiveness

ROS = reactive oxygen species

RNS = reactive nitrogen species

RT = room temperature

SCR = solar cosmic radiation

SOD = superoxide dismutase

SPEs = solar particle events

SSBs = single strand breaks

Sv = Sievert

TGF-β = transforming growth factor β

W_R = radiation weighting factor

CHAPTER 1

Introduction

1.1 Space Radiation Environment

The exceptional radiation field in space poses a significant threat to astronauts on long-duration missions to the moon or Mars. Many types of radiation exist in the space environment, including electromagnetic radiation, galactic cosmic rays (GCRs), and solar cosmic radiation (SCR). Of these sources, electromagnetic radiation is the most benign, consisting of soft X-rays with wavelengths from about 1 to 10 nm and the more penetrating hard X-rays with wavelengths from approximately 0.01 to 1 nm. The space ionizing radiation environment, in contrast, is dominated by the highly energetic and penetrating ions and nuclei that comprise the GCR and SCR spectra [7]. Table 1 below summarizes the relevant characteristics of the particles constituting the space radiation field.

Table 1: Characteristics of space radiation [8].

Characteristic	SCR	GCR	Trapped
Proton energy range (MeV)	Up to several 100	Up to several 1000	Up to several 100
Heavy ion energy range (MeV/nucleon)	Not significant	Up to several 1000	Not significant
LET range (keV/μm)	0.25-10	0.25-1000	0.25-10

1.1.1 Types of Space Radiation

Galactic Cosmic Radiation

Galactic cosmic rays originate from outside the solar system, for the most part within the Milky Way Galaxy. GCR and high-energy electrons are produced by supernova remnants, accelerated to nearly the speed of light with energies up to several TeV. They travel throughout space and the solar system, delivering a constant source of high energy, low-fluence radiation that consists of approximately 98% baryons and 2% electrons. The baryonic component is composed of 87% protons, 12% alpha particles, and about 1% of heavier nuclei with atomic numbers up to 92 (uranium) [7]. The relative abundance of each particle type generally decreases with increasing atomic number, although a significant increase occurs at iron-56 followed by a sharp decrease at higher numbers. The energy range of these particles extends over more than 15 orders of magnitude from less than 1 MeV to more than 10^{21} eV, although there is a peak in abundance in the vicinity of 1 GeV/nucleon [9].

Although GCRs are relatively constant in terms of the distribution of particle types and energies over time, they do decrease in intensity by roughly a factor of 10 during solar events because the increased energy emitted from the sun produces an increased interplanetary magnetic field that deflects a large fraction of the GCRs. Because the intensity of the solar wind varies according to an approximately 11-year cycle of solar activity, GCR fluxes also vary with the solar cycle in an effect known as solar modulation [10]. GCR levels differ between solar minimum and maximum by a factor of about 5. Consequently, the GCR flux is at its peak level during minimum solar activity and at its lowest level during the solar maximum. At peak energies of about 200-700 MeV/n during solar minimum, particle fluxes reach $2x10^3$ protons μm^{-2} $year^{-1}$ and 0.6 Fe-ions μm^{-2} $year^{-1}$. Nevertheless, there is significant uncertainty in the absolute

abundance of particles and their energies to factors of 2 to 4 at higher energies, and even larger uncertainties exist at lower particle energies.

Solar Cosmic Radiation

Solar cosmic radiation includes two primary constituents: low-energy solar wind particles that flow constantly from the sun as well as highly energetic solar particle events (SPEs) that originate from magnetically disturbed regions of the sun, which sporadically emit bursts of energetic charged particles. Collectively, the SCR spectrum is composed predominantly of protons with a minor contribution from helium ions (~10%) and an even smaller part of heavy ions and electrons (1%) [11]. The average 11-year solar cycle can be divided into four inactive years with a small number of SPEs occurring around solar minimum and seven active years with higher numbers of SPEs around solar maximum. Few significant SPEs occur during the solar minimum, whereas large events may occur several times during the solar maximum. For example, there were at least eight events yielding proton energies greater than 30 MeV during the solar cycle of 1986-1996. Simonsen et al. estimated the radiation doses and dose equivalents from the October 1989 SPE for various human organs as a function of thickness of water shielding. The doses to the skin, intestine, and bone marrow at a water thickness of 0.5 cm were 7.21, 0.5, and 0.8 Gy, respectively, corresponding to 11.32, 0.75, and 1.07 Sv [11].

In general, SPEs are unpredictable, develop rapidly, and last for only a few hours, although some can last more than several days. In a worst-case scenario, the solar particles can reach energies up to several GeVs per nucleon, and doses received could be immediately lethal for an astronaut in free space.

Van Allen Belts

The Van Allen Belts consist of protons and electrons trapped by the Earth's magnetic field. Energetic electrons form two distinct radiation belts, while protons form a single belt. Within these belts are particles capable of penetrating about 1 g/cm^2 of shielding [12].

The inner Van Allen Belt extends from an altitude of 700-10,000 km above the Earth's surface and contains high concentrations of energetic protons with energies exceeding 100 MeV and electrons in the range of hundreds of keV. It is hypothesized that protons of energies exceeding 50 MeV in the inner belts are the result of the beta decay of neutrons created by cosmic ray collisions with nuclei of the upper atmosphere. The source of lower energy protons may be proton diffusion due to changes in the magnetic field during geomagnetic storms.

In contrast, the outer belt extends from an altitude of 3-10 Earth radii above the Earth's surface. It consists of charged particles of both atmospheric and solar origin, the latter source consisting largely of helium ions from the solar wind. The protons of the outer belt have much lower energies than those of the inner belt, and their fluxes are much higher. The most energetic particles of the outer belt are electrons, whose energies reach between 0.1-10 MeV [13].

Secondary Particles

There are significant uncertainties in the distributions of galactic and solar cosmic radiation by particle type and energy at low energies, and significant variability is contributed by the uncertainty in the timing and intensity of the occasional SPEs. However, a major uncertainty in estimating the harmful effects of this radiation on astronauts is the uncertainty of the actual particle spectrum at the point of exposure of crew members inside a spacecraft, inside a space suit, or actually at the sites of specific organs of the astronauts. As the primary particles pass through the spacecraft and the bodies of the astronauts themselves, significant amounts of

secondary particles are produced, including: heavy secondaries, nuclear recoils, photons, electrons, neutrons, pions, and muons [9]. Even after particle traversal through a centimeter or less of shielding, the number of these secondary particles exceeds the number of primary particles. Furthermore, some of the secondaries, such as the low-energy nuclear recoils, have linear energy transfer (LET) values greater than those of most of the incident primary particles. Even the secondary electrons forming a low-LET radiation background may have some biological significance for intracellular effects such as DNA damage and subsequent mutations. Thus, the problem of spacecraft and space suit shielding is complicated as the reduction in primary radiation is partly counteracted by the formation of secondary species, which may be biologically even more hazardous [13].

1.1.2 Risks from Space Radiation Exposure

Although exposure to space radiation can result in appreciable cumulative doses to astronauts during long-duration missions, it is important to note that the radiation exposure occurs at low fluences, such that particle traversals through individual cells in an astronaut's body are well separated in tissue location and time. For example, fluence rates during solar maximum (with no solar event activity) have been estimated as: 4 protons/cm^2/sec, 0.4 helium ions/cm^2/sec, and 0.04 HZE (high atomic number and energy) particles/cm^2/sec with energies of a few hundred MeV to several GeV/nucleon [14]. Based on these fluence rates, it is predicted that for a typical cell nucleus of 100 μm^2, each nucleus in the body would receive a proton traversal every 3 days, helium traversal once a month, and a HZE particle traversal once per year [14].

At such low fluences, the primary risk from space radiation is late effects, such as cancer

induction. Risk estimation based on experimental measurement for the radiation in space is nearly non-existent. Current risk assessment is based largely on human epidemiology, with some support from animal studies, both generally based on high radiation doses delivered as a single shot at high dose rates of low-LET radiation. Risk in the low-dose regime characteristic of the space radiation field is then determined by linear back extrapolation to low doses, and assumptions are made to correct for low dose rates and for high-LET radiation qualities [15]. At doses below 1 Gy, risk estimation is based on one of several models, including the linear no-threshold, linear threshold, and linear quadratic models, although the linear no-threshold model is generally preferred [16-18]. The choice of model will greatly affect the associated radiation risk and necessary countermeasures developed for astronauts.

The critical issue for NASA regarding appropriate risk assessment is the fact that the space radiation environment is a continuous flux of low doses from both low- and high-LET radiation. Furthermore, the radiation environment is a mixed radiation field, which is much different from that used as the basis for the current risk assessment models. It is therefore crucial for NASA to have a basic understanding of the radiobiology relevant to the types of radiation encountered in space and to develop accurate and precise radiation risk models for space travel. There is currently an insufficient amount of data with HZE particles regarding biological effects to allow a fully informed risk assessment.

1.1.3 Current Guidelines for Space Radiation Risk

Long-term consequences of space radiation exposure are not well understood, and this absence of knowledge is preventing acceptable radiation exposure levels from being defined for missions traveling beyond low Earth orbit (LEO). Until results are obtained from ongoing

scientific studies investigating these issues, LEO radiation limits are being used as guidelines for lunar, Martian and other interplanetary missions [19]. In 1970, NASA first adopted a set of radiation protection guidelines that set the career limit of radiation exposure as 4.0 Sv [20]. Career limits were redefined by the National Council on Radiation Protection (NCRP) to take into account the age at first exposure and the sex of the crewmember. These career limits are based on a 3% lifetime excess risk of cancer mortality and are shown in Table 2 below [21].

Table 2: Recommended organ dose equivalent limits for all ages.

Exposure Interval	Blood-Forming Organ (BFO) dose (cSv)	Ocular Lens Dose (cSv)	Skin Dose (cSv)
30-Day	25	100	150
Annual	50	200	300
Career	200	400	600

1.1.4 Biological Effects of Space Radiation

Radiation effects can be generally grouped into acute and late effects. The former are deterministic in nature, whereby the severity of the effect increases with increasing dose. They occur only if certain dose thresholds are exceeded and include such responses as organ dysfunction (associated with acute radiation syndromes), erythema, and teratogenic effects. Such acute exposures from space radiation would only be present in the event of significant solar particle events, which are extremely rare and last only a matter of hours or days [19]. Accordingly, NASA is primarily concerned with the protection of astronauts against late stochastic effects including cancer induction [13]. The basic question outlined in the NASA Human Research Roadmap [22] pertaining to radiation is to determine the unique biological effects due to low fluences of HZE particles. Current research in animals and cell systems has shown that HZE particles lead to behavioral effects such as decreased motor performance,

premature aging, genomic instability, clustered DNA damage, cell cycle delays, cataracts, and CNS damage [23-26], although data from low fluences of HZE particles are lacking in the literature. In addition, biological responses from non-targeted cells such as the bystander effect may prove to be important in the overall radiation risk assessment.

1.1.5 Linear Energy Transfer

As an energetic charged particle traverses matter, its kinetic energy is lost largely through the excitation and ionization of atoms. However, the dynamics of energy deposition differ based on the mass of the traversing particle. For example, low-mass particles such as electrons and positrons deposit a large amount of their energy in single electronic collisions and follow torturous paths as a result of multiple Coulombic scattering processes. In contrast, heavy charged particles such as α-particles lose only a small amount of energy with each collision and therefore tend to follow more linear trajectories with fewer deflections. The electrons that are emitted through ionizations may have a large range of energies, and some of them can have energies sufficient to provoke further secondary ionizations. Such relatively high-energy electrons are called delta rays, which can travel distances on the order of tens of micrometers in biological targets. For example, an iron particle with an energy of 1 GeV/nucleon can yield delta rays with track lengths of up to 800 μm, which is a large distance compared to the diameter of a typical cell of 10 μm [27].

The term LET was coined to quantify the amount of energy lost by a charged particle over a given path length, or the ionization density. LET is generally described as the energy absorbed by the target in terms of keV/μm. It is important to note, however, that LET is an average quantity because at the microscopic level, the energy per unit length of track can vary

significantly; in other words, the energy loss of a charged particle is a discrete rather than continuous process. Furthermore, the peak energy loss for a beam of protons, α-particles, and other heavy ions occurs at the end of the particle tracks immediately before the particles come to rest. This is called the Bragg peak, which occurs because the energy loss due to electromagnetic reactions increases as the particles' energy decreases. As a comparison of LET values, a 1 GeV proton has an LET of 0.22 keV/μm, a 250-kVp X-ray beam has an LET of 2 keV/μm, a 290 MeV/nucleon carbon ion has an LET of 13.6 keV/μm, and a 1 GeV/nucleon iron ion has an LET of 151 keV/μm. Based on these beam energies, the X-rays and protons are considered to have a low LET, the carbon ions are considered to have an intermediate LET, and the iron ions have a high LET.

Also important in the characterization of radiation interactions with matter is the concept of track structure, which varies greatly with LET. For example, when cells are irradiated by low-energy, high-LET radiation such as α-particles, the energy will be deposited into a relatively small number of separate densely ionizing tracks of limited range. At low doses, an individual cell in a tissue is likely to receive either no dose or, if it is in the path of the particle track, a substantial dose. Alternatively, the energy deposited from low-LET ionizing radiation, such as γ-rays, is sparse and more uniform than that from high-LET radiation, with every cell receiving a similar dose (Figure 1). Thus, for particles of equal energy, fewer high-LET particles would be needed to give the same dose of 1 Gy compared to a low-LET particle because the high-LET particle will deposit this energy over a much shorter distance and has a dense formation of reactants along its track. Complicating matters in LET calculations is the matter of how to characterize the delta rays spawned by high-LET ions. For example, because delta rays have a low LET, a heavy ion will have both low- and high-LET track components.

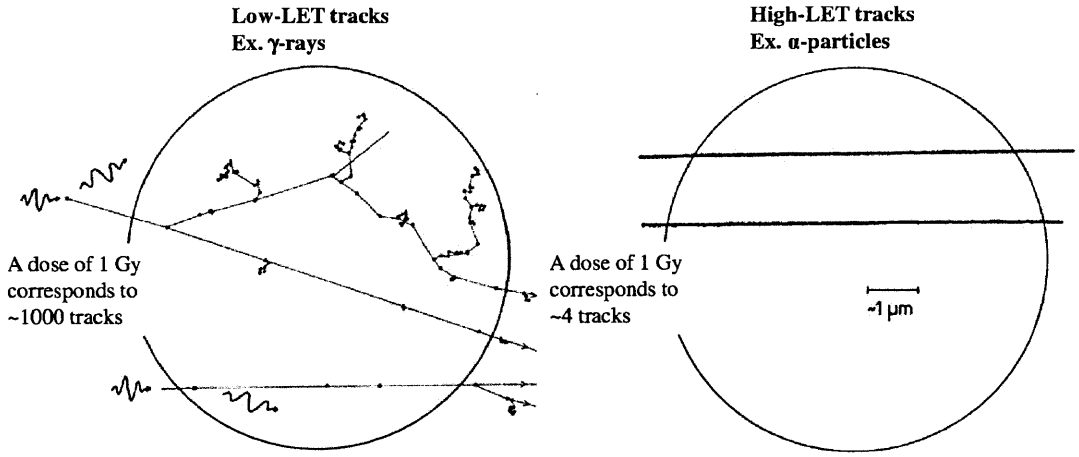

Figure 1: Schematic representation of a cell nucleus irradiated with either 2 γ-ray tracks (low-LET) or 2 α-particle tracks (high-LET) (adapted from [1]).

Although LET is a useful parameter to indicate the quality of different types of radiation, it does have some limitations. For example, because LET is an average quantity, it is of limited relevance when describing energy deposition in small volumes at the microscopic level where the energy per unit length of track varies over a wide range. This can be understood by considering a delta electron entering and terminating in a single cell. While there will be an overall cellular dose (for example, several hundred millirads for an electron with an energy of 0.022 MeV [27]), that dose is not distributed evenly over the total volume of the cell. Thus, subcellular areas of equal sizes will receive potentially very different doses depending on the particular trajectory of the electron. As an alternative physical parameter to LET, the mean free path can be used to describe radiation quality at low particle fluences such as those present in the space radiation field. This parameter describes the distance between lethal ionization events due to the traversal of a charged particle through a medium (for example, the distance between two delta electron ionizations) [28]. Using the quality parameter 'mean free path for linear primary ionization', Watt successfully developed a model to predict the risk of inactivation of irradiated

mammalian cells due to any radiation type and was able to use it to determine effects in cellular targets due to low doses of either low- or high-LET radiations. This work demonstrates the potential of defining a new unified fluence-based dosimetry system based on the mean free path concept [29].

1.1.6 Relative Biological Effectiveness and Quality Factor

Investigations regarding the biological effectiveness of high-LET radiation have generally been more limited than studies utilizing low-LET radiation sources, primarily because high-LET ions other than alpha rays must often be produced in accelerators and are not as readily available as conventional X-rays for characterization studies. However, a few important differences between low- and high-LET radiation are well established. Regarding cell survival curves, a repair shoulder is visible in the low-dose region for low-LET radiation, but the survival curve is generally a straight line for high-LET radiation [30]. It has also been shown that high-LET radiation causes much more complex chromosome rearrangements than low-LET radiation, with the aberrations involving a greater number of chromosomes and breakpoints as well as both intra- and inter-chromosome exchanges [31-34]. Other findings suggest that high-LET radiation causes more complex clustered DNA lesions than low-LET radiation, as evidenced by, for example, the smaller DNA fragments found following high-LET irradiation [35-38] and the demonstration that ionizing particles (i.e., protons and iron ions) produce more lesion clusters relative to double-strand breaks than do X-rays or γ-rays in irradiated T7 DNA [39].

An important concept in the discussion of risk incurred from space radiation is the relative biological effectiveness (RBE) of various particles. RBE is the ratio between the dose of low-LET radiation, i.e., X-rays, compared to the dose of a particular high-LET radiation needed to produce the same biological effect. RBE values are dependent on LET, dose rate, dose

fractionation, and the biological endpoint used. For example, as the LET increases, the RBE increases slowly at first and then more rapidly at LET values beyond 10 keV/μm. The RBE increases rapidly with increasing LET between 10 and 100 keV/μm and reaches a maximum at approximately 100 keV/μm [30]. As the LET continues to increase beyond this value, the RBE decreases. This decrease in RBE at LET values greater than about 100 keV/μm has been interpreted as an overkill effect whereby the ionization events within a single cell are too close together and energy is effectively "wasted."

Because radiation types differ in their biologic effectiveness per unit of absorbed dose, the radiation weighting factors (W_R) were introduced to provide a simpler way to consider the differences in biologic effectiveness of different radiations. Radiation weighting factors are chosen by the International Commission on Radiation Protection (ICRP) based on a consideration of experimental RBE values. The factors are biased for biologic end points relevant to radiation protection, such as cancer, at low doses and low dose rates. The ICRP also introduced the dose equivalent value that takes into account the weighting factors; namely, the equivalent dose (in Sievert, or Sv) is the product of the absorbed dose in Gy and the weighting factor. The currently recommended radiation weighting factors are shown in Table 3.

Table 3: Recommended radiation weighting factors (table reproduced from ICRP Publication 103 [40]).

Radiation Type	Radiation Weighting Factor (W_R)
Photons	1
Electrons and muons	1
Protons and charged pions	2
Alpha particles, fission fragments, heavy ions	20
Neutrons	Continuous function of neutron energy

The equivalent dose has been utilized to set radiation exposure limits for both the general population and radiation workers. However, a problem that is encountered in setting exposure limits for astronauts is that there are significant uncertainties in the weighting factors of biological effects due to the high-LET radiation characteristic of the space radiation field. For example, radiation in space is found at low fluences and is a combination of multiple particle types. It is not yet clear how to define a weighting factor and, eventually, risk due to a small population of cells receiving low doses of mixed radiation types. Risk models will also have to be adjusted to take into account the potentially significant contribution of bystander effects to overall cell/tissue damage [2].

1.2 The Bystander Effect

According to the classical dogma of radiation biology, a cell can only be damaged if it is directly traversed by radiation. However, experiments in the last two decades have demonstrated the existence of "bystander effects," defined as the induction of biologic effects in cells that are not directly traversed by radiation but that are in close proximity to cells that are [41, 42]. Interest in this phenomenon was sparked by the report in 1992 by Nagasawa and Little who showed that a larger proportion of cells showed biologic damage than the number of cells estimated to have been hit by a high-LET α-particle; specifically, 30% of the cells showed an increase in sister chromatid exchanges even though less than 1% were calculated to have undergone a nuclear traversal by a particle [43]. Subsequent studies have also shown the occurrence of bystander effects after low LET γ-rays [44] and X-rays [45], but few studies have investigated their occurrence after irradiation with heavy ions such as those encountered in space [46-48].

Recent studies have focused on elucidating the mechanisms involved in bystander signaling. The response of cells to the bystander signal may include induction of apoptosis, genomic instability or delayed death, enhanced cell growth, or mutations [49-51]. Alterations in the levels of proteins associated with these effects and a generalized stress response have also been detected [52-54]. At least two modes of bystander signal transmission have been demonstrated to date: medium-mediated diffusion or via gap junctions between cells in direct contact with each other [55]. The nature of the transmittal agent remains unclear, although several molecules have been highlighted as potential mediators of the response, such as: reactive oxygen species (ROS) [45, 56], cytokines such as interleukin-8 (IL-8) [57] and transforming growth factor-β (TGF-β) [58], calcium [59], nitric oxide [58], and enzymes such as Cox-2 [60] and NADPH oxidase [61]. The mixed results from these studies suggest that the mode of transmission is likely to depend on factors such as cell type, cell density, radiation dose, and biological endpoint assessed.

An important characteristic seen in all bystander studies is that the effect is triggered by low radiation doses and then rapidly saturates with increasing dose, generally by 10-30 cGy. The relevance of this dose effect to a space mission was investigated by Brenner and Elliston, who developed a quantitative model to assess the contributions of directly hit and bystander cells to cancer risk on a Mars mission as a function of the mean number of particle traversals per nucleus [2]. The results, shown in

Figure 2, clearly suggest that a linear extrapolation of risk from epidemiologically-available, high-dose exposures (where the bystander effect may be negligible), to estimate risks at very low doses relevant for space travel (where the bystander effect may be dominant) could underestimate the risk from low doses of high-LET radiation. It is important to note that this

model assumes bystander effects to be detrimental, which may not always be the case as discussed in Section 6.1.

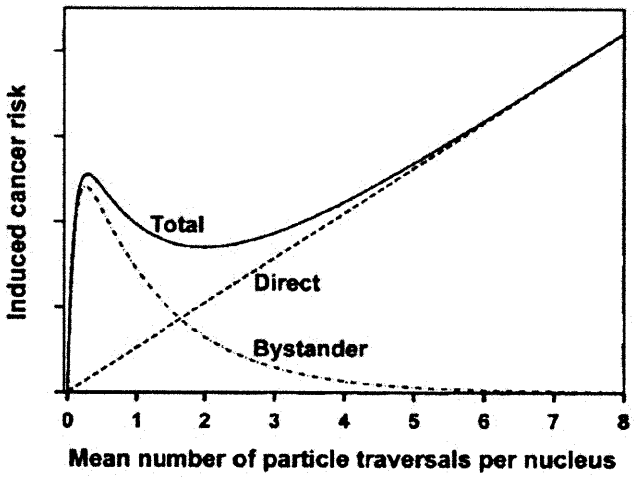

Figure 2: Relative contribution of bystander effects to cancer risk for low-dose radiation exposures (figure is reproduced from [2]).

1.2.1 In Vitro Bystander Studies

1.2.1.1 Gap-Junction-Mediated Bystander Signaling

One pathway that has been implicated in the propagation of the bystander signal is gap junction intercellular communication (GJIC). Gap junctions are specialized intercellular connections that directly connect the cytoplasm of two cells and allow ions and small molecules to pass through. While the nature of the factors passing through the gap junctions from the irradiated cells to the neighboring cells has not yet been verified, GJIC appears to require connexin 43 [62, 63], indicating that the size of the signaling factor is relatively small.

Azzam et al. presented evidence for the involvement of GJIC in the molecular events

leading to the modulation of gene expression in bystander cells. In this study, confluent cultures of normal human fibroblasts were exposed to low fluences of α-particles in the presence or absence of lindane, a chemical inhibitor of GJIC. Western blotting was then performed to evaluate changes in the p53/p21^{wafl} cell signaling pathway as well as changes in the expression levels of proteins involved in cell cycle regulation, namely CDC2, CCNB1 and RAD51. Based on observations that the gene expression levels were more significantly modulated than expected given the fraction of irradiated cells in the population, it was inferred that bystander cells participated in the overall cellular response to the radiation stress. Furthermore, GJIC was implicated in bystander signaling because gene expression changes were found to be reduced in the presence of lindane [54].

The involvement of GJIC in the response of bystander cells in confluent cultures exposed to low fluences of α-particles was further explored in a subsequent study by Azzam et al. Six cell lines were used in the study: AG1522 normal human-diploid skin fibroblasts, HLF1 normal human-diploid lung fibroblasts, wild-type and connexin 43$^{-/-}$ mouse embryo fibroblasts (MEFs), and rat epithelial cells WB-F344 and WM-aB1 (GJIC-competent and GJIC-deficient, respectively). All cells were grown to confluency on a mylar membrane and irradiated with low-fluence α-particles from a ^{238}Pu source. In addition to lindane, which may have effects other than inhibition of connexin 43-mediated intercellular communication, the GJIC inhibitors DDT [1,1'bis(pchlorophenyl)-2,2,2-trichloroethane] and dieldrin were also employed. The end points assessed in this study were the induction of p53, p21^{wafl}, and micronuclei (MN) formation. It has been well documented in the literature that cells with wild-type p53 respond to ionizing radiation by increasing p53 levels, which in turn leads to cell cycle arrests until either the damage is repaired or the cells are triggered to undergo apoptosis, or programmed cell death. As p21^{wafl} is a

direct downstream response protein of p53 that is involved in G1 cell cycle arrest, the induction of $p21^{waf1}$ indicates that p53 was activated. MN are nuclei that form when a chromosome or chromosome fragment is not incorporated into the daughter cell nucleus during cell division, predominantly from DNA double-strand breaks. It was found that p53 and $p21^{waf1}$ levels were significantly enhanced in AG1522 skin and HLF-1 lung fibroblasts exposed to low doses of α-particles. For example, after exposure of AG1522 cells to a dose of 0.16 cGy, a 2.0- to 2.5-fold increase in $p21^{waf1}$ levels was found, where only 1% of the cells were calculated to have been directly traversed by a particle. All three GJIC inhibitors were found to reduce $p21^{waf1}$ and p53 expression to control levels only at doses below 10 cGy. At doses greater than 10 cGy, where greater than 50% of cells were directly traversed by α-particles, $p21^{waf1}$ was induced in the majority of cells regardless of whether lindane was present. These results suggest that at doses below 10 cGy, the bystander effects were blocked by gap junction inhibitors, whereas at doses above 10 cGy, the gap-junction-mediated bystander effects were insignificant compared to the damage induced by irradiation of the cells by α-particles. In the rat liver epithelial cells, a bystander response was evident in the gap-junction-proficient WB-F344 cell line as evidenced by an increase in $p21^{waf1}$ levels following irradiation with doses as low as 0.3 cGy. In WM-aB1 cultures, which were deficient in GJIC, an increase in $p21^{waf1}$ levels was seen only at mean doses of 5 cGy or higher, most likely as a result of direct rather than bystander effects. These results were similar in the MEF cell lines, where $p21^{waf1}$ bystander induction was found in the wild-type line but not in the connexin $43^{-/-}$ line. The $p21^{waf1}$ levels were also found to correlate with MN levels. Specifically, a 3-fold MN induction was found in AG1522 cells at 1 cGy, and no increase in MN was seen following the addition of lindane. Therefore, this study provided strong evidence that GJIC is one pathway involved in the propagation of the bystander effect [64].

1.2.1.2 Medium-Mediated Bystander Signaling

Several adaptations of the medium-transfer approach have been employed over the years, utilizing a variety of biological endpoints. This signaling mode was first demonstrated by Mothersill and Seymour, who found a highly significant reduction in cloning efficiency in both non-irradiated normal cells as well as malignant epithelial cell lines that had received medium from ^{60}Co-gamma-ray-irradiated cultures [49]. These results suggested that irradiated cells secreted a cytotoxic factor into the medium that was capable of killing non-irradiated cells. Further studies showed that the transfer of medium from cultures irradiated with low-LET radiation to unirradiated cells increases the levels of bystander effects as manifested by cell killing [52, 65], neoplastic transformation [66], and genomic instability [49].

To determine whether irradiated medium, with or without accompanying cell cultures, can induce a bystander effect in a human hamster hybrid cell line, custom-designed double mylar dishes were used in an experiment by Zhou et al. One side (either with or without cells) was irradiated with α-particles using a broad beam from the track segment mode of a 4-MeV Van de Graaff accelerator [67]. Because α-particles can only traverse a limited distance, cells that were plated on the other side of a mylar dish filled with culture medium would not be irradiated by the particles. Non-irradiated target cells attached to the top mylar layer were found to have a greater number of chromatid-type aberrations when there was a bottom layer of cells in the medium-filled chambers than when just medium was present [68]. These results suggested that certain factor(s) excreted from the irradiated cells on the bottom mylar layer induced non-repairable chromosomal changes, resulting in an increased incidence of chromosome breaks.

Another method developed to test medium-mediated bystander effects is a transwell insert co-culture system [45, 47]. In this system, cells are plated in both a 6-well plate and in a

companion permeable membrane insert, which allows for the passage of small molecules but not cells. The cells on the 6-well plates are irradiated, and the inserts with the unirradiated cells are immediately added to the wells. Thus, the irradiated and unirradiated cells are cultured together in the same medium but are not in direct contact. Yang et al. utilized the transwell co-culture system to study the bystander effect in normal human skin fibroblasts (AG01522) using 250 kVp X-rays. The bystander fibroblasts exhibited a two-fold increase in the induction of both micronuclei and $p21^{waf1}$. Furthermore, all bystander results in the fibroblasts were found to plateau following X-ray doses to the irradiated fibroblasts in the range of 0.1-2 Gy, indicating a dose-independent characteristic of the bystander response over this dose range. The generation of ROS in the cells was also measured using DCFH-DA (2',7'-dichlorodihydrofluorescein diacetate). A four-fold increase in ROS production was detected in the bystander cells 30 h after the initiation of co-culture, and the ROS production had returned to background levels by 60 h. Using the antioxidant enzymes copper, zinc-superoxide dismutase (Cu-ZnSOD), and catalase, Yang et al. showed that the previously-observed induction of micronuclei and $p21^{waf1}$ in the bystander fibroblasts was effectively removed. However, these enzymes did not eliminate the reduction in the survival fraction of bystander fibroblasts that was previously observed [45]. These data suggest that irradiated cells release toxic factors other than ROS into the medium.

1.2.1.3 Bystander Studies Using a Microbeam

The development of single-particle microbeams has significantly enhanced the complexity and flexibility of bystander studies. Through the use of microbeams, which make it possible to deliver a known number of particles through the nucleus or cytoplasm of specific cells, studies have been conducted with both confluent as well as sparsely populated human and other mammalian cells using a variety of biological endpoints. Most microbeam studies have

utilized α-particles because it is easier to focus them accurately, but a bystander effect has also been observed among non-hit cells using protons and soft X-rays when either a single or a defined proportion of cells was targeted. Furthermore, increasing the number of particle traversals per cell [48, 69] or the total dose delivered to the irradiated fraction [70] did not increase the intensity of the bystander response. Thus, as with the medium-mediated bystander studies, these data demonstrate a lack of a dose response in bystander effects. In further microbeam studies employing α-particles, the addition of the calcium blocker calcicludine [71] or NS-398, an inhibitor of cyclooxygenase (COX)-2, significantly reduced the bystander response in human lung fibroblasts [60].

Several other studies have also utilized various types of microbeams to investigate bystander effects in both cell monolayer and tissue experimental systems. See Section 1.2.2.2 for further discussion of the use of microbeams in bystander studies.

1.2.1.4 DNA Repair Pathways in Bystander Cells

In irradiated cells, DNA damage can be caused either directly or indirectly via chemical reactions with various radiolytic reactive species such as $O_2^{\bullet}$, $H^{\bullet}$, $OH^{\bullet}$, and H_2O_2 (Figure 3). In contrast, DNA damage in bystander cells is caused exclusively by indirect reactions because ionizing particles do not pass directly through the cells. Nevertheless, both direct and indirect processes cause various radiation-induced DNA lesions such as: base damage, DNA-DNA and DNA-protein cross-links, single strand breaks (SSBs), double strand breaks (DSBs), and multiply damaged sites [30]. The factors that determine the amount of energy transferred to the DNA and the type of lesion created include dose, dose rate, and LET of the radiation. Base damage and SSBs do not generally correlate with cell killing and are thus not considered to be

lethal. However, DSBs can lead to chromosomal changes and can cause a significant loss of genetic material during cell division, thereby contributing to cell killing or the induction of mutations [30].

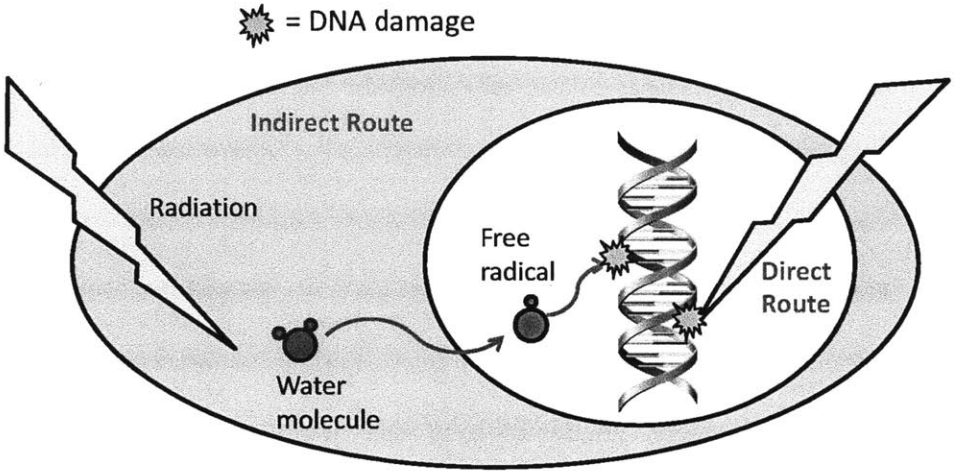

Figure 3: Qualitative depiction of the direct and indirect actions that cause DNA damage in irradiated cells.

In response to DNA damage, mammalian cells usually activate two important cell functions: DNA repair mechanisms or cell cycle regulation [72]. Shortly after DNA lesion recognition and assessment, a cell must decide whether to commit suicide (generally through apoptosis) or to try to repair damage, aiming first to preserve the reproducibility and integrity of the genome, by following one of four main pathways [73]:

I. ***Cells arrest their cell cycle progression***. The regulation of cell propagation through the cell cycle is governed by specific intracellular enzymes known as cyclin dependent kinases (CDKs). These enzymes are activated by phase-specific proteins (cyclins) and allow cell transitions from one phase to another. Events that

occur during each phase of the cell cycle are strictly controlled to ensure that the next event is not initiated before the previous event is completed. A number of checkpoint genes regulate these processes at three primary points within the cell cycle: G_1/S checkpoint, S-phase checkpoint, and G_2/M checkpoint. The lesion(s) is sensed by sensor proteins, which then initiate checkpoint signals and activate protein kinases. These kinases will phosphorylate critical targets and result in cell cycle arrest.

II. ***Repair of DNA damage.*** Following damage recognition and cell cycle arrest, a cell may initiate an attempt to repair itself. Two main pathways exist for the repair of DSBs, namely nonhomologous end joining (NHEJ) and homologous recombination (HR). NHEJ is initiated by the DNA dependent protein kinase complex (DNA-PK), which localizes broken ends of the DNA and binds to them. Alternatively, HR utilizes the availability of the sister chromatid on the homologous chromosome and uses it as a template to repair damage.

III. ***Mitotic catastrophe.*** Many cells may experience de novo delayed DNA damage that may occur hours or days after exposure to radiation [74]. It has been found that cells with compromised p53 function are transiently delayed in late S and G2 phases after irradiation, at which time an overaccumulation of cyclin B1 and activation of cyclin B1-dependent kinase may occur [75, 76]. An increased accumulation of this positive regulator of mitosis leads to disruption of the G2/M checkpoint with a premature entry of cells into mitosis. This, in turn, causes nuclear fragmentation and delayed DNA damage, both of which are hallmarks of

mitotic catastrophe. There is an ongoing debate in the literature regarding whether mitotic catastrophe is itself a mode of cell death or whether it is a process that leads to cell death via apoptosis or necrosis [77-79].

IV. ***Initiation of cell death via apoptosis***. If a cell determines that a DNA lesion can not be repaired, it will commit suicide. This generally occurs via apoptosis, which is the process of programmed cell death for the purpose of removing cells that are damaged beyond repair. Apoptosis is characterized by biochemical changes that lead to cell changes and death. Such changes include blebbing, cell shrinkage, nuclear fragmentation, chromatin condensation, and chromosomal DNA fragmentation. Cell fragments called apoptotic bodies are produced that phagocytic cells are able to engulf and quickly remove to ensure that the contents of the cell do not spill out onto neighboring cells and cause further damage.

One of the early cellular responses to DSBs is the serine-139 phosphorylation of the H2AX histone (γH2AX) near the lesion site. It has been found that this phosphorylation can take place within minutes in irradiated cells; therefore, the detection of γH2AX foci can be used as an early biomarker for cell damage in the form of DSBs [80]. Although the exact function of γH2AX foci formation is unknown, a correlation has been found between these foci and DSB locations [81]. Furthermore, co-localization of γH2AX with MN has been found in irradiated human fibroblasts [82]. In addition to γH2AX, many other DNA repair-related proteins have been used as surrogate markers for DNA DSBs, including DNA-PKcs and 53BP1, both of which have been shown to co-localize with γH2AX [83]. DNA-PKcs plays a key role in DSB repair

mediated through non-homologous end joining [84], and its phosphorylated form has been shown to be localized at DSBs [85]. 53BP1 is a DSB sensing protein and has been shown to interact with γH2AX and to respond to DNA DSBs following exposure to ionizing radiation [86].

Although the initial studies investigating surrogate markers of DSBs were conducted in irradiated cells, many studies have now shown that such markers are also present in bystander cells. For example, Yang et al. utilized the transwell insert co-culture method to study DSB formation and repair in bystander human fibroblasts (AG01522) that were co-cultured with AG01522 fibroblasts that had been irradiated with 250 kVp X-rays [45]. A two-fold induction of γH2AX foci was detected in the fibroblasts after a 1- or 24-h co-culture time with the irradiated fibroblasts but not after 48 h. In contrast, in AG01522 fibroblasts that were irradiated with either 0.1 or 2 Gy of X-rays, γH2AX foci induction was detected at 1 h post-irradiation but not at 24 or 48 h. Furthermore, the addition of catalase or superoxide dismutase (SOD) was found to successfully eliminate the foci formation in the bystander fibroblasts. Therefore, this study suggested that either (i) the DSB repair mechanism is slower in bystander cells or (ii) the bystander signal is more persistent and thus can continue to produce DSBs over a longer period of time in bystander compared to irradiated cells. Prompted by the growing evidence that DSBs form in bystander cells, several research groups began to investigate whether cells that are deficient in DNA repair exhibit an enhancement of bystander effects. For example, Little et al. investigated the participation of the NHEJ repair pathway in bystander cells in the induction of chromosome aberrations [87]. Mouse knockout cell lines that had deficiencies in four proteins involved in NHEJ repair were studied: Xrcc5 (Ku80), G22p1 (Ku70), Prkdc (DNA-PKcs), and Adprt (PARP). Wild-type S or SV cells were used as NHEJ repair-proficient controls. Cells were grown on a mylar layer to confluence and irradiated with low fluences of α-particles (doses

between 0.17 and 1.7 cGy), where only 2-15% of the cells were expected to be traversed by an α-particle. At 0.33 cGy (3.3% of the cell nuclei irradiated), 9.3 and 9.4% of the wild-type S or SV cells showed an increase in chromosomal aberrations, respectively, representing a four-fold increase over control levels. In comparison, a 40-50-fold increase in chromosome aberrations compared to background levels was found in Ku70-/- and Ku80-/- cells, and around a 20-fold increase over background was found in DNA-PKcs-/- and Adprt-/- cells. Thus, in addition to demonstrating that DSBs occur in bystander cells, this study showed that the involvement of NHEJ repair of DSBs in these cells is crucial and that deficiency in this pathway results in a significant susceptibility of the cells to bystander effects.

1.2.1.5 LET Dependence of the Bystander Effect

Bystander experiments have utilized a wide variety of radiation types, which differ in their radiation quality and/or LET. In addition to the most commonly used radiation sources (i.e., γ-rays, X-rays, and α-particles), bystander effects have been studied after irradiations with protons [88], Auger electrons [89], high-energy electrons [90], neutrons [91], and heavy ions such as carbon, nitrogen, lithium, iron, neon, argon, nickel and uranium ions [46, 92-95]. However, the majority of studies have been conducted using only one radiation type, making the analysis of the LET dependence of bystander effects difficult.

Nevertheless, a few studies have been carried out where two or more radiation types have been tested in parallel using a single experimental system to allow comparisons of the dependence of the bystander effect on LET. For example, Yang et al. conducted studies in which 0.5 and 2.0 Gy of 250 kVp X-rays (LET: 2 keV/μm) or 1 GeV/nucleon iron ions (LET: 151 keV/μm) was used to irradiate AG01522 human fibroblasts. Bystander effects were monitored in a separate population of AG01522 cells co-cultured with the irradiated cells for various times

ranging from 1-24 h [46, 47]. These authors reported no differences in levels of MN induction, γH2AX formation, or the surviving fraction of the bystander cells between the X-rays and iron ions. Furthermore, they found that both Cu-Zn SOD and catalase blocked the γH2AX foci induction in bystander fibroblasts co-cultured with either iron or X-ray irradiated fibroblasts. These data demonstrated that ROS were involved in the medium-mediated bystander signal produced by both radiation types. Therefore, this study suggested that the bystander responses in AG01522 fibroblasts were independent of LET. Similarly, in a medium transfer experiment by Baskar et al., no LET-dependent differences were reported between ^{137}Cs γ-rays and α-particles [96]. In this study, medium from either irradiated normal human fetal lung fibroblasts or irradiated ataxia telangiectasia mutated fibroblasts was transferred to unirradiated normal fibroblast cells. When the unirradiated cells were treated with the medium from either irradiated cell line following either α-particle or γ-ray irradiation, a 10-30% enhancement in colony formation efficiency was observed.

Shao et al. used the transwell co-culture system to study the medium-mediated bystander effect in human salivary gland tumor cells [97]. Carbon beams with LETs of 13 keV/μm and 100 keV/μm were used to irradiate the tumor cells, and the cells were then placed in co-culture with a bystander population of the same cell type for 24 h. A 2-fold increase in MN formation was seen in the bystander tumor cells that were co-cultured with the cells irradiated with the 13 keV/μm carbon beam, while a 2.5-fold increase was seen in the bystander cells co-cultured with cells irradiated with the 100 keV/μm beam. Furthermore, nitric oxide was measured in the co-cultured medium, and the concentration was found to be higher in the medium of the cells irradiated with the higher LET carbon beam. Thus, this study showed that MN formation and nitric oxide concentration are LET dependent in this particular cell signaling combination.

Based on studies that have been conducted, the LET dependence of the bystander effect appears to strongly depend on the cell types, endpoints, and experimental systems studied. As many experiments capture only a snapshot of the complex relationship between LET and bystander effects, the studies to date have resulted in seemingly paradoxical findings that will only be elucidated with further experiments comparing multiple radiation types in parallel within a single experimental system.

1.2.1.6 Bystander Signaling Between Different Cell Lines

While numerous bystander studies have now been conducted using a variety of cell and radiation types, there is a dearth of information related to bystander signaling between different cell types. Such studies are important to more accurately assess bystander signaling *in vivo*, where multiple cell types are present. In a study by Anzenberg et al., bystander signaling between human prostate carcinoma cells and AG01522 fibroblasts was studied [98]. Specifically, DU-145 prostate carcinoma cells were irradiated with either X-rays or α-particles, and the cells were co-cultured with either unirradiated DU-145 or AG01522 cells. The three experimental end points studied were MN formation, γH2AX focus induction, and the surviving fraction. After 4 h of co-culture with DU-145 cells that had been irradiated with either X-rays or α-particles, there was a 1.5-2-fold increase in MN formation in both tumor and fibroblast bystander cells. An increase in γH2AX focus induction (1.5-fold) and a decrease in the surviving fraction (to 0.8) were observed only in AG01522 cells when co-cultured with X-irradiated tumor cells. In contrast, α-particle irradiation of the DU-145 tumor cells caused neither a decrease in the surviving fraction nor an increase in the induction of γH2AX foci in either bystander cell line. These data indicate that not only are there LET-dependent differences in the signal released from the DU-

145 cells but also that bystander AG01522 and DU-145 cells respond differently to the same medium-mediated signal, thereby highlighting the importance of investigating bystander signaling between different cell lines.

1.2.2 Tissue Models and *In Vivo* Bystander Studies

For the bystander effect to have any relevance to the prediction of radiation risk to astronauts, the effect must be demonstrated to occur not only *in vitro*, but also *in vivo*. Although the number of *in vivo* studies that have been conducted to date is still limited compared to the number of *in vitro* studies, bystander effects have been investigated by several authors in cell cluster models, 3D artificial tissue models, and animal models.

1.2.2.1 Bystander Effects in Cell Clusters

One approach that has been used to study bystander effects is a three-dimensional multicellular model. Such a model was utilized by Bishayee et al. to investigate the bystander effect due to a nonuniform distribution of radioactivity incorporated into a three-dimensional tissue culture model. Chinese hamster V79 cells were labeled with tritiated thymidine and mixed with unlabeled cells to achieve multicellular clusters composed of 100, 50, or 10% radiolabeled cells. Furthermore, to study the mechanisms underlying bystander effects, the clusters were assembled in the presence of the free radical scavenger DMSO and/or an inhibitor of GJIC, lindane. The clusters were maintained at 10.5°C for 72 h to allow the decay of ^{3}H in the absence of cell division. Following this incubation period, the clusters were vortexed to disperse them and then plated for colony formation. When 100% of the cells were labeled, the surviving fraction was exponentially dependent on the mean level of radioactivity per cell. However, a two-component exponential response was observed when either 50 or 10% of the cells were

labeled, the first representing killing of the radiolabeled cells and the second representing killing of unlabeled bystander cells. The addition of either DMSO or lindane significantly protected the unlabeled or bystander cells when 50 or 10% of the cells were labeled; however, the effect of lindane was greater than that of DMSO. In both cases, the maximum protection of the bystander cells was elicited by the combined treatment (DMSO+lindane). In addition to showing that the bystander effects caused by nonuniform distributions of radioactivity are affected by the fraction of cells that are labeled, these results also show that at least a portion of the bystander effects demonstrated in this study are initiated by free radicals and are likely to be mediated by GJIC [99]. Similar results have been found in other multicellular cluster models [100, 101].

1.2.2.2 Bystander Effects in 3D Tissue Models

Belyakov et al. conducted the first study of bystander responses in a three-dimensional, normal human tissue system [3]. Two types of reconstructed skin systems were used in this study that were generated by growing differentiated keratinocyte cultures on either acellular or fibroblast-populated dermal substrates, corresponding to a human epidermis model (EPI-200) and a "full-thickness" skin model corresponding to the epidermis and dermis of normal human skin (EFT-300), respectively. The EPI-200 tissue is about 75-μm thick, corresponding to about 8-12 cell layers, and the EFT-300 tissue is about 700-μm thick; both are commercially available from MatTek (Ashland, MA). For the EPI-200 epidermal tissue, a charged particle microbeam delivering 7.2-MeV α-particles was used to irradiate 400-800 cells along a single thin, vertical plane, resulting in an average dose of about 1 Gy/cell. This arrangement guaranteed that cells more than a few micrometers away from the plane of irradiated cells would receive no radiation because the α-particles scatter very little as they pass through the tissue sample. The EFT-300 tissue was irradiated in a similar fashion but with two different protocols; one protocol targeted

only keratinocytes in the epidermis, and the second targeted only fibroblasts in the dermis. A schematic of the irradiation setup and analysis method is shown in Figure 4.

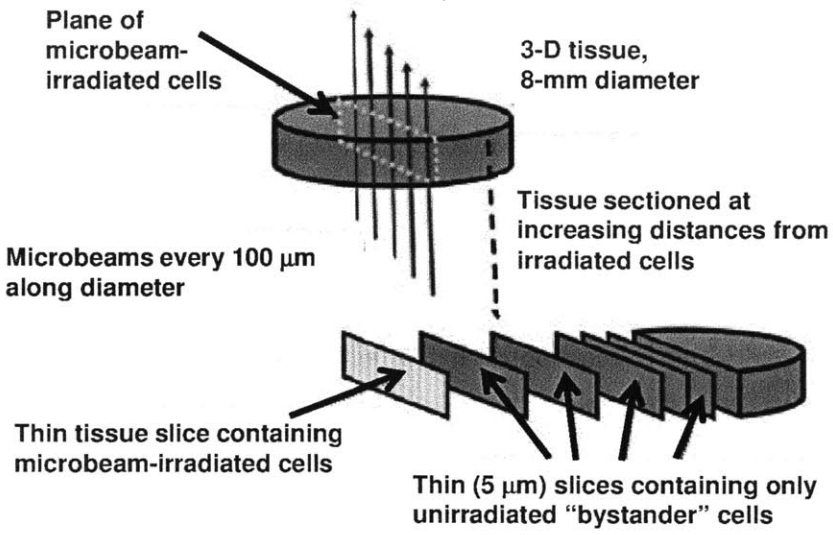

Figure 4: Schematic of the irradiation procedure used by Belyakov et al. After irradiation, the tissue was sectioned into 5-μm-thick slices parallel to, and progressively further from, the plane of irradiation. Diagram was reproduced from Belyakov et al. [3].

At 72 h post-irradiation, apoptosis and MN induction were assessed in unirradiated cells in tissue sections parallel to the irradiated section at increments of 5 μm up to 1,100 μm from the plane of irradiated cells. In the EPI-200 tissue, a 3-fold increase in apoptosis induction was found in unirradiated keratinocytes up to 1,000 μm from the irradiated cells, and a 2-fold increase in MN induction was detected in the unirradiated keratinocytes up to 600 μm from the irradiated cells. In the EFT-300 tissue, a bystander response similar to that in the EPI-200 tissue was found when the epidermal layer was irradiated. However, when only the dermis layer was irradiated, no bystander response was seen in the keratinocytes. These data suggest that the irradiated keratinocytes emitted a signal that induced a response in the unirradiated keratinocytes. It is not

clear, however, if the lack of observed bystander response following irradiation of the dermis was due to the extended distance between the dermal fibroblasts and assayed keratinocytes or if there is no signaling from the dermal to epidermal layers in terms of a bystander response. This study was significant in that it showed the ability of unirradiated cells in a 3D human tissue model system to respond to radiation-induced cellular damage over long distances (up to 1 mm).

In a follow-up study, Sedelnikova et al. performed similar microbeam irradiations of both the EFT-300 and Epi-Airway (Air-100) tissue systems [4]. The Air-100 system consists of three to four layers of normal, human-derived tracheal/bronchial epithelial cells that are cultured to form a highly differentiated tissue with a thickness of approximately 40 μm, which closely resembles the epithelial tissue of the respiratory tract. The bottom layer of each tissue model was irradiated with a 7.0-MeV α-particle microbeam. Unirradiated cells were assayed over a 7-day time course in serial sections perpendicular to the irradiated plane of the tissue. A schematic of the irradiation setup and analysis method is shown in Figure 5.

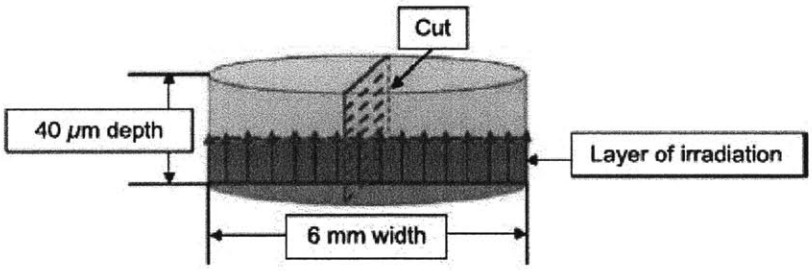

Figure 5: Schematic of the tissue irradiations performed using an α-particle microbeam. The arrows represent the beam of α-particles, and the square "Cut" section represents the serial cuts made perpendicular to the plane of irradiation for assay [4].

All three types of bystander cells (airway epithelium, dermal fibroblasts, and epidermal keratinocytes) of both tissues responded with a similar increase in the incidence of DNA DSBs, as measured by γH2AX foci induction, involving 40-60% of the cells in the bystander regions. Furthermore, the levels of γH2AX foci persisted up to 7 days in both tissue models. These increases in bystander DSB formation were accompanied by increased levels of apoptosis (6-fold increase) and MN formation (2.5-fold increase), by loss of nuclear DNA methylation, and by an increased fraction of senescent cells. An interesting difference between this study and that of Belyakov et al. [3] is that the former study detected a bystander response in the keratinocytes induced by irradiated fibroblasts whereas the latter study did not. This suggests that the fibroblasts do emit a bystander signal that was perhaps only detected in the more recent study due to the use of a more sensitive apoptosis assay. Overall, this study demonstrated the involvement of DNA DSBs in bystander responses occurring in tissues and provided evidence that such DSBs are precursors to widespread downstream effects in human tissues. Because bystander cells exhibiting post-irradiation signs of genomic instability may be more prone than unaffected cells to becoming cancerous, this study suggests the importance of considering the indirect biological effects of radiation in performing cancer risk assessment.

1.2.2.3 "Bystander Effects" in Animal Models

Until recently, very few studies have explored the potential impact of radiation exposure on distant organs and tissues in animal models. To investigate the possibility that X-irradiation induces DNA damage in out-of-field tissue *in vivo*, Koturbash et al. placed lead shielding over half the body of a mouse before exposing it to 1 Gy of X-rays [102]. Subsequently, ventral skin was taken from the area adjacent to the thigh at least 0.7 cm away from the exposed half of the

mouse, and the levels of DNA damage, DNA methylation, and protein expression were evaluated in both the irradiated and shielded cutaneous tissue. Six hours following the half-body irradiations, the levels of γH2AX foci, a surrogate marker of DNA DSBs, were found to be significantly elevated (1.3-fold increase) in the shielded tissue. By 4 days post-irradiation, the number of foci had returned to background levels. Interestingly, RAD51 expression, which is an important protein in DNA repair, was found to be significantly elevated at both 6 h and 4 days post-irradiation. This study also assessed epigenetic changes, including DNA methylation, which have been shown to be involved in both cancer development and genomic instability. Although a significant decrease in DNA methylation was found in exposed skin 6 h post-treatment, only a slight (non-significant) decrease in methylation changes was found in shielded tissue. In mammals, DNA methylation patterns are established and maintained by three DNA methyltransferases: DNMT1, DNMT3a, and DNMT3b. In particular, DNMT1 has been shown to maintain existing methylation patterns. In this study, a 1.4- and 1.8-fold increase in DNMT1 expression was found in tissue from shielded regions at 6 h and 4 days post-irradiation, respectively. Furthermore, DNMT3a and DNMT3b, which catalyze de novo methylation, were found to be slightly down-regulated in the shielded tissue 6 h post-irradiation. As it has been well established that clinical exposure to radiation therapy can result in cutaneous injury, which involves complex physiological changes, it is possible that the suppressed levels of DNMT3a and DNMT3b reflect an early injury response. In summary, the principle findings of this study were: (1) an increased level of DNA DSBs was present 6 h post-irradiation in shielded tissue; (2) significant repair (via homologous recombination) of the strand breaks occurred in the shielded tissue up to 4 d post-irradiation; and (3) DNA methylation genes were involved in the response in shielded tissue. However, the relationship between these *in vivo* out-of-field responses and the *in*

vitro bystander effect is not clear.

In another study by Mancuso et al., tumor induction was investigated in the cerebellum of radiosensitive Patched-1 (Ptch1) heterozygous mice [103]. The mice were irradiated with 8.3 Gy of X-rays to the whole body except their heads, which were protected by individual cylindrical lead shields. A highly significant induction of γH2AX foci occurred in the cerebellum at 4.5 and 6 h post-irradiation, with a decrease to control levels at 18 h. Furthermore, a 7-fold increase in apoptosis was detected in the cerebellum 6 h post-irradiation that declined to background levels by 18 h. Accompanying these changes, tumor induction in the cerebellum of these mice was also shown to be enhanced. To determine whether the response in these mice was propagated by GJIC, 12-O-tetradecanoylphorbol-13-acetate (TPA), a potent inhibitor of GJIC, was injected into the mice 0.5 h prior to irradiation. The TPA treatment abrogated DNA-DSB responses in the cerebellum post 8.3-Gy irradiation to the rest of the body, and apoptotic damage was reduced by 3.3-fold. This suggests that the expression of the connexin43 (Cx43) protein, the most abundant gap junction protein in the CNS, is associated with the communication of damage signals between adjacent CNS cells. In summary, this study demonstrated tumor induction in shielded brain tissues *in vivo*.

1.3 Thesis Work

1.3.1 Specific Aims

Most published studies of bystander effects to date have been conducted using either α-particles or low-LET γ- or X-rays at high fluences, which have little relevance to the space radiation field. Furthermore, current studies are generally limited to the use of cell monolayers and do not investigate the potential modulation of bystander responses by the microenvironment

present in 3D tissue models.

In light of these current limitations to space radiation bystander studies, the purpose of this thesis was to investigate bystander signaling between different cell types in both 2D and 3D skin models. Irradiations of the cells and tissues were conducted at the NASA Space Radiation Laboratory at Brookhaven National Laboratory, which provides particle beams over a broad LET range and at low fluences to mimic the space radiation environment. Mechanistic investigations were also performed to gain insight into the nature of the bystander signaling process. Ultimately, results from these studies will be utilized to better quantify radiation risks to astronauts and will eventually be used in the determination of appropriate countermeasures to mitigate astronauts' risk of exposure to space radiation. The specific aims of this thesis are summarized below.

SPECIFIC AIM 1: Test the hypothesis that bystander signals can be transmitted between different cell types, but the characteristics of the responses depend on the cell type, radiation quality and endpoint. The purpose of this aim is to serve as a prelude for analysis of bystander effects in a 3D model, which is described in Aim 2. In this aim, bystander signaling was investigated from irradiated fibroblasts to bystander keratinocytes and vice versa using proton and iron beams at both low and high particle fluences. DNA damage was measured in both irradiated and bystander cells with endpoints of MN (which arise from either whole lagging chromosomes or acentric chromosome fragments that do not integrate into the daughter nuclei during cell division) and 53BP1 foci formation (which is a commonly used marker of DNA double-strand breaks, a type of complex DNA lesion [30, 86]).

SPECIFIC AIM 2: Develop a 3D skin model to test the hypothesis that radiation-induced bystander signals are dependent upon the architecture of cellular systems. Increasing evidence suggests that the microenvironment influences intercellular signaling, not only in response to radiation, but also more generally in induction of endpoints such as apoptosis and tumorigenesis [104]. Several studies implementing microbeam irradiation have demonstrated bystander responses in tissue models over distances up to 1 mm [3, 4]. The goal of this aim was to first develop a skin construct consisting of a fibroblast-containing collagen layer and an epidermal layer containing keratinocytes. Constructs were then irradiated using both proton and iron ion beams, and cell damage (53BP1 foci) was assessed in sections prepared from the tissue constructs to test the hypothesis that the architecture of cellular systems modulates bystander signaling.

SPECIFIC AIM 3: Investigation of the roles of ROS and nitric oxide (NO) in eliciting bystander responses. For this aim, both the 2D and 3D skin models developed in Aims 1 and 2 were utilized to investigate potential mechanisms involved in medium-mediated bystander signaling. Namely, catalase, superoxide dismutase, and 2-phenyl-4,4,5,5-tetramethylimidazolineoxyl-1-oxyl-3-oxide (PTIO) were used to scavenge hydrogen peroxide and superoxide (types of ROS), as well as nitric oxide, respectively, which are postulated to be involved in the intercellular signaling following exposure to ionizing radiation. Additionally, the dependence of the efficacy of these scavengers to alter bystander signaling induced by various radiation qualities was investigated by irradiating samples with either protons or iron ions as in Aims 1 and 2.

1.3.2 Thesis Organization

The radiation bystander phenomenon was introduced in this chapter, as well as its potential importance in defining risks to astronauts on long-duration missions. Additionally, the two primary modes of bystander signal propagation were described, namely through gap-junction and medium-mediated communication, and relevant studies in the bystander literature were discussed. The specific aims of this thesis were also described in light of the current limitations of bystander studies.

Chapter 2 introduces the assays used to quantify bystander signaling as well as the protocols used to develop the 3D tissue model employed in Aims 2 and 3. Methods used to evaluate bystander signaling at the low particle fluences characteristic of the space radiation environment are also introduced, in addition to methods used to investigate the potential mechanisms involved in bystander signaling.

The results and discussion of the 2D bystander experiments are presented in Chapter 3, including quantifications of bystander signaling within the three cell signaling combinations investigated, at both high and low particle fluences, and due to both low- and high-LET radiation exposures. The modulation of the bystander signaling via the introduction of ROS/RNS scavengers into the medium is also presented.

The results and discussion of the 3D bystander experiments are presented in Chapter 4, including quantifications of bystander signaling at both high and low particle fluences and due to both low- and high-LET radiation exposures. The modulation of the bystander signaling via the introduction of ROS/RNS scavengers into the medium is also presented.

A comparison of the bystander signaling demonstrated in the 2D and 3D models developed in this thesis is provided in Chapter 5, and Chapter 6 concludes with a summary of the

thesis and discussion of future directions of this work.

CHAPTER 2

Materials and Methods

2.1 Cell Lines

The two cell lines used in this thesis are the hTERT immortalized keratinocytes, which were obtained from Dr. Irene Kochevar (Wellman Center for Photomedicine at Massachusetts General Hospital, Boston, MA) [105], and AG01522 normal human skin diploid fibroblasts, which were obtained from the Genetic Cell Repository at the Coriell Institute for Medical Research (Camden, NJ). The keratinocytes were grown at 37°C in 95% air and 5% CO_2 in keratinocyte medium (KSFM) containing Keratinocyte-SFM (Gibco) supplemented with 100 U/ml penicillin, 0.1% of 0.3 mM $CaCl_2$, L-glutamine, epidermal growth factor, and bovine pituitary extract. The fibroblasts were grown at 37°C in a humidified atmosphere of 95% air and 5% CO_2 with alpha-modified MEM (Sigma, St. Louis, MO) supplemented with 20% fetal bovine serum (FBS; Hyclone, Logan, UT), 100 µg/ml streptomycin, and 100 U/ml penicillin.

2.2 Cell and Tissue Irradiation

Charged particle irradiation of the cells and tissues for this project was conducted at the NASA Space Radiation Laboratory (NSRL) at Brookhaven National Laboratory (BNL) in Upton, NY. While NSRL now has the capability to generate many different particle beams, the emphasis of our experiments focused on bystander effects generated by: 1.0 GeV/n Fe ions, because Fe is the high Z ion of greatest abundance in the GCR spectrum, and 1.0 GeV/n protons, because they are the dominant particle type in both the GCR and SPE spectra. These particles have LET values of 0.24 keV/µm (protons) and 150 keV/µm (iron ions), thereby allowing us to investigate

the LET dependence of the bystander effect. The dose rates of particle irradiations ranged from 0.05 Gy/min to 2 Gy/min, and

Figure 6 shows a Bragg curve obtained for 1 GeV/nucleon iron ions.

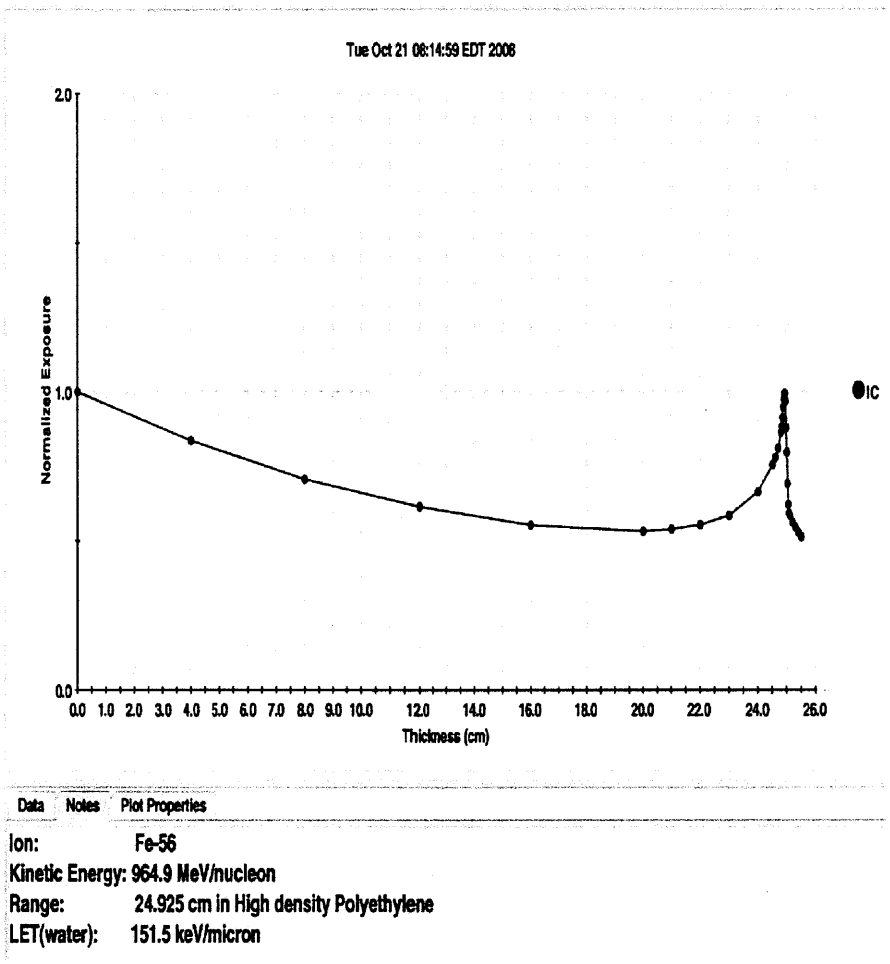

Figure 6: Bragg curve for 1 GeV/nucleon iron ions. The distance traveled by a particle in tissue-equivalent plastic is displayed on the x-axis. This curve was generated by Dr. Adam Rusek at NSRL.

The Bragg curves obtained at NSRL are generated by a beam traveling through a thickness in plastic with density equivalent to that of tissue. Because the particle beams at NSRL travel primarily though air before encountering the plastic of the 6-well plates containing cells,

the samples to be irradiated were placed at the beginning portion of the Bragg curve where little energy or LET loss occurs through the sample. Figure 7 shows an image of an experimental set-up consisting of two, 6-well plates taken by the digital beam imager during irradiation with 1 GeV/nucleon Fe ions. The target (6-well plates) had an area of 18x12 cm^2, which was well within the 20x20-cm^2 central region of the beam characterized by a flat intensity within 3% [5].

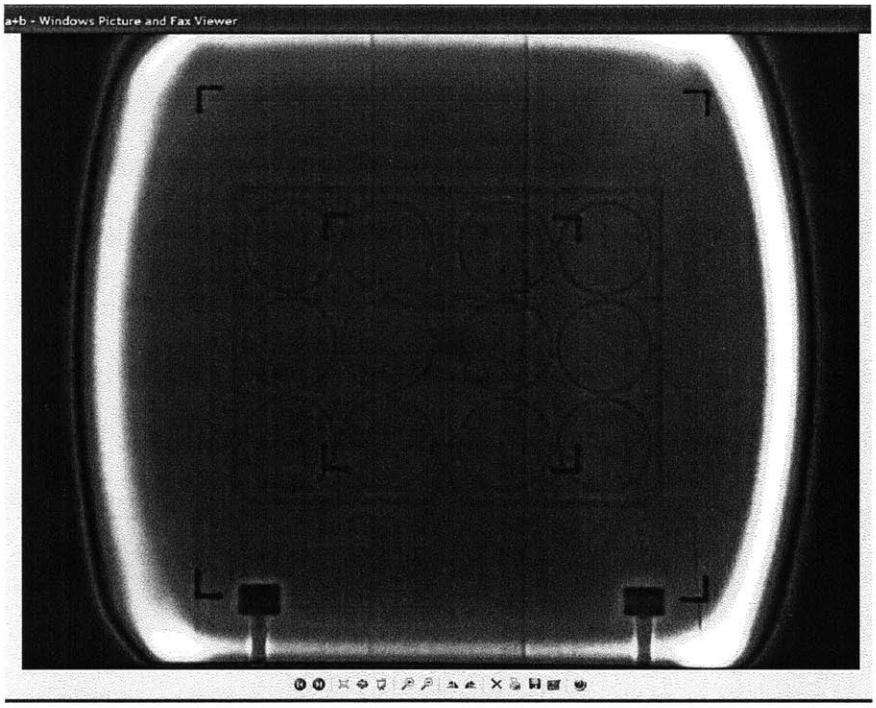

Figure 7: Image captured by the digital beam imager during setup with a Fe beam. The purple-pink, square-like area surrounded by the thin, bright frame defines the beam region. This particular experimental set-up consisted of two, 6-well plates placed next to each other against a foam target stand [5].

Figure 8 shows the experimental setup in the target room at NSRL, with the 6-well plates containing the samples placed upright against a foam holder, perpendicular to the beam (coming from the right side of the photograph). The primary method of calibrating the dose delivered at NSRL is via a small ion chamber called a "Calibration Ion Chamber" (EGG counter; Far West

Technology, Inc., Goleta, CA), which is an air-filled bulb with electrodes for collecting ionization inside a tissue-equivalent plastic cap. Prior to each set of exposures, the EGG counter is used to measure the dose delivered by the beam at the same time as measurements from a series of large ion chambers are being read out. This reading serves to transfer the calibration from the EGG counter to the large ion chamber, which remains just upstream of the samples during exposures. This secondary ion chamber is used to measure the integrated dose delivered, as well as to cut off the beam when the specified total dose has been reached.

Ionization chambers generally consist of two parallel plates within a gas-filled chamber attached to a voltage source. As the radiation passes through the gas chamber, the gas is ionized, and the ions and free electrons move to the electrodes of the opposite polarity, thereby creating an ionization current or voltage drop that can be measured. Ultimately, an ionization chamber provides a count of the number of particles that pass through it during a certain amount of time, or the fluence rate. To calculate the dose rate (and dose delivered to the samples), the following expression can be used:

$$\dot{D} = \dot{\varphi}\left(-\frac{dE}{\rho dx}\right)$$

where the dose rate ($\dot{D}$) is equal to the fluence rate ($\dot{\varphi}$) times the stopping power ($-dE/dx$) divided by the density (ρ) of the material. Once the predetermined dose is reached, the computer-controlled ionization chambers at NSRL cut off the beam, ensuring a dose accuracy within 0.5% [106].

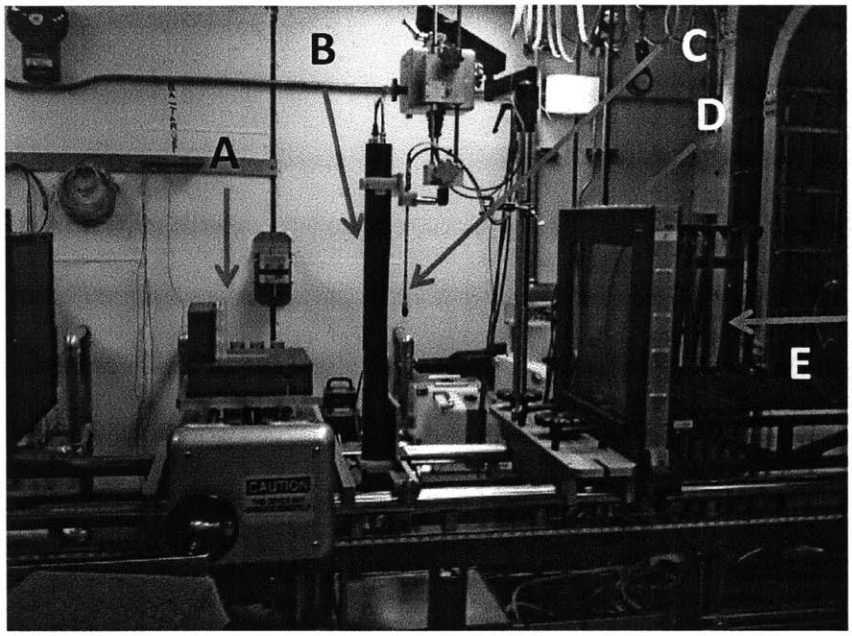

Figure 8: Experimental setup at the NSRL. Photograph shows: (A) 6-well plate placed vertically against a foam holder, (B) scintillation counter, (C) EGG counter, (D) ion chamber, and (E) direction of the beam.

For doses below 1 cGy, the fluence of the beam ions was measured using scintillation counters rather than the ion chamber, as the output of the latter is obscured by electronic and readout noise. Details of the scintillation counters used for the proton and iron ion fluence measurements can be found in the paper by Yang et al. [5].

2.3 2D Co-Culture Experiments

2.3.1 Cell Preparation

When the fibroblasts were used in experiments, the medium was changed to keratinocyte medium. All experiments involving the use of fibroblasts were initiated by trypsinizing flasks of confluent cells and replating them at numbers of $4x10^4$-$1x10^5$ cells, depending on the time of assay. Because keratinocytes begin to differentiate when confluent, they were trypsinized after

reaching ~60% confluency. During experiments, they were similarly kept at low densities to ensure that they would not become confluent at the time of assay. Accordingly, all plating of the keratinocytes used in the 2D co-culture experiments was conducted while they were in the stable exponential growth phase. Cells were transported to Brookhaven National Laboratory and given at least 1 day in the incubator prior to plating for experiments to allow the pH and temperature to restabilize. Cells were then plated 24 hours prior to irradiation to allow time for cell attachment.

2.3.2 Experimental Setup

Critical to the success of conducting bystander studies is the development of a method to co-culture irradiated and non-irradiated cells. Our group has developed a transwell insert system that has been successfully utilized in the study of medium-mediated bystander effects [45]. As shown in Figure 9, cells are plated on coverslips in wells of a 6-well plate as well as in companion Falcon® transwell culture inserts (Becton, Dickinson and Company, Franklin Lakes, NJ). The inserts have a membrane with pores of 1.0 μm diameter at a density of $1.6 \times 10^6/cm^2$ to allow the passage of molecules. Using this system, cells plated in the 6-well plates are irradiated, and immediately after irradiation, inserts with the unirradiated bystander cells are placed in the wells. Therefore, medium is allowed to pass between the bystander and irradiated cells at a cell population separation distance of 0.9 cm.

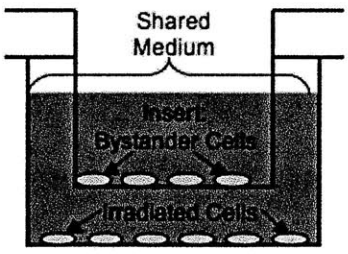

Figure 9: Schematic of the transwell insert co-culture system.

2.3.3 Micronucleus Assay

A micronucleus (MN) is a small nucleus that forms when a chromosome or fragment of a chromosome is not incorporated into one of the daughter nuclei during cell division. It has sufficient information to form its own nuclear membrane and thus appears as a mini nucleus in the cytoplasm. MN formation following irradiation has traditionally been assessed using the cytokinesis-block technique [107], in which cytochalasin B is added to the medium following irradiation. The cytochalasin B blocks cells in cytokinesis by hindering the formation of contractile microfilaments, thereby leaving the cells in a binucleated state. These binucleated cells are then scored to quantify cell damage. However, cytochalasin B was not used in this thesis work because the concentration needed to produce MN in fibroblasts was too toxic for the keratinocytes. Instead, samples were fixed at 48 hours after irradiation with 3.7% formaldehyde and washed 3x5 min with PBS. The samples were then kept in PBS, transported to Boston, and stored at 4°C until stained with the nuclear stain 4', 6'-diamidimo-2-phenylindole (DAPI) at a concentration of 10 μg/ml in water. Cells were then mounted with Vectashield® mounting medium (Vector Laboratories, Inc., Burlingame, CA) and viewed using a fluorescence microscope (Olympus, Center Valley, PA). At least 1000 cells in at least 20 fields of view were examined for each sample.

2.3.4 53BP1 Foci Formation Assay

The kinetics of 53BP1 foci formation were assessed by fixing both irradiated and bystander cells at 1, 5, 12, 24, 48, and 72 hours after the start of co-culture following either proton or iron irradiation. Cells were fixed in 3.7% formaldehyde for 15 min at room temperature (RT) and washed in PBS for 3x5 min. They were then transported to Boston in PBS

and stored at 4°C until staining. To prepare cells for staining, they were first permeabilized in 0.5% Triton X-100 solution for 15 min on ice. Cells were then blocked with blocking buffer containing 5% goat serum, 0.2% dry non-fat milk for 1 h at RT, then incubated with anti-53BP1 antibody (Abcam, Cambridge, MA) for 30 min at RT. After washing the cells with PBS for 4x5 min, they were incubated with Alexa Fluor® 488 goat anti-rabbit IgG secondary antibody (Invitrogen, Carlsbad, CA) for 45 min at RT. The cell monolayers were washed at least four times with PBS and then stained with 10 μg/ml DAPI for 2 min, mounted with Vectashield® mounting medium (Vector Laboratories, Inc.), and viewed using a fluorescence microscope (Olympus). At least 500 cells in at least 15 fields of view were examined for each sample, and cells with at least five foci were considered as positive cells.

2.3.5 Cell Cycle Analysis

To compare the degree of cell cycle arrest in cells irradiated with protons or iron ions, cell cycle analysis was performed on irradiated keratinocytes. Cells were seeded 24 hours prior to irradiation in T-75 flasks at cell densities that ensured the cells would not become confluent by the time of assay but that they would yield at least $1x10^6$ cells on the day of processing. Cells were processed at 5, 24 and 48 hours after proton and iron irradiation. At the time of processing, cells were trypsinized, collected, and washed twice with PBS. After discarding the supernatant, the cells were vortexed to break up the cell pellet. As the cells were being vortexed, the cells were fixed by slowly adding 1 ml of ice-cold 100% ethanol. Samples were stored at -4°C for up to two months until the time of processing for flow cytometry.

To prepare the cells for flow cytometry, they were spun down and washed twice with PBS. They were then stained with 0.5 mg/ml RNase (Sigma), 0.1 mg/ml Propidium Iodide (PI;

Sigma), and 0.1% NP40 (Sigma) detergent in PBS for a total working volume of 0.5 ml/sample. The cell suspension was passed through filter tubes wrapped in aluminum foil to eliminate any cell clumps. Cells were then analyzed for DNA content using a FACSCalibur flow cytometer (BD Bioscience) and accompanying FlowJo software (TreeStar Inc., Ashland, OR).

2.4 3D Tissue Construct Development

Artificial skin constructs are a well-characterized model used in dermatology and skin cancer biology studies [108, 109]. Although skin tissue equivalents are commercially available for purchase, we chose to develop our own skin constructs because it allows us to use the same cells as used in the 2D studies. Furthermore, in future studies, genetically modified variants of the keratinocytes could also be used to gain insight into molecular processes involved in the development of radiation-induced cancers.

In general, skin is composed of two tissue layers: connective tissue (dermis), which provides structural support, and a covering epithelium (epidermis), which provides biological feedback to the dermis through the release of cytokines and other mediators. In our tissue constructs, the dermis layer consisted of AG01522 fibroblasts embedded in a type I collagen matrix, and the epidermis layer consisted of sequentially-differentiated keratinocytes.

The dermal layer was constructed by mixing a solution consisting of 7.4% NaOH (0.3 M), 14.3% 10X M199 media (Gibco), and 78.3% type I rat tail collagen (Fisher Scientific) with a total volume of 1.4 ml/tissue construct. The solution was carefully mixed to avoid the formation of bubbles, and up to an additional 500 µl of NaOH was added to the mixture as necessary until the solution turned a pinkish-orange color (corresponding to a pH of ~7). During the mixing process, the solutions were kept on ice to prevent the collagen from solidifying. Finally, between 1-2x10^6 AG01522 fibroblasts/construct were added to the solution, and the mixture was plated in

a Falcon® transwell culture insert (Becton, Dickinson and Company, Franklin Lakes, NJ) added to a well of a 6-well plate and then left in the incubator at 37°C (5% CO_2) for an hour to solidify. Following solidification of the gel, alpha-modified MEM (Sigma, St. Louis, MO) was added to both the well and the insert (3 and 2.5 ml, respectively) so that the construct was effectively submerged in medium. The constructs were placed back in the incubator and left for at least one day to allow the fibroblasts to become embedded within the collagen matrix.

The following day, the medium was aspirated out of the well and off the top of the construct. Between 1-2x10^6 keratinocytes were added in 3 ml KSFM to the top of each construct, and fresh alpha-modified MEM was added to the well. The constructs were then incubated for about 4 days, with the MEM and KSFM changed daily, to allow the keratinocytes to become confluent and form a basement membrane (Figure 10). The constructs were then cultured for 4 days at an air-liquid interface by transferring the transwell inserts containing the constructs into deep well plates (BD Biosciences) containing 10 ml MEM with no medium added on the top of the inserts. The MEM was changed each day in the well. The air-liquid interface caused the keratinocytes to form a skin-like, stratified epithelium with proliferating basal cells and sequentially differentiated layers as is found in human skin. The constructs were then irradiated at ~Day 10 of culture.

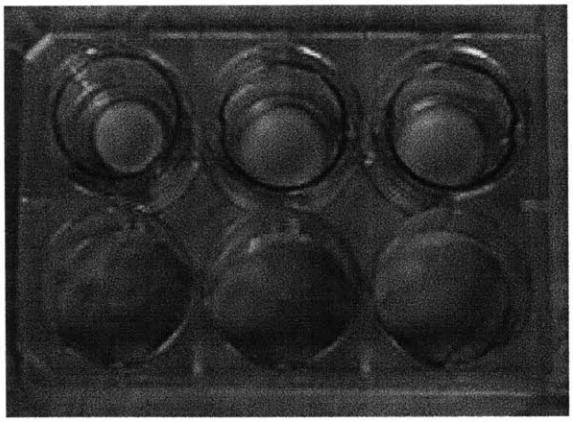

Figure 10: Skin tissue constructs in transwell inserts placed within the wells of a 6-well plate.

2.5 3D Tissue Construct Experiments

Bystander experiments were conducted by splitting each construct in half and exposing half to radiation (either protons or iron ions) then placing the other half in direct contact with the irradiated tissue on a transwell insert (Figure 11). The medium was aspirated prior to tissue irradiation, and 10 ml of fresh AGO medium was added to the wells of the deep well plates immediately after irradiation (no medium was added to the top of the constructs to maintain the air-liquid interface in effect prior to irradiation). The constructs were returned to the incubator until the time of processing.

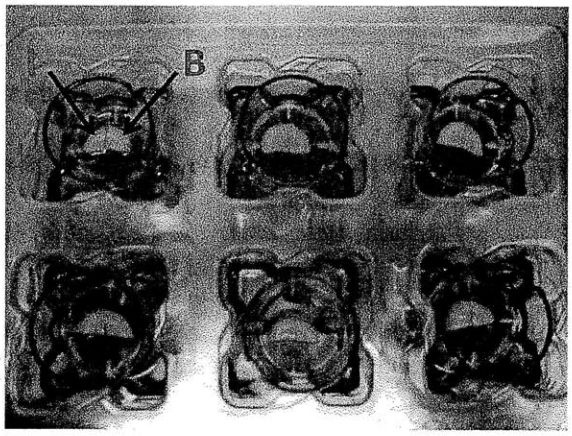

Figure 11: Image of the constructs as they appear after being split into an irradiated section ("I") and bystander section ("B") prior to irradiation.

At the time of processing, the constructs were washed twice in PBS and then fixed in 4% paraformaldehyde in PBS (Fisher Scientific) for 30 minutes. The constructs were then washed twice in PBS and fixed in a 15% sucrose solution overnight on a horizontal shaker at the lowest setting to preserve the cell layers. The following day, the 15% sucrose solution was removed and replaced with a 30% sucrose solution, and the constructs were again gently shaken in solution overnight on a horizontal shaker. The next day, the sucrose solution was aspirated off the constructs, and the constructs were placed in dilution vials (Fisher Scientific) and fixed with 10% buffered formalin phosphate (Fisher Scientific) for 48 hours. Following fixation, the tissue constructs were cut into approximately 5x10-mm pieces and were either immediately sent for processing/embedding by placing them in biopsy tissue cassettes (Tissue-Tek), or they were kept in 70% ethanol at 4°C for up to a week prior to processing/embedding due to travel logistics from BNL back to Massachusetts General Hospital (MGH).

Tissue processing was completed overnight at the Dana Farber/Harvard Cancer Center (DF/HCC) Research Pathology Core facility located at MGH. Briefly, the constructs were dehydrated with gradient ethanol solutions for 1 h each (70%, 80%, 95%x2, 100%x3), cleared in

three washes of xylene for 1 h each, and then infiltrated with paraffin wax for 1 h. Paraffin embedding of the constructs was performed by us to ensure that the samples were mounted sideways to provide cross-sectional slices for assay (i.e., so that both cell types were present in the same section). Sectioning was performed by the DF/HCC Core facility, during which 5-μm-thick sections were mounted onto glass slides.

2.5.1 Histological Analysis

Histological analysis was performed throughout the protocol development phase of the tissue constructs to ensure that a tissue morphology similar to that of normal human skin was obtained, namely to ensure that the fibroblasts were distributed throughout the dermal layer and that the keratinocytes formed sequentially differentiated layers and were attached to the dermal layer. The construct morphology was assessed using traditional hematoxylin and eosin (H&E) histological staining. Briefly, the tissue was deparaffinized in xylene (10 min), rehydrated in gradient ethanol solutions (100%, 5 min; 90%, 3 min; 70%, 2 min), washed in PBS for 2 min, stained with hemotoxylin for 2 min, rinsed in deionized water (dH_2O) until all of the excess stain was washed off, dipped in eosin 2-3 times, rinsed in dH_2O, dehydrated in gradient ethanol solutions (70%, 2 min; 90%, 2 min; 100%, 2 min), cleared in xylene for 3 min, and sealed with a coverslip. A representative H&E image of the tissue used in the bystander experiments is shown in Figure 12.

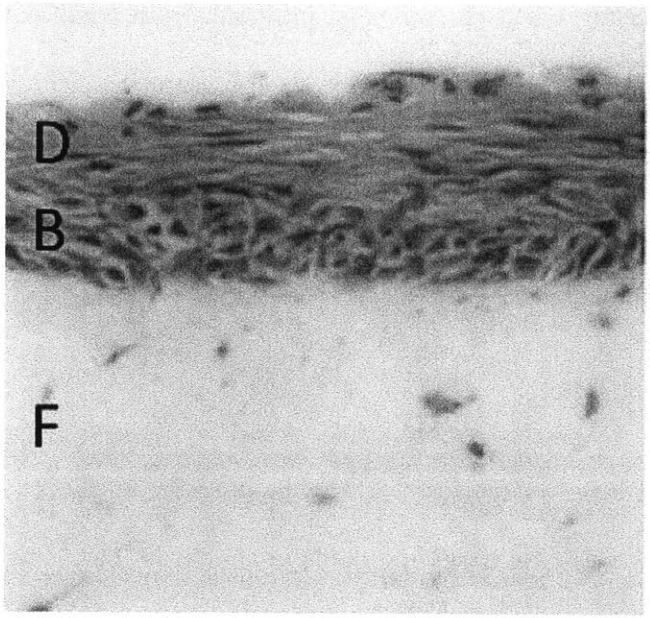

Figure 12: H&E image of a construct cross-section at 40x magnification. "F", "B", and "D" indicate the fibroblasts, basal-layer keratinocytes, and differentiated keratinocytes, respectively.

In Figure 12, the fibroblasts can clearly be seen dispersed throughout the collagen-matrix comprising the dermal skin layer. The stratified squamous epithelium is maintained by cell division within the basal layer, which can be identified by the keratinocytes with large nuclei that are attached to the dermal layer. Differentiating cells delaminate from the basement membrane and are displaced outwards through the epidermal layers. In the outermost epidermal layers, individual cells are difficult to identify because: 1) nuclei can no longer be identified, 2) the cells are very flat, and 3) the space between the cells is filled with lipids that serve to cement the cells together into a continuous membrane.

2.5.2 53BP1 Foci Formation Assay

Deparaffinization and rehydration

Before the tissue construct sections can be stained, they must first be deparaffinized and

rehydrated. Deparaffinization was accomplished by washing the construct slides in CitriSolv (Fisher Scientific) 2x8 min. The tissue was subsequently rehydrated through washes in gradient concentrations of ethanol: 100% for 2x3 min, 95% for 1x3 min, 70% for 1x3 min, and 50% for 1x3 min. The slides were then dipped a few times in three changes of dH_2O and then washed in dH_2O for 2x2 min, followed by a wash in PBS for 1x2 min.

Antigen retrieval

Most formalin-fixed tissues require an antigen retrieval step before the immunohistochemical staining can proceed. This is due to the formation of methylene bridges during fixation, which cross-link proteins and therefore mask antigenic sites. There are generally two methods of antigen retrieval, heat-mediated and enzymatic, which serve to break the methylene bridges and expose the antigenic sites to allow the antibodies to bind. Following a consultation with Abcam, the company that produces the 53BP1 antibody, it was determined that a heat-mediated retrieval process would be more optimal for use with this particular antibody. Accordingly, all tissue samples underwent retrieval via a water bath protocol. Specifically, a retrieval solution was prepared via a 10% solution of Target Retrieval Solution (DAKO) in water. The slides were placed in a slide rack inside a slide tray containing the unmasker solution. The slide tray was then kept inside a pre-heated water bath at 98°C for 35 min. The slide tray was then taken out and allowed to cool for 5 min on the lab bench and then 5 min in a tap water bath.

Immunostaining

Following the antigen retrieval process, the slides were washed in dH_2O for 2x2 min and then PBS for 1x2 min. The slides were then prepared for immunostaining by carefully wiping the area around the tissue section and circling the tissue with a PAP pen. The sections were

permeabilized using a 0.5% Triton X-100 solution for 15 min on ice. The tissue was then blocked using a 2.5% goat serum solution in PBS for 1 hour. Immediately following tissue blocking, the tissue was incubated with anti-53BP1 antibody (Abcam) diluted 1:1000 in antibody diluent solution (DAKO, Carpinteria, CA) at 4°C overnight in a humidified chamber.

The next day, the slides were washed by dipping them a few times in 1 change of PBS and then washing with Tris-Tween 2x5 min and then PBS 1x5 min. The tissue was incubated in a secondary antibody solution consisting of Alexa Fluor® 488 goat anti-rabbit IgG secondary antibody (Invitrogen) at a 1:400 concentration in antibody diluent solution (DAKO) for 45 min at RT. The slides were then washed by dipping them a few times in 1 change of PBS and then washing in Tris-Tween 2x5 min and PBS 1x5 min on a horizontal shaker plate at low speed. After carefully wiping around the tissue to remove any remaining solution, coverslips were mounted on the slides using Vectashield® mounting medium (Vector Laboratories, Inc.) combined with 20 µl of DAPI at a concentration of 10 µg/ml. The sections were viewed using a fluorescence microscope (Olympus). At least 500 fibroblasts and keratinocytes in at least 10 fields of view were examined in each section, and the number of foci/cell was recorded.

2.6 Low Fluence Experiments

Although astronauts could receive a high cumulative radiation dose on a long-duration mission (for example, the dose is estimated at 1-2 Sv on a three-year trip to Mars [110], it is important to note that the exposures would occur at very low dose rates from mixed radiation fields. For example, on a three-year trip to Mars, it has been estimated that astronauts would be exposed to about 250 µGy/day of protons (or ~0.4 hits per cell nucleus per day), 35 µGy/day of α-particles, and 3 µGy/day of HZE particles [111]. Under such conditions, where particle

traversals are well separated in tissue location and time, low-dose phenomena such as the bystander effect could contribute to the overall biological effects of space radiation [112]. To address the magnitude or existence of the bystander effect under conditions of low particle fluences in both the 2D and 3D skin models, we utilized the novel techniques developed at NSRL to measure very low particle fluences by using a large ionizing chamber to visualize the radiation beam and a scintillation counter to quantify the particle fluence. Details of this technique can be found in the study by Yang et al. [5].

For the low fluence studies conducted at NSRL, ion exposures were conducted in the particle counting mode. The particle fluence was converted to dose using the following equation:

$$Dose\ (Gy) = 1.6x10^{-9}\ x\ LET\left(\frac{keV}{\mu m}\right)\ x\ F\left(\frac{particles}{cm^2}\right)$$

It should be kept in mind that the above dose essentially represents the dose to the 6-well plate, and the dose to the cells is highly non-uniform. For example, at fluences so low that only a fraction of cells are actually traversed by a particle, the traversed cells would receive a large dose, the cells traversed by delta rays derived from the traversal of the particle through the sample would receive a low dose, and other cells would receive no dose. The average number of particle traversals per cell was calculated as:

$$n = \frac{Dose\ (Gy)x\ cellular\ area\ (\mu m^2)}{0.16\ x\ LET\ \left(\frac{keV}{\mu m}\right)}$$

where a cell area of 1000 μm^2 was assumed. The fraction of cells traversed (f) can be expressed using Poisson statistics as:

$$f = 1 - e^{-n}$$

2.7 Scavenger Experiments

The role of ROS/RNS in eliciting bystander effects in response to both proton and iron ion irradiation was investigated by adding the ROS/RNS scavengers catalase (200 μg/ml [8000 U/ml]; EMD Chemicals, Gibbstown, NJ, USA), SOD (200 μg/ml [500 U/ml]; EMD Chemicals), and PTIO (20 μM; EMD Chemicals) (which scavenge hydrogen peroxide, superoxide, and NO, respectively) into the medium of both tissue constructs and 2D cell monolayers immediately following irradiation. The reactions of catalase with hydrogen peroxide, superoxide dismutase with superoxide, and PTIO with NO are shown in Figure 13, Figure 14, and Figure 15, respectively.

$$2H_2O_2 \xrightarrow{\text{Catalase}} 2H_2O + O_2$$

Figure 13: Reaction of catalase with hydrogen peroxide.

$$2O_2^{\bullet -} + 2H^+ \xrightarrow{\text{SOD}} O_2 + H_2O_2$$

Figure 14: Reaction of SOD with superoxide.

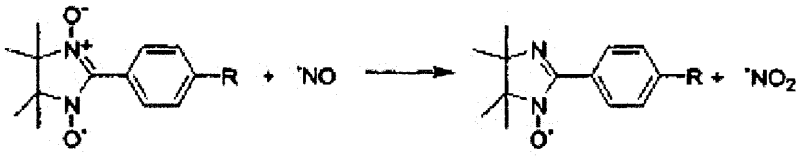

Figure 15: Reaction of PTIO with NO.

Tissue constructs and cells were fixed at 12 hours (protons) and 24 hours (iron) (time points identified in Aim 1 for the peak bystander responses) after irradiation and assayed for 53BP1 foci formation.

2.8 Statistical Analysis

All data shown in this thesis are representative of at least three independent experiments unless otherwise noted, and the results are presented as means ± standard deviation. Statistical comparisons between the treatment groups and controls were performed using the Student's t-test.

CHAPTER 3

2D Experiments

3.1 Results

Results of the 2D experiments are presented in this section, which include investigations of cell signaling between keratinocytes and fibroblasts under both low- and high-LET irradiations over a wide fluence/dose range as well as the modulation of the effects by ROS/RNS scavengers.

3.1.1 Micronucleus Assay

Using the DAPI nuclear stain, micronuclei were seen in both irradiated and bystander cells following both iron and proton irradiation. Three different cell signaling combinations were investigated: bystander keratinocytes co-cultured with irradiated AG01522 cells (A→K), bystander AG01522 cells co-cultured with irradiated keratinocytes (K→A), and bystander keratinocytes co-cultured with irradiated keratinocytes (K→K). Figure 16 shows a typical immunofluorescence DAPI-stained field showing cells with MN (arrows show locations of MN).

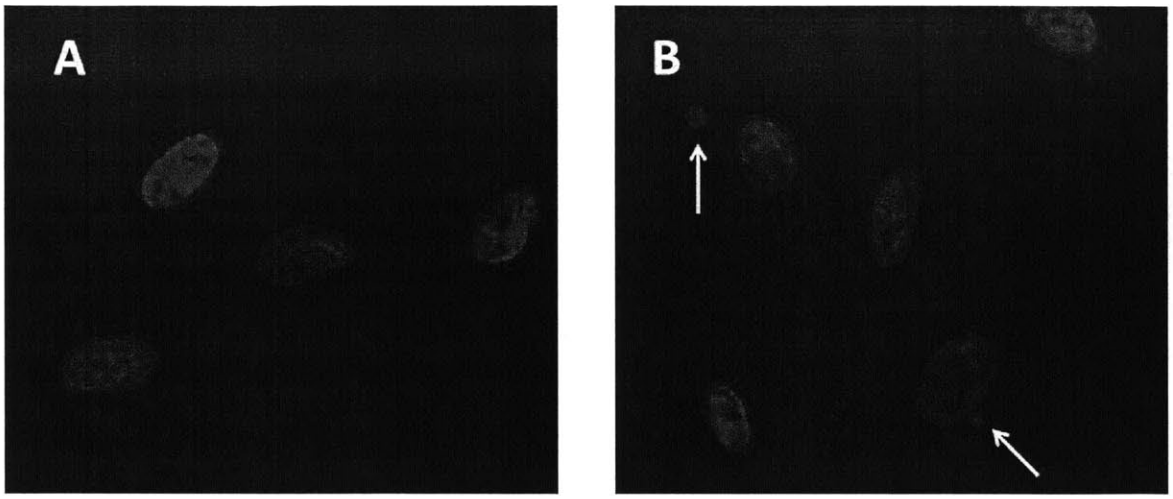

Figure 16: Immunofluorescence detection of MN in unirradiated AG01522 fibroblasts (A) and in fibroblasts 1 h following irradiation with 1 Gy iron ions (B). Arrows indicate locations of MN.

The percentages of both irradiated and bystander cells exhibiting MN were determined simultaneously in the same experiments, but the data are presented separately for each cell population. The percentages of cells exhibiting MN in the irradiated cell populations are shown in Figure 17. It can be seen that at 0.1 Gy, the levels of MN are elevated in cells of only 1 or 2 of the signaling combinations under either proton or iron ion irradiation, whereas at either 1 Gy (iron) or 2 Gy (protons), cells in all three combinations exhibit statistically significant increases in MN formation. Based on Figure 17, it can be seen that iron ions are more effective than protons at inducing cell damage, with 14% of cells expressing MN after only 1 Gy of iron ions compared to only 9% having MN after 2 Gy of protons.

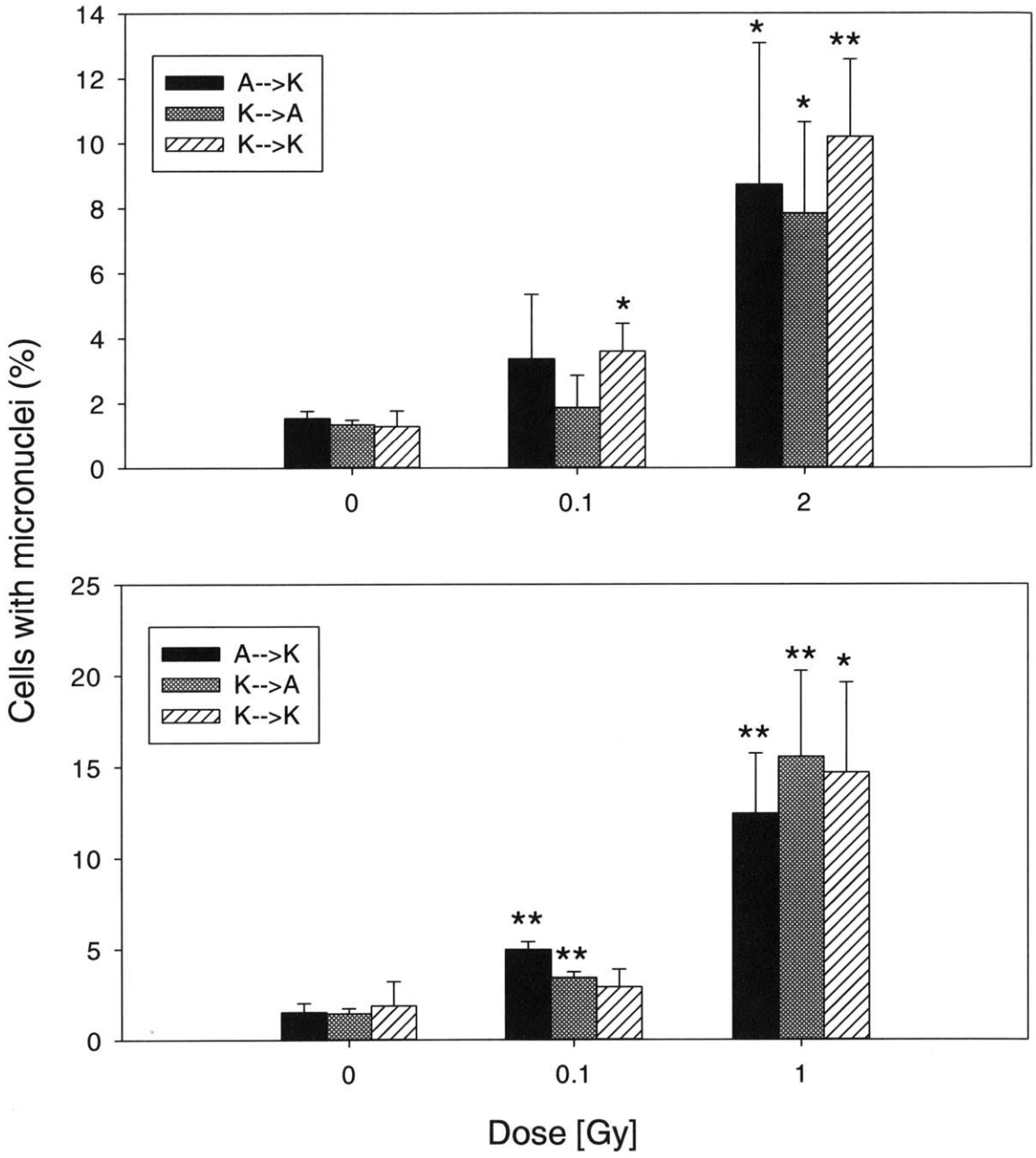

Figure 17: Dose response for the induction of MN in irradiated AG01522 fibroblasts (A) or keratinocytes (K) 48 h after exposure of cells to either 1 GeV protons (top) or 1 GeV/n iron ions (bottom). *, $p<0.05$; **, $p<0.01$ versus the unirradiated control. In the legend, the first letter (A or K) corresponds to the irradiated cells, and the second letter indicates the bystander cells.

As shown in Figure 18, there is a 1.5-2.0-fold increase in MN formation in bystander fibroblasts or keratinocytes after proton irradiation of either cell type. Interestingly, data obtained for MN bystander induction from the mixed cultures exposed to iron ions showed differences from the results with the low-LET protons. Namely, a bystander effect was seen in unirradiated keratinocytes co-cultured with irradiated AG01522 cells, with a two-fold increase in MN expression, but no visible bystander effect was seen in unirradiated AG01522 cells co-cultured with iron-irradiated keratinocytes (Figure 18, bottom). Furthermore, there was no apparent dose-dependence of the bystander effect for either radiation quality tested; the higher dose of either 1 Gy (iron ions) or 2 Gy (protons) did not yield a significant increase in MN formation compared to the lower dose of 0.1 Gy (for both protons and iron ions). This dose-response plateau feature is typical of the bystander response.

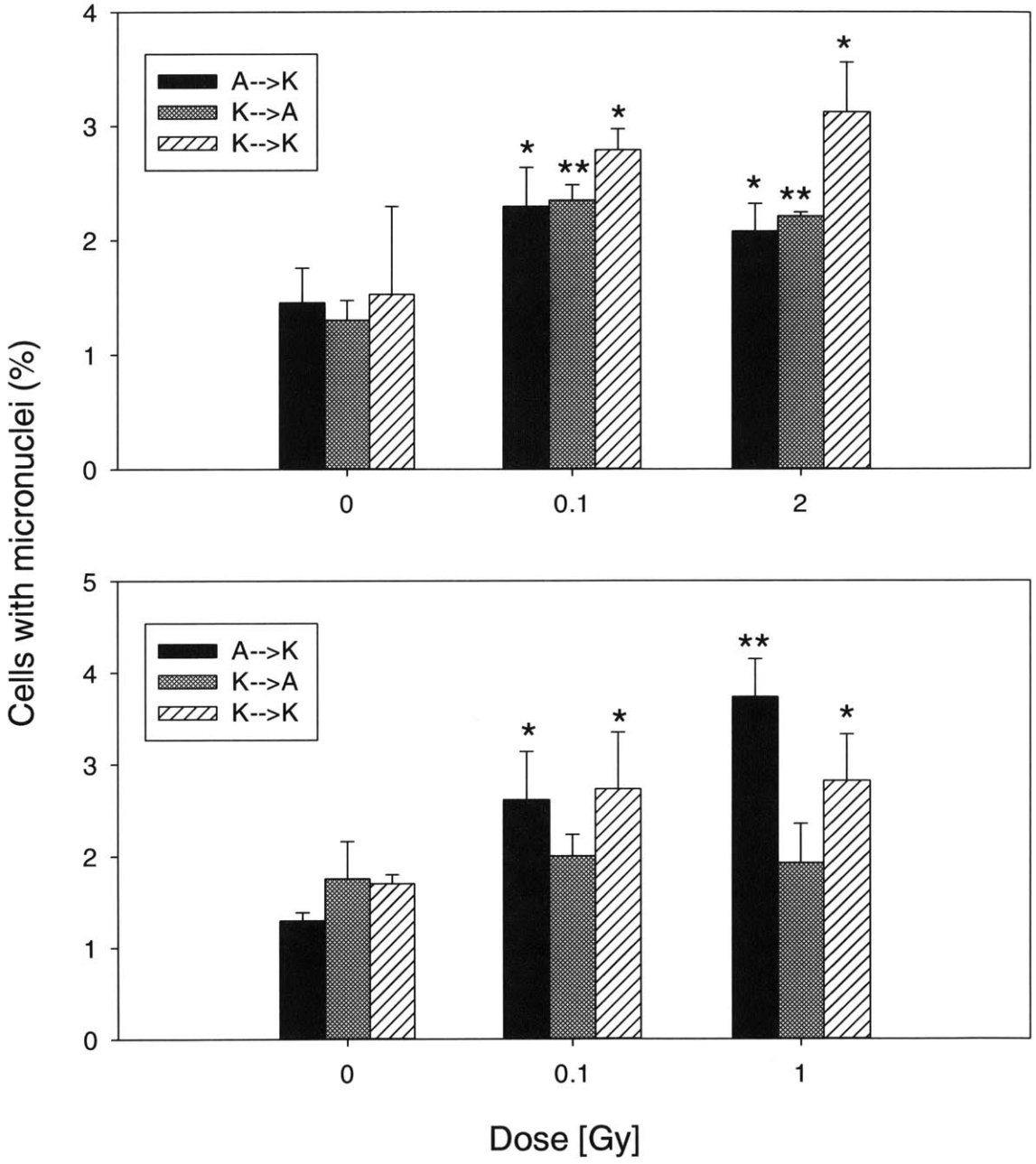

Figure 18: Induction of MN in unirradiated AG01522 fibroblasts (A) or keratinocytes (K) 48 h after the start of their co-culture with cells exposed to either 1 GeV protons (top) or 1 GeV/n iron ions (bottom). *, $p<0.05$; **, $p<0.01$ versus the unirradiated control. In the legend, the first letter (A or K) corresponds to the irradiated cells, and the second letter indicates the bystander cells.

3.1.2 53BP1 Foci Formation

To determine how the patterns of double strand break formation and rejoining kinetics change with particle LET, dose, and cell signaling combination, the formation and dissolution of 53BP1 foci in cells at 1, 5, 12, 24, 48, and 72 h after irradiation with either 0.1 and 2 Gy of protons or 0.1 and 1 Gy of iron ions were examined. The formation of 53BP1 foci was determined visually in irradiated and bystander cells using a fluorescent antibody. Cells with 5 or more foci were considered positive. Figure 19 shows a representative time course of 53BP1 foci formation in AG01522 fibroblasts in both control cells and in cells at 1, 5, 12, 24, 48, and 72 h post-irradiation with 2 Gy of protons.

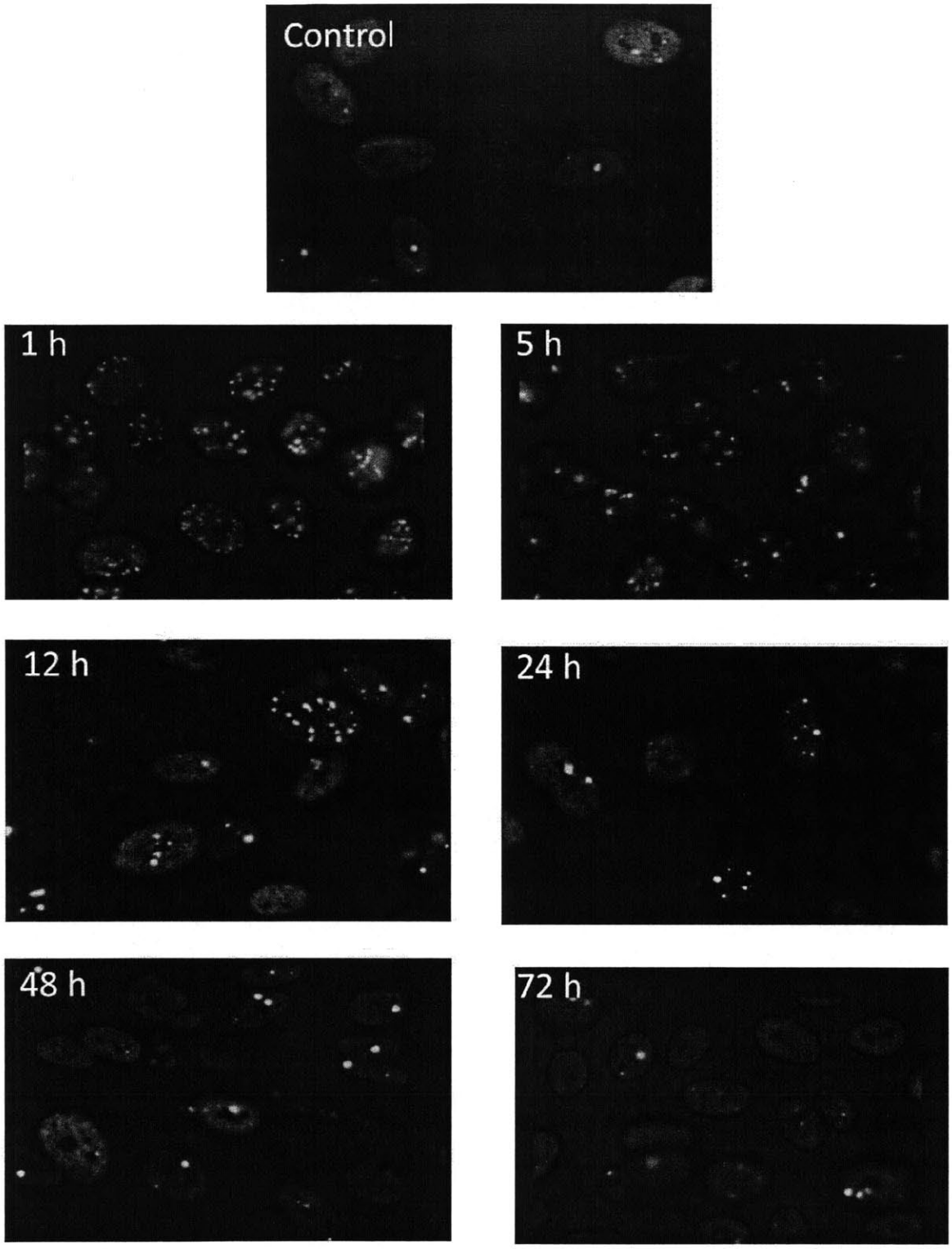

Figure 19: In situ immunofluorescence detection of 53BP1 foci in AG01522 fibroblasts in control cells (top) and in cells at different time points after irradiation with 2 Gy of protons.

Foci expression in irradiated cells is shown in Figure 20, Figure 21, and Figure 22. These figures demonstrate a direct correlation between foci formation and dose; namely, the number of cells positive for foci formation was significantly greater in cells exposed to either 1 or 2 Gy of iron ions and protons, respectively, compared to 0.1 Gy of either protons or iron ions. For all irradiated cells, foci formation was found to be maximum at 1 h after irradiation and decreased to control levels by 72 h with the exception of iron-irradiated fibroblasts co-cultured with keratinocytes (Figure 20, left), where the fraction of cells with foci remained elevated even at 72 h. The decreasing foci number with time reflects the continued DNA rejoining and repair that occurs following irradiation. Following proton irradiation at 0.1 Gy, foci formation in irradiated cells peaked at 1 h and was at background levels by 5 h. Following iron ion irradiation at 0.1 Gy, foci formation in irradiated cells peaked at 1 h and decreased to background levels by either 12 h (K→K and K→A) or 5 h (A→K). Thus, in general, the double strand breaks induced by protons were rejoined faster than those induced by iron ions.

53BP1 foci are also formed in the bystander cells, as shown in Figure 23, Figure 24, and Figure 25 (A→K, K→A, K→K, respectively). Following proton irradiation, foci formation in the bystander cells remained at control levels at 1 and 5 h, peaked at 12 h at doses of both 0.1 and 2 Gy, and returned to background levels by either 48 h (A→K and K→K) or 24 h (K→A). Following iron irradiation, foci formation in the bystander cells remained at background levels from 1-5 h, was increased at 12 hours although not statistically significant, reached a maximum at 24 h at both 0.1 and 1 Gy, and returned to background levels by either 48 h (K→A) or 72 h (A→K and K→K). Furthermore, the magnitude of the bystander effect was found to be independent of dose, LET, and cell signaling combination. Based on these preliminary experiments, 12 h (proton) and 24 h (iron) were chosen as the co-culture time points for the

subsequent low fluence and scavenger studies.

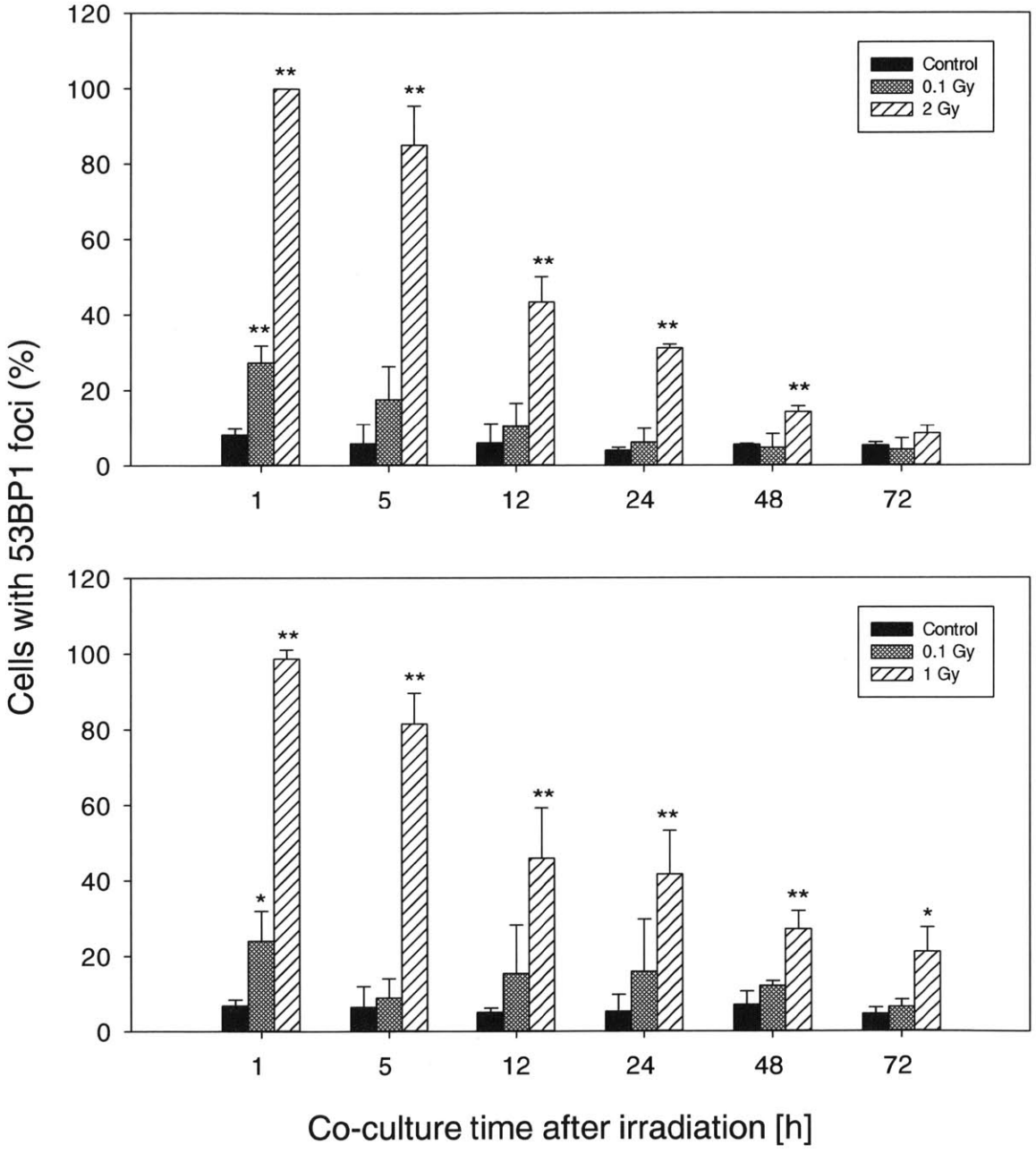

Figure 20: 53BP1 foci formation in irradiated AG01522 fibroblasts placed in co-culture with bystander keratinocytes. Top: proton irradiation; Bottom: iron irradiation. Cells with at least 5 foci were considered positive for foci formation (*, $P < 0.05$; **, $P < 0.01$ vs. unirradiated control).

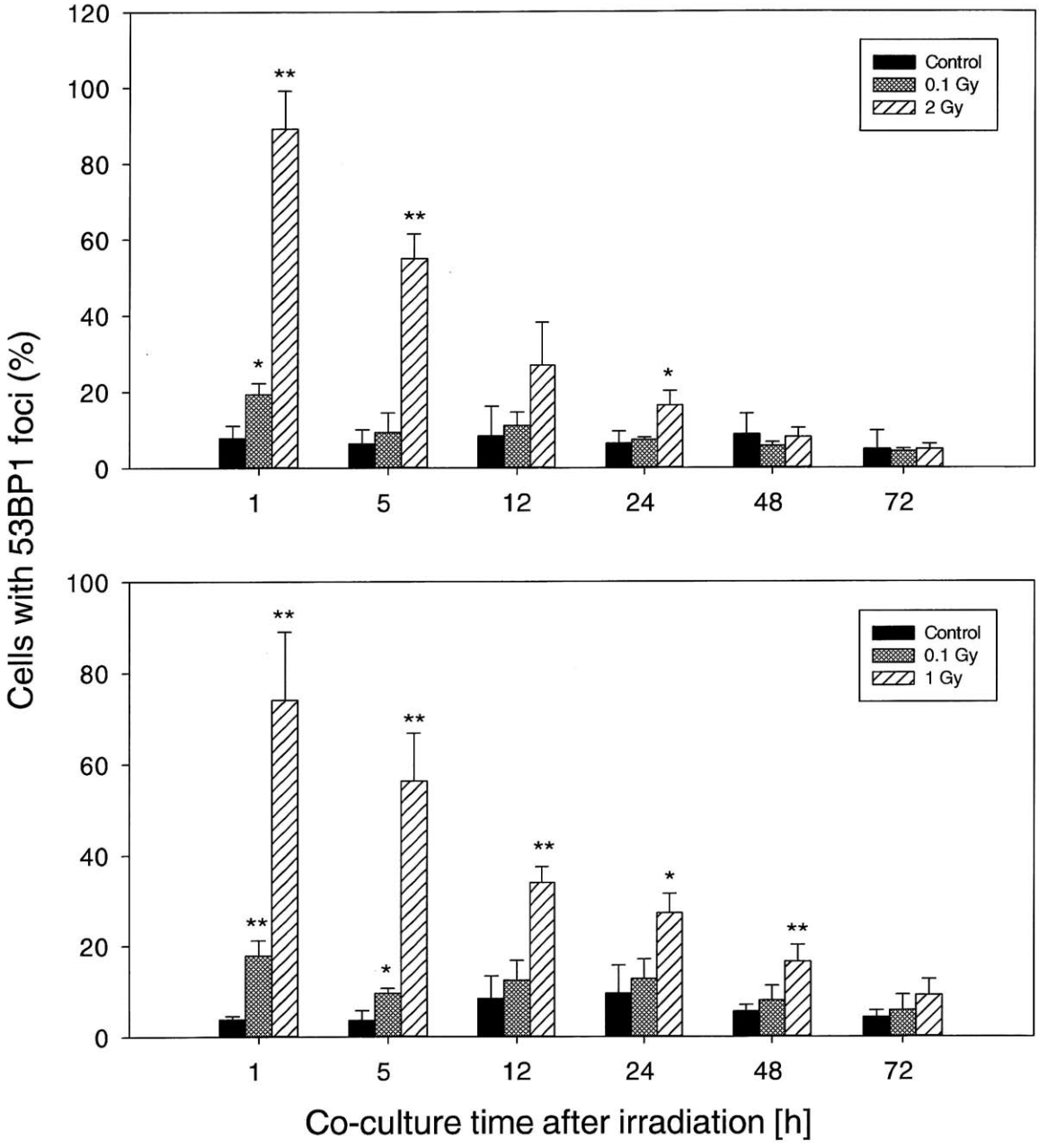

Figure 21: 53BP1 foci formation in irradiated keratinocytes placed in co-culture with bystander AG01522 fibroblasts. Top: proton irradiation; Bottom: iron irradiation. Cells with at least 5 foci were considered positive for foci formation (*, $P < 0.05$; **, $P < 0.01$ vs. unirradiated control).

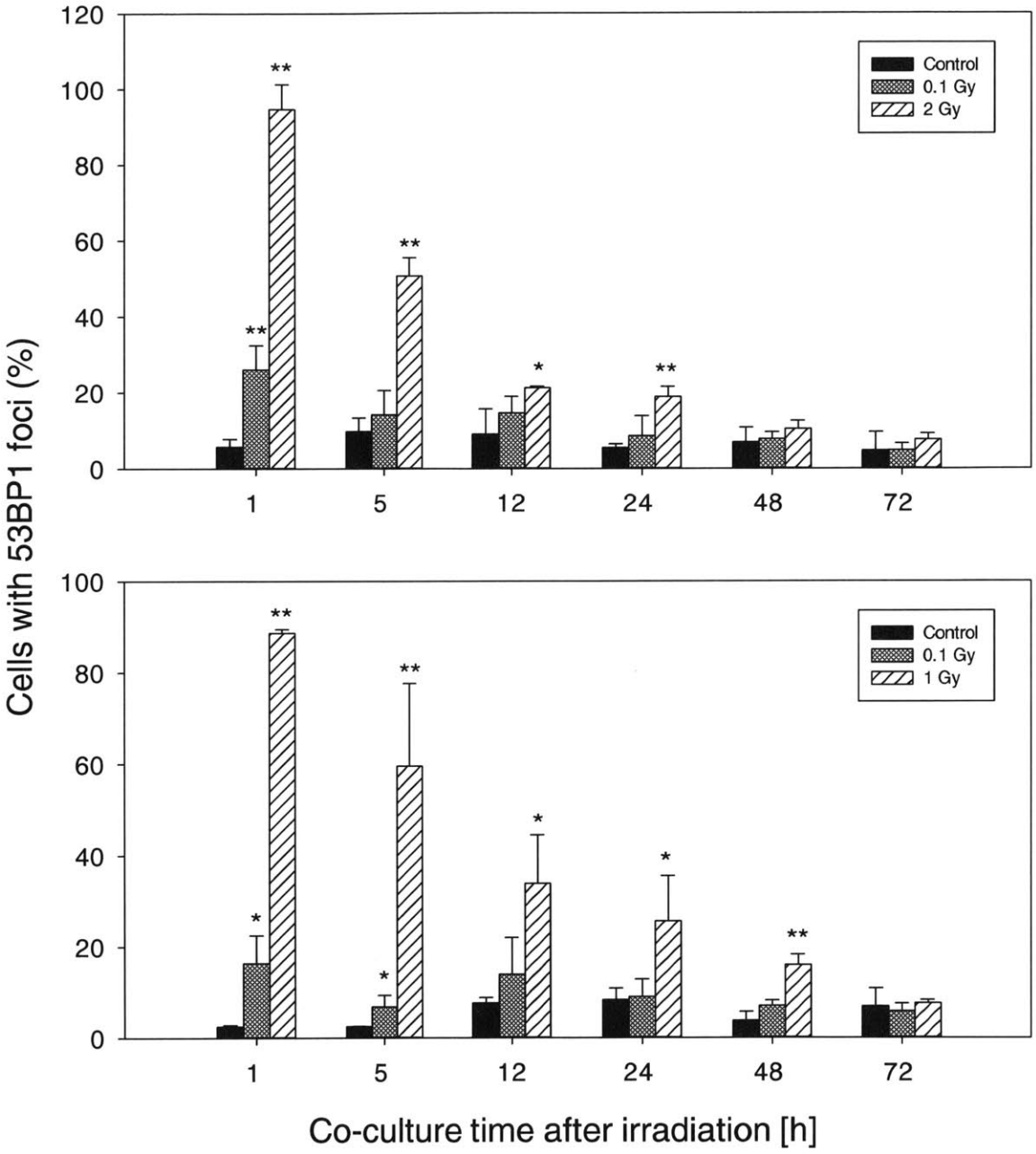

Figure 22: 53BP1 foci formation in irradiated keratinocytes placed in co-culture with bystander keratinocytes. Top: proton irradiation; Bottom: iron irradiation. Cells with at least 5 foci were considered positive for foci formation (*, $P < 0.05$; **, $P < 0.01$ vs. unirradiated control).

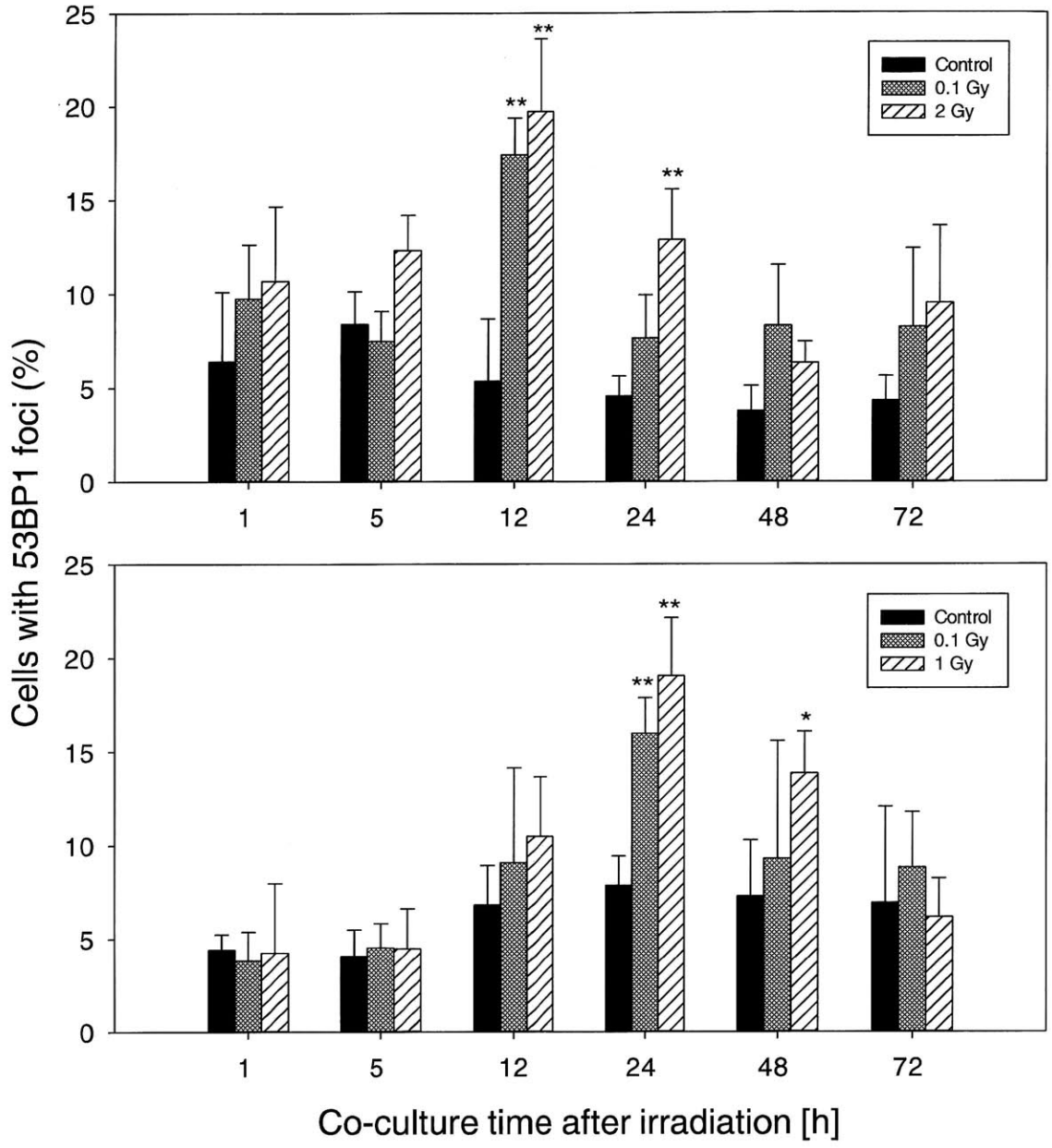

Figure 23: 53BP1 foci formation in bystander keratinocyte cells following the irradiation of AG01522 fibroblasts as a function of time that irradiated and unirradiated cells were in co-culture. Top: proton irradiation; Bottom: iron irradiation. Cells with at least 5 foci were considered positive for foci formation (*, $P < 0.05$; **, $P < 0.01$ vs. unirradiated control).

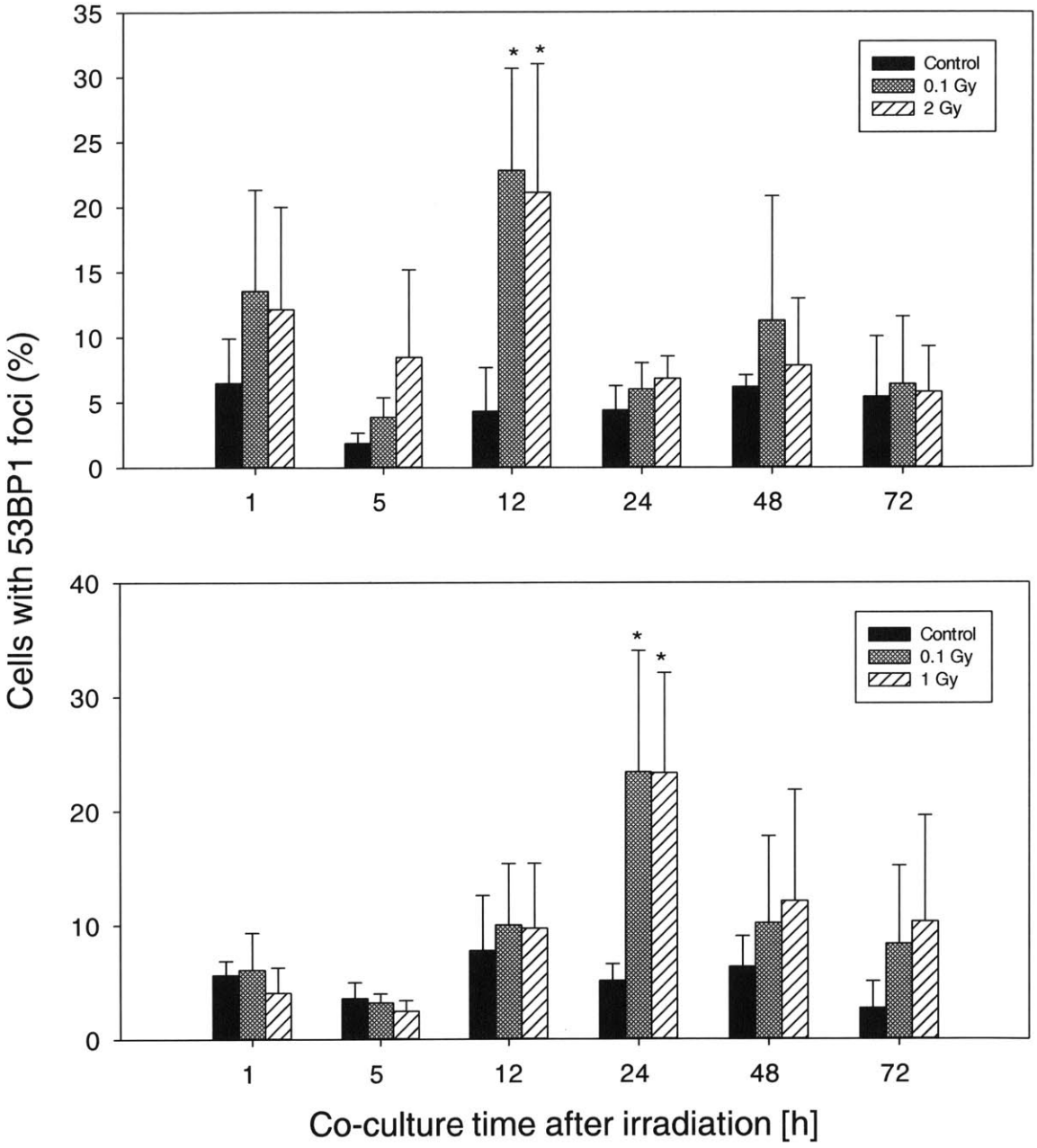

Figure 24: 53BP1 foci formation in bystander AG01522 fibroblasts following the irradiation of keratinocytes as a function of time that irradiated and unirradiated cells were in co-culture. Top: proton irradiation; bottom: iron irradiation. Cells with at least 5 foci were considered positive for foci formation (*, $P < 0.05$; **, $P < 0.01$ vs. unirradiated control).

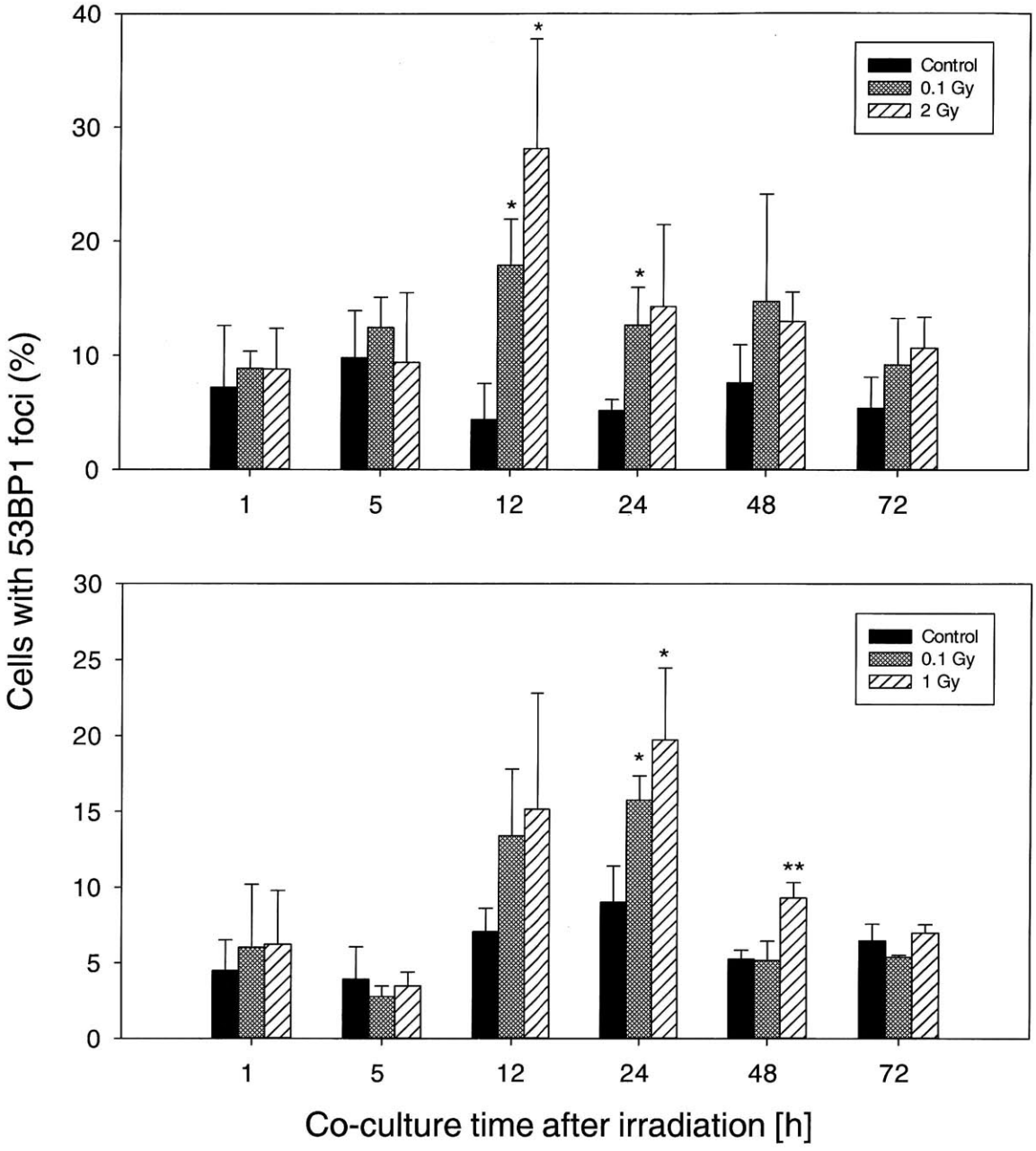

Figure 25: 53BP1 foci formation in bystander keratinocytes following the irradiation of keratinocytes as a function of time that irradiated and unirradiated cells were in co-culture. Top: proton irradiation; bottom: iron irradiation. Cells with at least 5 foci were considered positive for foci formation (*, $P < 0.05$; **, $P < 0.01$ vs. unirradiated control).

In summary, irradiation with either protons or iron ions induces 53BP1 foci formation in both keratinocytes and fibroblasts that is maximal at 1 h and decreases out to 72 h. Foci appear to be removed slightly more quickly in irradiated keratinocytes than in irradiated fibroblasts, and foci are removed more rapidly by both cell types after proton compared to iron ion irradiation. In bystander cells, foci formation was found to peak at 12 and 24 h following co-culture with proton- and iron-irradiated cells, respectively, in all three cell signaling combinations.

3.1.3 Cell Cycle Delays

As it is known that radiation can induce cell cycle arrests, we hypothesized that an arrest of keratinocytes could explain why a bystander effect was not seen in the induction of micronuclei in fibroblasts co-cultured with iron-irradiated keratinocytes. This possibility was investigated by conducting cell cycle analysis in keratinocytes at 5, 24, and 48 h after both proton and iron irradiation. Figure 26–28 show the cell cycle distribution of keratinocytes following proton irradiation, and Figure 29-31 show the distribution of keratinocytes following iron irradiation (data from Anzenberg, 2005). It can be seen that there is a G2 arrest in the keratinocytes 5 h after 2 Gy of protons that is resolved by 24 h. No significant differences in cell cycle distribution are noted after 0.5 Gy of protons. Following 2 Gy iron irradiation, however, a large G2 arrest occurs from 5 h until at least 48 h, along with a corresponding decrease in the percentage of cells in the G1 and S phases due to the accumulation of cells in the G2 phase. Similar trends are seen following 0.5 Gy of iron irradiation, although at a lower magnitude.

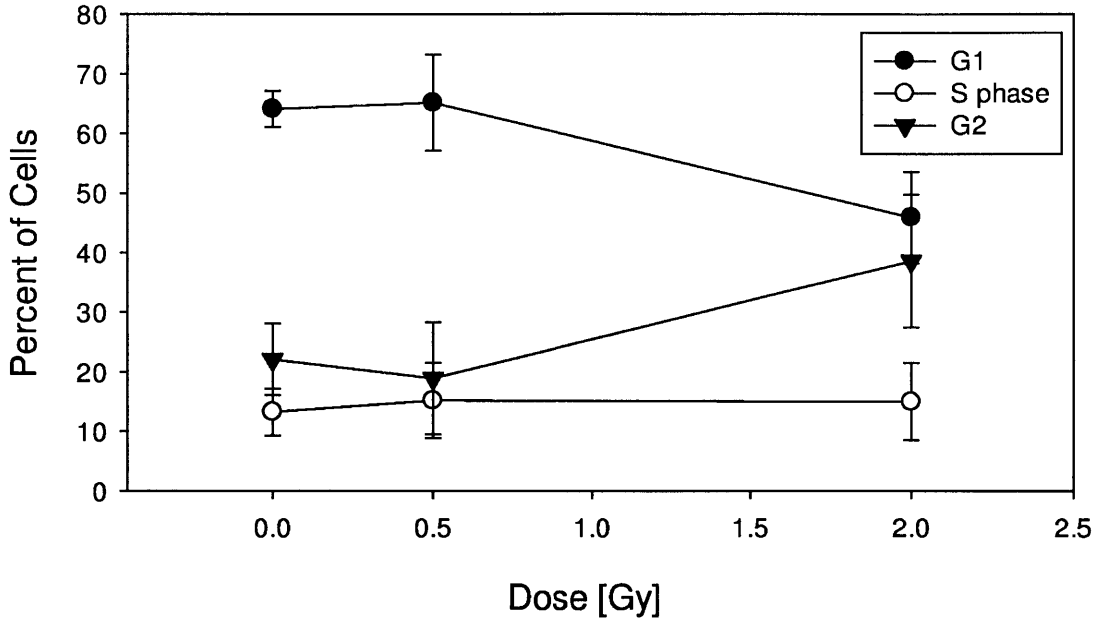

Figure 26: Cell cycle distribution in irradiated keratinocytes 5 h after proton irradiation.

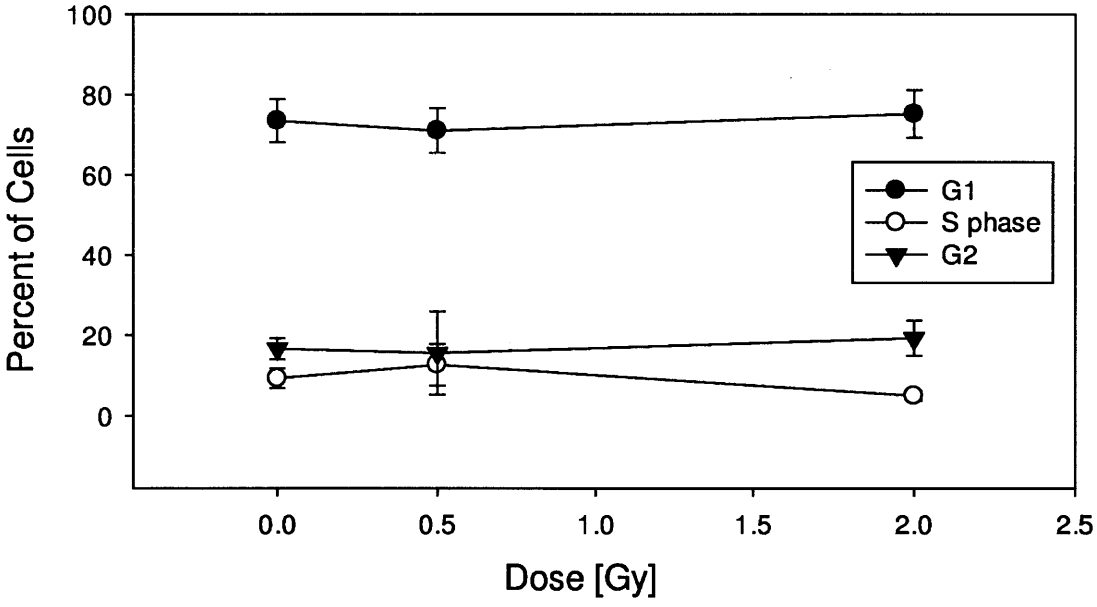

Figure 27: Cell cycle distribution in irradiated keratinocytes 24 h after proton irradiation.

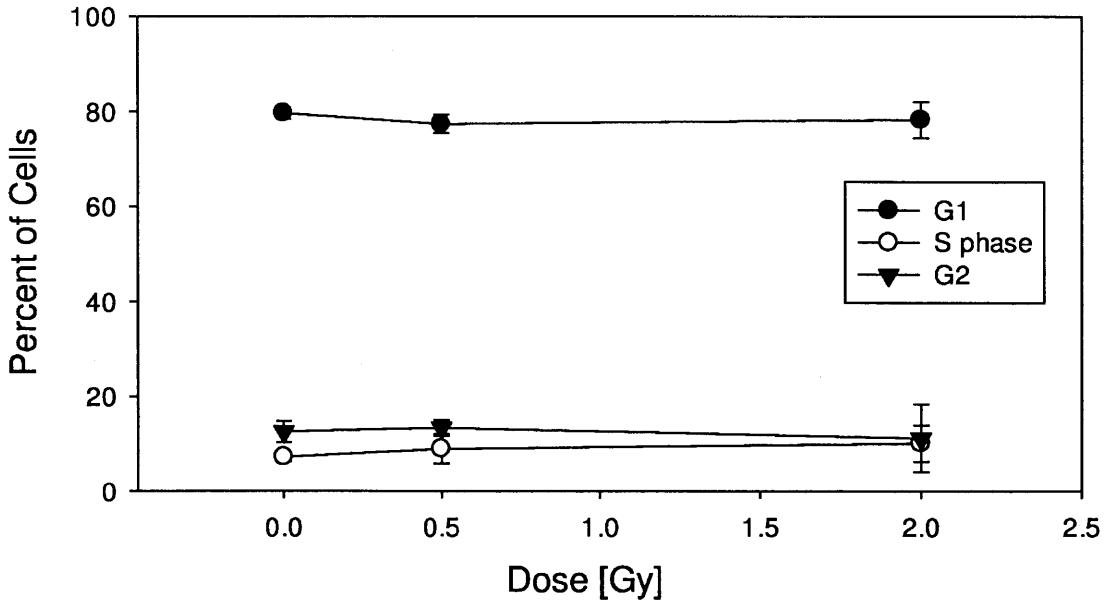

Figure 28: Cell cycle distribution in irradiated keratinocytes 48 h after proton irradiation.

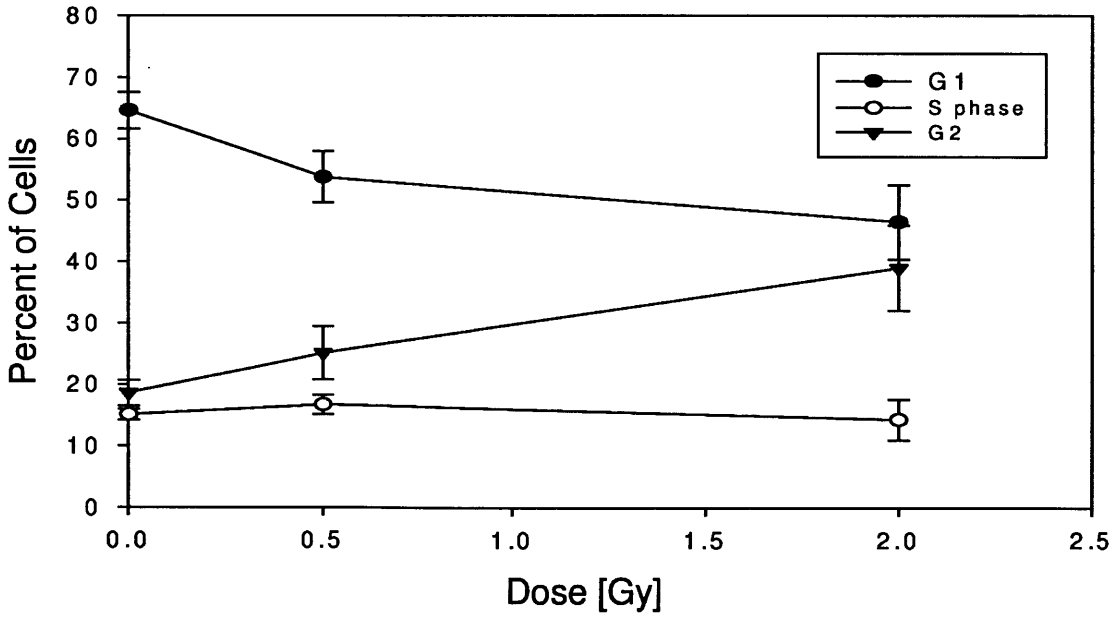

Figure 29: Cell cycle distribution in irradiated keratinocytes 5 h after iron irradiation [Source: [6]].

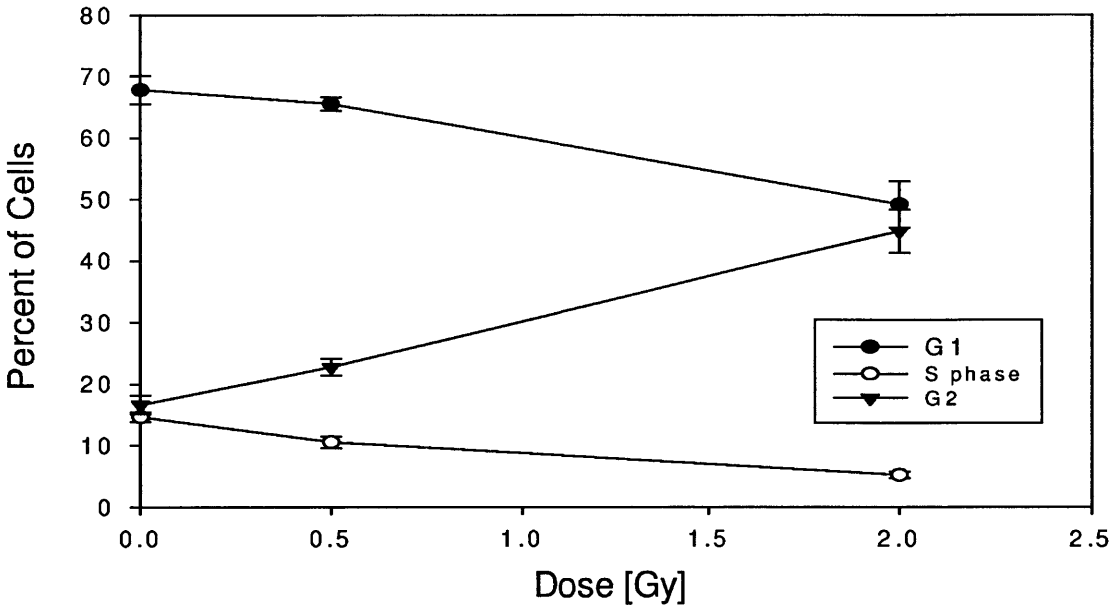

Figure 30: Cell cycle distribution in irradiated keratinocytes 24 h after iron irradiation [Source: [6]].

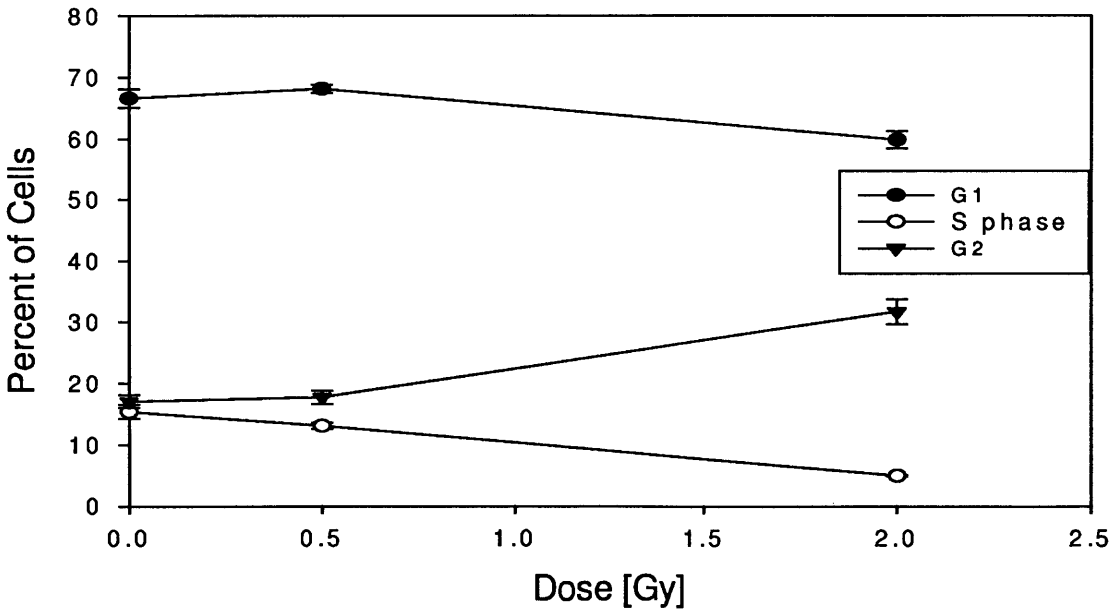

Figure 31: Cell cycle distribution in irradiated keratinocytes 48 h after iron irradiation [Source: [6]].

3.1.4 Low Fluence Studies

To determine whether a bystander response is present in cells under the more relevant low particle fluences found in the space radiation field, a set of experiments was conducted in which bystander cells were placed in co-culture with cells irradiated with low fluences of either protons or iron ions. The particle fluence, corresponding absorbed dose, and corresponding particle traversals per cell (calculated using the equations in Section 2.6) are shown in Table 4.

Table 4: Characteristics of low and high particle fluences investigated.

	Ions/cm^2	Ions/cell	Dose [Gy]
Protons	0	0	0
	2.00E+04	2.00E-01	8.00E-06
	2.00E+05	2.00E+00	8.00E-05
	2.00E+07	2.00E+02	8.00E-03
	2.50E+08	2.50E+03	1.00E-01
	5.00E+09	5.00E+04	2.00E+00
Iron Ions	0	0	0
	2.00E+03	2.00E-02	4.83E-04
	2.25E+04	2.25E-01	5.44E-03
	2.25E+05	2.25E+00	5.44E-02
	4.14E+05	4.14E+00	1.00E-01
	4.14E+06	4.14E+01	1.00E+00

Figure 32 shows the percentage of cells positive for 53BP1 foci formation in bystander cells corresponding to all three signaling combinations at 12 h after exposure to low fluences of protons. Data for the previously used higher doses of 0.1 and 2 Gy are also included for comparison. It can be seen that all three bystander cell populations exhibit a statistically significant increase in 53BP1 foci formation at a fluence of $2x10^7$ protons/cm^2 (~8 mGy), with bystander cells corresponding to the K→A and A→K signaling combinations also exhibiting a significant increase at the lower fluence of $2x10^5$ protons/cm^2 (~80 μGy). Slight increases are

also seen at the lowest fluence of $2x10^4$ protons/cm^2 investigated, but it should be noted that these data are the result of only a single experiment; therefore, the significance of this increase can not be determined. Of particular note is the result that, for all three bystander populations, the levels of 53BP1 foci are not statistically significantly different between the fluences of $2x10^5$ to $5x10^9$ protons/cm^2, indicating a plateauing of the bystander effect.

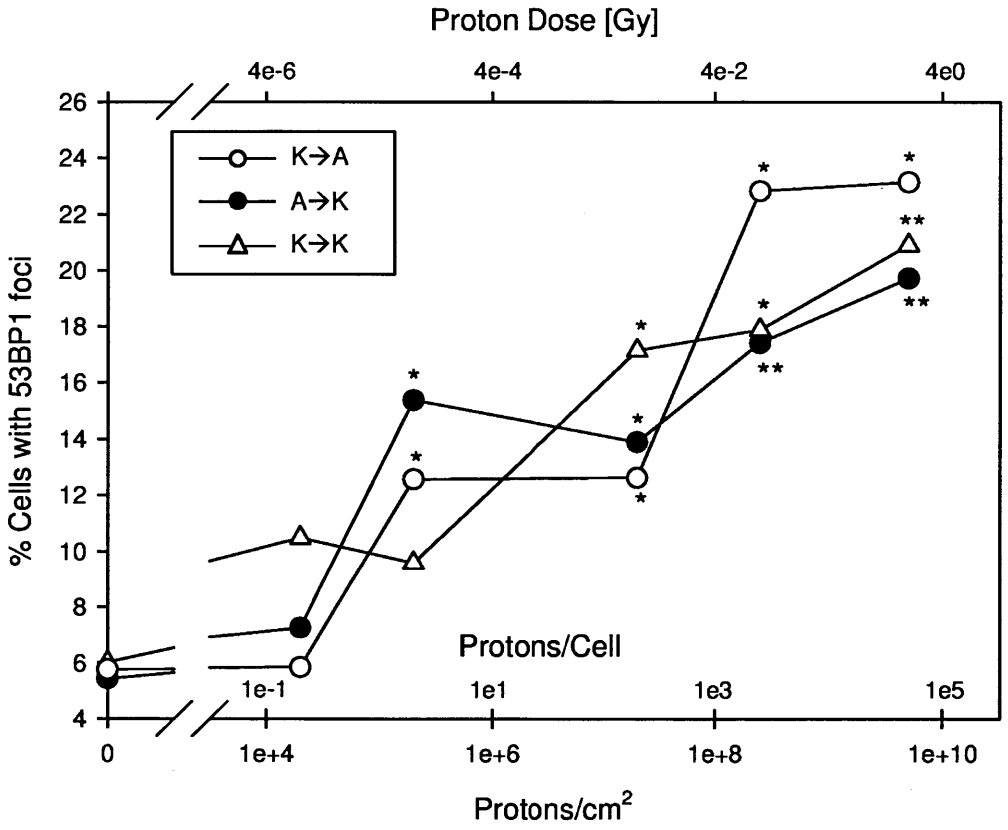

Figure 32: Dose responses for the induction of 53BP1 foci in bystander cells at 12 h for all three signaling combinations following irradiation with low fluences of protons. Data are the result of three independent experiments with the exception of the data point at 2e4 protons/cm^2, which is the result of one experiment (*, P < 0.05; **, P < 0.01 vs. unirradiated control). Error bars were omitted to improve clarity of the figure.

Figure 33 shows the percentage of bystander cells positive for 53BP1 foci at 24 h for all

three signaling combinations after exposures of irradiated cells to low fluences of iron ions. Data for the previously used higher doses of 0.1 and 1 Gy are also included for comparison. It can be seen that at the lowest fluences ($2x10^3$ and $2.25x10^4$ iron ions/cm^2), there is no statistically significant increase in the levels of 53BP1 foci formation in any of the three bystander cell populations investigated. Levels of foci formation are increased at the fluence of 2.25e5 ions/cm^2 (2.4-, 1.5-, and 2.1-fold increase in bystander cells in the A→K, K→K, and K→A signaling combinations, respectively), but the significance of this increase can not be determined as this was the result of a single experiment. As with the proton data, a plateauing of the bystander effect seems to occur starting at a dose of 0.1 Gy.

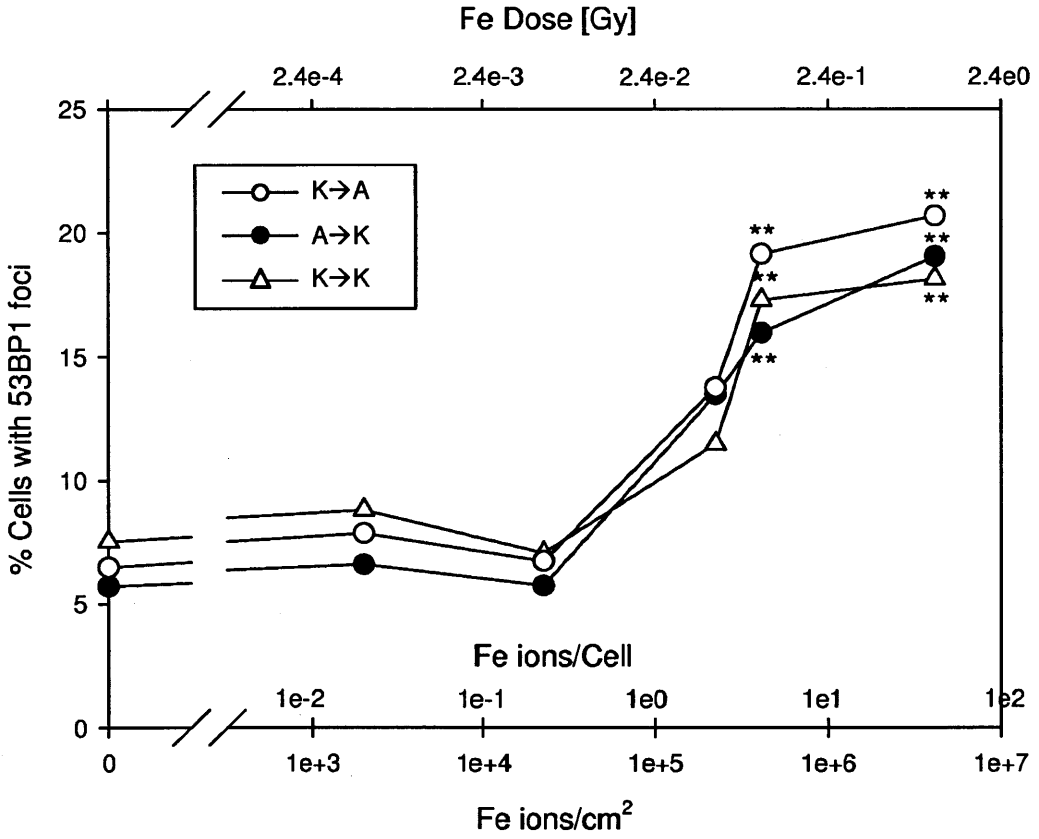

Figure 33: Dose responses for the induction of 53BP1 foci in bystander cells at 24 h for all three signaling combinations following irradiation with low fluences of iron ions. Data are the result of three independent experiments with the exception of the data point at 2.25e5 Fe ions/cm^2, which is the result of one experiment (, P < 0.01 vs. unirradiated control).**

3.1.5 Scavenger Effects

To investigate possible signaling molecules involved in eliciting the bystander effect, namely reactive oxygen and nitrogen species, scavenger experiments were conducted by introducing either catalase, superoxide dismutase, or PTIO into the medium containing cells in co-culture following the irradiation of one cell population with either 0.1 and 2 Gy of protons or 0.1 and 1 Gy of iron ions.

The modulation with scavengers of the bystander response in keratinocytes co-cultured with proton- and iron-irradiated AG01522 fibroblasts is shown in Figure 34. Similarly, the response modulations using the combination of bystander AG01522 fibroblasts in co-culture with irradiated keratinocytes and bystander keratinocytes in co-culture with irradiated keratinocytes are shown in Figure 35 and Figure 36, respectively. It was found that the addition of either SOD, catalase, or PTIO resulted in a significant reduction of the fraction of cells exhibiting 53BP1 foci compared to foci levels in the absence of scavengers in all signaling combinations and following both proton and iron ion irradiation, with only a few exceptions. Namely, when keratinocytes were co-cultured with irradiated keratinocytes, the levels of 53BP1 foci were reduced following the addition of SOD and catalase after proton irradiation at 2 Gy, but this decrease was not statistically significant. Similarly, PTIO reduced the levels of 53BP1 foci in the bystander keratinocytes following iron irradiation at 0.1 Gy, but this decrease was also not statistically significant.

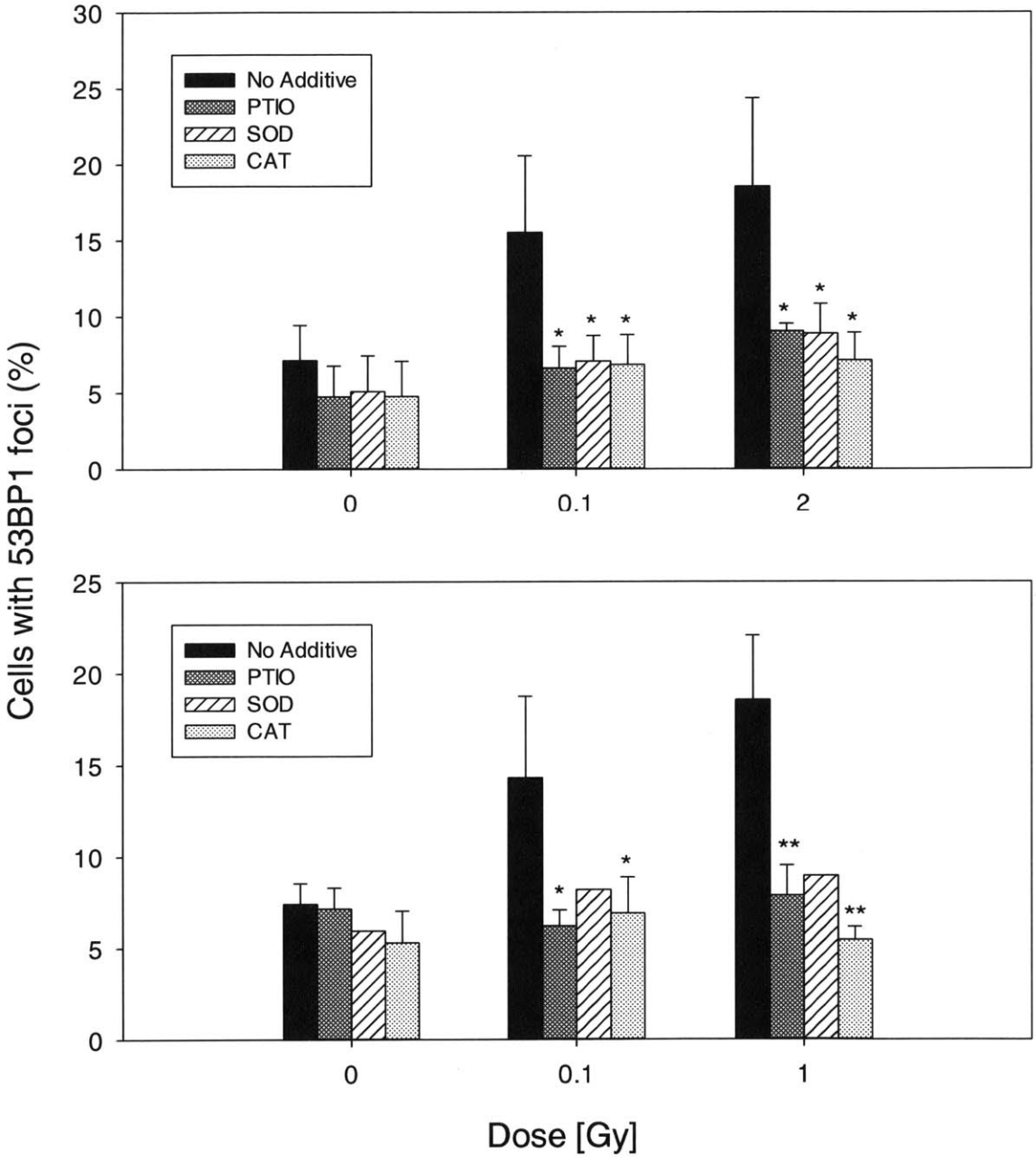

Figure 34: Dose responses for the induction of 53BP1 foci in bystander keratinocytes at either 12 h (proton; top) or 24 h (iron; bottom) after start of co-culture with irradiated AG01522 fibroblasts, following the addition of ROS/RNS scavengers to the medium (*, $P < 0.05$; **, $P < 0.01$ compared to foci formation in the corresponding bystander cells at the same dose in the absence of scavengers). It should be noted that the SOD data for iron irradiation are the result of only a single experiment; therefore, no error bars are shown.

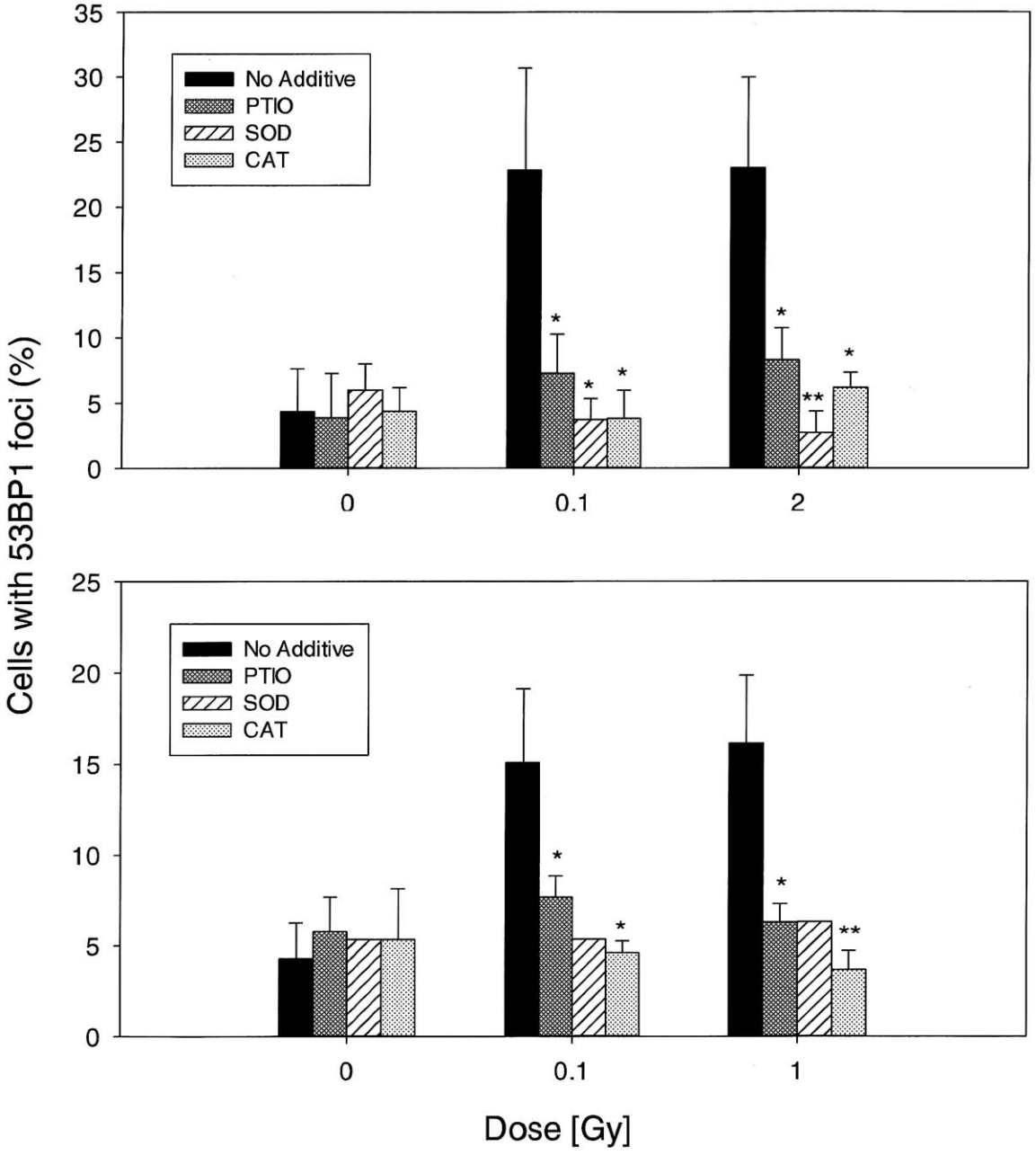

Figure 35: Dose responses for the induction of 53BP1 foci in bystander AG01522 fibroblasts at either 12 h (proton; top) or 24 h (iron; bottom) after start of co-culture with irradiated keratinocytes, following the addition of ROS/RNS scavengers to the medium (*, $P < 0.05$; **, $P < 0.01$ compared to foci formation in the corresponding bystander cells at the same dose in the absence of scavengers).

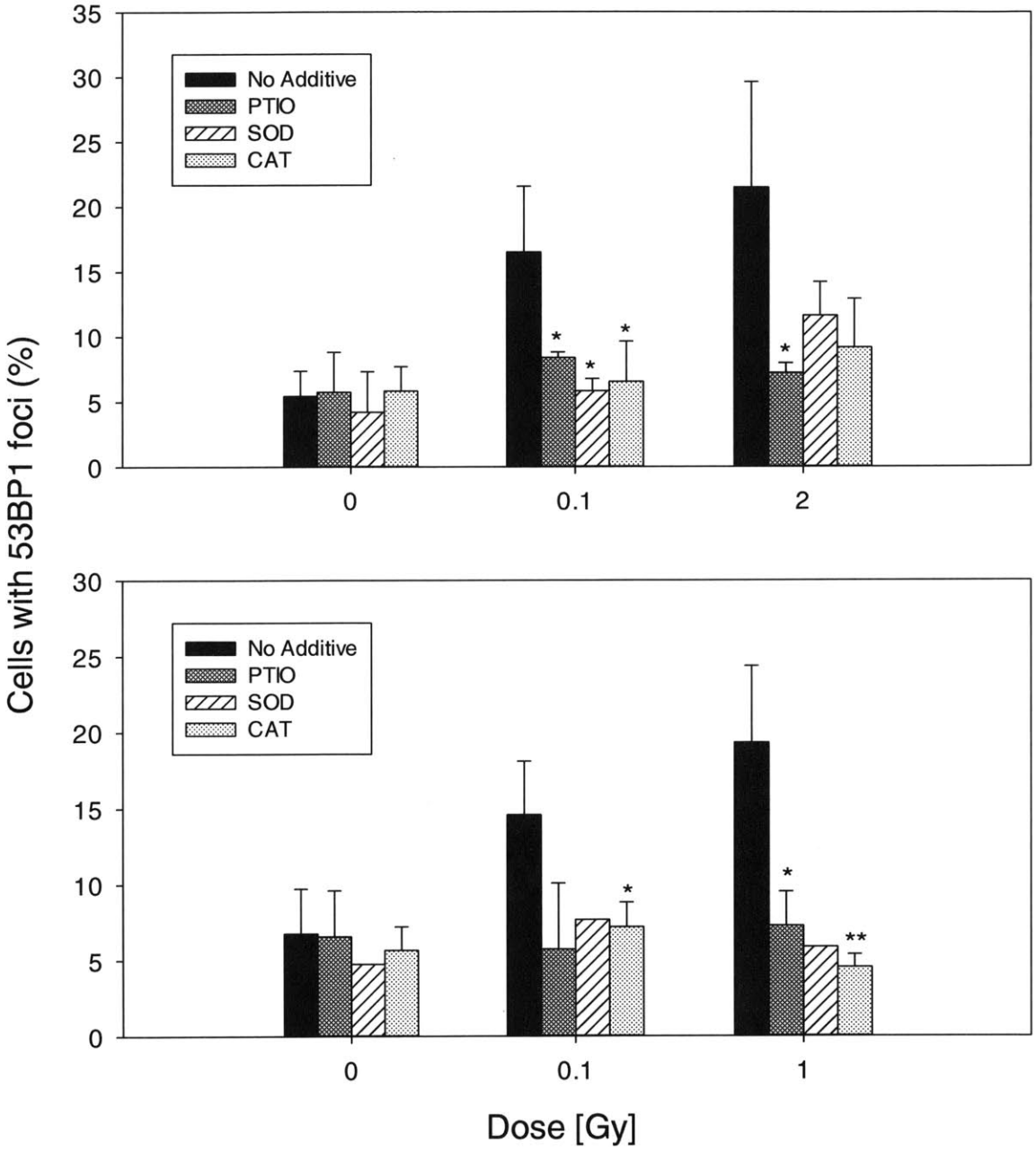

Figure 36: Dose responses for the induction of 53BP1 foci in bystander keratinocytes at either 12 h (proton; top) or 24 h (iron; bottom) after start of co-culture with irradiated keratinocytes, following the addition of ROS/RNS scavengers to the medium (*, $P < 0.05$; **, $P < 0.01$ compared to foci formation in the corresponding bystander cells at the same dose in the absence of scavengers).

3.2 Discussion

The experiments presented in this chapter demonstrate that both AG01522 fibroblasts and keratinocytes are capable of eliciting a medium-mediated bystander response in unirradiated populations of both fibroblasts and keratinocytes. However, the data indicate that the bystander response is modulated by LET, cell type, and endpoint studied. For example, evidence is presented that bystander fibroblasts and keratinocytes respond differently to the same signal emitted by irradiated keratinocytes and that LET-dependent differences exist in the response of bystander fibroblasts to signals emitted by irradiated keratinocytes. These differences are discussed in more detail in this section.

3.2.1 LET, Cell Type, and End Point Dependence

Although bystander responses of similar magnitudes were seen in most unirradiated populations of fibroblasts or keratinocytes in co-culture with either fibroblasts or keratinocytes irradiated by protons or iron ions, the work presented in this chapter demonstrates several LET-dependent differences in the responses. One of the differences found was the timing of the peak bystander response, which has been shown to vary based on end point. For example, some studies have shown the peak response for γH2AX foci induced in bystander cells to occur approximately 30 min after irradiation [70, 113], whereas many bystander end points peak several hours or days after irradiation [114-116]. Using the end point of 53BP1 foci formation, it was found that there was a delay in the bystander effect from a peak at 12 h following proton irradiation to a peak at 24 h following iron ion irradiation for all three cell signaling combinations. While the mechanism causing this delay in the bystander response is not clear, the cell cycle studies suggest that the release of the signaling molecule could be dependent on the

cell cycle phase of the irradiated cells. For example, a prolonged G2 arrest was found in keratinocytes following irradiation with low and high doses of iron ions (0.5 and 1 Gy), whereas only a short-lived G2 arrest was present in keratinocytes following irradiation with 2 Gy protons that resolved between 5 and 24 h.

Another example of LET dependence was seen using the endpoint of MN. A bystander effect was found in all signaling combinations following irradiation with either 0.1 or 2 Gy of protons, but no bystander effect was seen in bystander fibroblasts placed in co-culture with irradiated keratinocytes following irradiation with either 0.1 or 1 Gy of iron ions. For MN induction, the finding that the fibroblasts received and responded to a bystander signal from keratinocytes treated with protons but not iron ions might suggest that the irradiated keratinocytes are emitting a bystander signal(s) following proton and not iron ion exposure. However, this hypothesis is not consistent with the finding that bystander keratinocytes co-cultured with irradiated keratinocytes exhibited a bystander effect in the form of MN induction following either proton or iron ion irradiation. Thus, it would seem instead that keratinocytes are capable of eliciting a bystander signal following either proton or iron ion exposure but that either (i) different bystander cell types respond differently to the same signal or (ii) the irradiated keratinocytes send out different signals depending on LET quality and different bystander cell types respond differently to particular signals. Furthermore, the data also suggest that different signals are responsible for eliciting various end points in bystander cell populations. For example, a bystander response in all cell signaling combinations was seen using the end point of 53BP1 foci formation regardless of LET, whereas an increase in MN formation in bystander cells was present in all cell combinations following low-LET irradiation but only in two of the three combinations following high-LET irradiation.

Ultimately, these data portray a complex dependence of bystander effects on LET, cell type, and end point utilized. This set of studies is unique in that it is one of the few experiments conducted to date that investigates all of these factors within a single experimental system. Many experiments to date capture only a snapshot of the complex relationship between these experimental parameters, resulting in findings that are generally incohesive and seemingly paradoxical.

Experiments concerning the LET-dependence of the bystander effect that are most directly comparable to the results reported in this section are those of Yang et al., who used either 250 kVp X-rays (2 keV/μm) or 1 GeV/n iron ions (151 keV/μm) to irradiate AG01522 fibroblasts and then assessed bystander effects in a separate population of fibroblasts that was co-cultured in the same medium on an insert [45, 47]. The endpoints studied were survival fraction, MN induction, and γH2AX foci formation. Based on the finding that there were no differences in the bystander effect between the X-rays and iron ions, they concluded that the bystander effect was independent of LET in their experimental setup. In a similar co-culture experiment in which AG01522 fibroblasts were used as both the irradiated and bystander cell population, no difference in bystander MN formation was found regardless of whether cells were irradiated with 250 kVp X-rays or α-particles (LET: 128 keV/μm) [117].

However, an LET-dependence has been found in other studies such as that by Anzenberg et al., who investigated bystander signaling between human prostate carcinoma cells and AG01522 fibroblasts [98]. Specifically, DU-145 prostate carcinoma cells were irradiated with either X-rays or α-particles, and the cells were co-cultured with either unirradiated DU-145 or AG01522 cells. The three experimental end points studied were MN formation, γH2AX focus induction, and the surviving fraction. After 4 h co-culture with DU-145 cells that had been

irradiated with either X-rays or α-particles, there was an increase in MN formation in both tumor and fibroblast bystander cells. An increase in γH2AX focus induction and decrease in the surviving fraction were observed only in AG01522 cells when co-cultured with X-irradiated tumor cells. In contrast, α-particle irradiation of the DU-145 tumor cells caused neither a decrease in the surviving fraction nor an increase in the induction of γH2AX foci in either bystander cell line. These data indicate that not only are there LET-dependent differences in the signal released from the DU-145 cells but also that bystander AG01522 and DU-145 cells respond differently to the same medium-mediated signal, thereby highlighting the importance of investigating bystander signaling between different cell lines.

In a study investigating the long-term consequences of radiation-induced bystander effects, Buonanno et al. exposed normal human diploid skin fibroblasts (AG1522) to low or high doses of 1 GeV/n iron ions (LET ~ 151 keV/μm), 600 MeV/n silicon ions (LET ~ 51 keV/μm), or 1 GeV protons (LET ~ 0.2 keV/μm) [118]. A non-irradiated population of AG1522 cells was placed in co-culture with the irradiated cells for 5 h and was then harvested and allowed to grow for 20 generations. Their results showed that there was a reduced cloning efficiency and higher levels of chromosomal damage, protein oxidation, and lipid peroxidation in the bystander cells that were co-cultured with cells irradiated with either iron or silicon ions but not with protons. Therefore, this study demonstrated the long-term consequences of bystander effects and indicated a clear LET-dependence of the response.

3.2.2 Dose Dependence

In addition to investigating the LET, cell type, and end point dependence of the bystander effect in this thesis, dose dependence was also investigated. Using the three aforementioned cell signaling combinations and endpoints of MN induction and 53BP1 foci formation, the dose

dependence was investigated by irradiating cells with either 0.1 and 2 Gy of protons or 0.1 and 1 Gy of iron ions. A typical dose dependence for 53BP1 foci formation was found in the irradiated cells, whereby a significantly greater amount of foci was found following either 2 Gy of protons or 1 Gy of iron ions compared to the number of foci seen at 0.1 Gy of either protons or iron ions. This dose dependence was maximal at the first time point studied (1 h) and decreased non-linearly out to 72 h. Furthermore, dose was also found to be directly correlated with the degree of cell cycle arrest in irradiated cells. However, no significant dose dependence was found in any of the bystander cell populations under any experimental condition for the two doses studied (the exception to this is in the lower fluences studied).

Among the studies in the literature that have investigated the dose dependence of the bystander effect, most have reported that the magnitude of the induced effects has no simple relationship with dose. For example, in a study by Schettino et al., microbeam irradiations of a single cell with X-ray doses as low as 50 mGy showed that increasing doses resulted in an increased probability of a bystander effect being triggered, although the effects were of equal magnitude when they were induced [119]. Regarding α-particle irradiations, *in vitro* bystander effects have been observed after single particle traversals, which represent the lowest cellular dose for any particulate radiation [120]. Furthermore, several studies have shown that the magnitude of the induced bystander effect is similar when comparing single and multiple α-particle traversals to one or more cells [120-123]. In a different study by Tomita et al., no significant bystander effect was induced from X-ray microbeam irradiation of five cells within a population of normal human fibroblast WI-38 cells at a dose of 90 mGy per cell, although doses in the range of 0.25-1.5 Gy per cell induced bystander effects of similar magnitude [124]. Unfortunately, while a number of studies have demonstrated the plateauing effect of the

bystander response in several cell lines, the nature of this effect due to low fluences of heavy charged particles, such as those found in space, is not clear due to the dearth of studies conducted using these types of particles.

There are three primary explanations regarding the apparent saturation of the bystander response at low doses. (i) Saturation may exist due to a limit of how much signal can be produced by irradiated cells, whereby an increase in dose is not able to induce an increase in signal. For example, low-LET radiations that deposit a low amount of energy per track may show dose-dependent increases in bystander responses, but only up to a certain saturation level. In contrast, in the case where a single high-LET α-particle traversal deposits energy over the saturation level, variations in the number of α-particles used would cause the bystander response to seem dose-independent. Such saturation effects could be due to limitations in signal production capacity or to a more fundamental effect in which molecular sensors are capable of only an on-or-off state. (ii) Alternatively, the apparent saturation of the bystander effect could be due to a maximum signal level in bystander cells above which an increase in dose to the irradiated cells does not correspond to an increase in the bystander response, regardless of whether the degree of signal induction is proportional to dose. Thus, bystander cells may reach their full response at a certain signal level and be insensitive to increases in this level. Furthermore, the induction of different bystander end points may saturate at different thresholds. (iii) A third possible explanation for the saturation of the bystander effect could be that only a limited fraction of bystander cells can respond to signals from the irradiated cells. Thus, increases in the dose to the irradiated cell population would not correspond to an increased response in the bystander population. These hypotheses suggest that the dose dependence of the bystander signal can only be determined by elucidating the nature of bystander signals and the

mechanisms by which they are propagated.

3.2.3 Low Fluence Effects

Many bystander studies to date have utilized radiation doses that are much higher than those that would be received by astronauts on long-duration missions. The induction of chromosome damage and changes in gene expression in bystander cells following low fluences of high-LET α-particles at doses as low as 0.3 mGy was shown in the pioneering studies of the bystander effect by Little et al. [43]. Following the development of microbeams, which are capable of delivering a beam of radiation to regions of micrometer or submicrometer dimensions, it has been shown that the traversal of a single cell by a single charged particle can induce DNA damage in unirradiated cells [48]. To determine whether a bystander response is present in cells under the more relevant doses found in the space radiation field, a set of experiments was conducted in which bystander cells (either AG01522 fibroblasts or keratinocytes) were placed in co-culture with cells (either AG01522 fibroblasts or keratinocytes) irradiated within a low fluence range corresponding to doses below 0.1 Gy.

In the low fluence experiments in this study, the data suggest that the lowest doses (fluences) that induce statistically significant effects on all three populations of bystander cells are 8 mGy ($2x10^7$ protons/cm^2) of protons (although significant effects are also present in 2 of the 3 signaling combinations at a lower fluence of 2×10^5 protons/cm^2) or 0.1 Gy of iron ions, although these threshold doses were modulated slightly by cell signaling combination as discussed previously. With both ion species, the level of damage (expressed as 53BP1 foci formation) does not increase with increasing dose or fluence, thereby demonstrating the saturation or plateauing effect that is commonly seen in bystander studies (reviewed in [125]). Therefore, these data provide potentially important evidence that the magnitude of the bystander

response is independent of radiation type and dose above a certain threshold.

The low fluence experiment that is most comparable to the experiment in this thesis is that by Yang et al., who performed similar low-fluence irradiations with either protons or iron ions and investigated DNA damage in terms of both MN induction and 53BP1 foci formation [5]. The primary difference between their study and the study presented in this thesis is that they investigated bystander signaling in bystander AG01522 fibroblasts co-cultured with irradiated AG01522 fibroblasts. Interestingly, they found that the lowest doses (fluences) that induced statistically significant bystander effects in terms of 53BP1 foci induction were 0.44 mGy ($2x10^3$ iron ions/cm^2) of iron ions or 60 μGy ($2x10^5$ protons/cm^2) of protons. Thus, irradiation with iron ions induced bystander effects at a lower fluence than that identified in this thesis, whereas bystander effects were seen at the same proton fluence level of $2x10^5$ protons/cm^2 in both studies (with the exception of the K→K signaling combination investigated in this thesis). The difference in bystander induction due to iron ion irradiation described above suggests that the bystander effect at low fluences of iron ions is highly dependent on cell type, assay time, and/or cell culture medium, as these were the primary variables between the study by Yang et al. and this thesis work. Similar to this thesis work, however, they also demonstrated a plateauing of the bystander effect above a certain dose/fluence threshold.

3.2.4 Response Modulation by Scavengers

In an effort to elucidate potential signaling molecules responsible for eliciting the bystander responses described in this section, the scavenging molecules catalase, superoxide dismutase, and PTIO were introduced into the medium of the irradiated and bystander cell populations in co-culture immediately following irradiation. Catalase and superoxide dismutase scavenge the reactive oxygen species hydrogen peroxide and superoxide, respectively, while

PTIO scavenges the reactive nitrogen species nitric oxide. In the scavenger experiments presented in this section, it was found that the addition of either SOD, catalase, or PTIO reduced the fraction of cells exhibiting 53BP1 foci to background levels in all signaling combinations and following both proton and iron ion irradiation, with only a few exceptions. Overall, these results suggest that hydrogen peroxide, superoxide, and nitric oxide are all involved in medium-mediated bystander signaling irrespective of cell type, radiation quality, and dose.

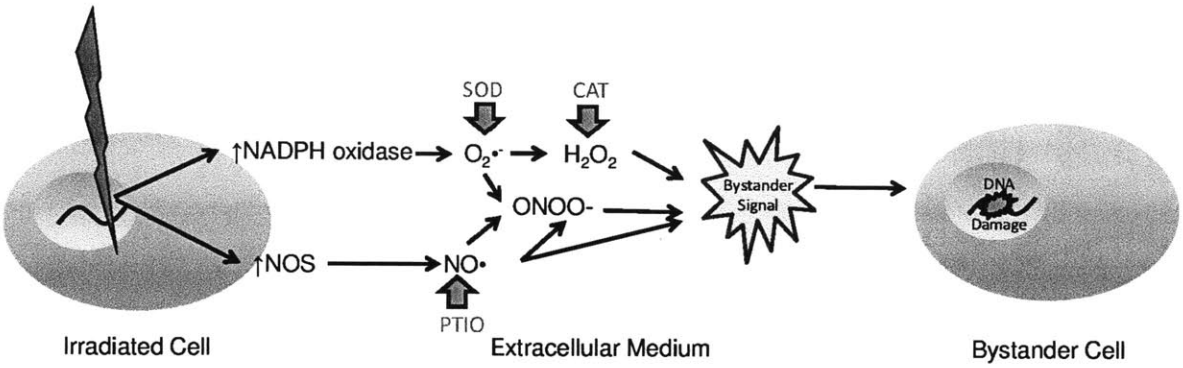

Figure 37: Depiction of our hypothesis for the role of ROS/RNS in bystander signaling. In red are the scavengers used in this study, with green arrows pointing to the targeted molecule to be scavenged.

According to our working hypothesis for the roles of ROS/RNS in bystander signaling depicted in Figure 37, the traversal of an ionizing radiation particle through a cell (either the nucleus or cytoplasm) activates NADPH oxidase in the membrane of that cell. NADPH oxidase then produces superoxide anion that is released into the medium and converted into H_2O_2. This molecule, either alone or in combination with other molecules, is then the bystander signaling agent that causes DNA damage in neighboring cells. In addition to the activation of NADPH oxidase, ionizing radiation simultaneously activates inducible nitric oxide synthase (iNOS) that produces nitric oxide (NO•). This is released into the medium and can either directly serve as a

bystander signaling molecule or react with superoxide to produce peroxynitrite ($ONOO^-$), which can then propagate the bystander signaling.

Reactive oxygen and nitrogen species have been implicated in a number of medium-mediated bystander responses using a variety of endpoints [45, 54, 70]. However, because nearly all reactive oxygen species have relatively short half-lives, it is likely that they are generated either very close to the target bystander cells or are produced through a continuous cascade of events [126]. For example, evidence exists that NADPH oxidase, a membrane-bound enzyme complex, is involved in the bystander response [56, 61]. NADPH oxidase can generate superoxide, which is a reactive free radical, through the transfer of electrons from NADPH inside the cell across the membrane and the coupling of these to molecular oxygen. The downstream products of superoxide include hydrogen peroxide, another reactive oxygen species. Additionally, these short-lived ROS are thought to be important in the secondary generation of longer-lived organic radicals that are known to cause mutations and transformation in human cells [127].

In addition to the role of reactive oxygen species in the induction of bystander effects, the role of reactive nitrogen species, particularly nitric oxide, has also been investigated using a variety of endpoints. For example, in bystander cells treated with the NO scavenger PTIO, the induction of γH2AX foci [128] and MN [48] was significantly reduced, suggesting the role of NO in mediating bystander effects.

CHAPTER 4

3D Experiments

4.1 Results

Results of the 3D experiments are presented in this section, including the assessment of DNA damage in bystander tissue constructs resulting from irradiations of neighboring constructs with a wide range of particle fluences/doses and two different particle types. The modulation of the bystander response seen in the constructs by ROS/RNS scavengers is also presented.

4.1.1 53BP1 Foci Formation

Similar to the 2D experiments, studies were conducted using the 3D skin tissue model to investigate the kinetics of DNA double strand break formation and repair and to determine if and when there is a bystander response in a 3D model following either proton or iron ion irradiation. The formation of 53BP1 foci was determined visually in irradiated and bystander tissue sections using a fluorescent antibody. In contrast to the 2D protocol for assessing 53BP1 foci formation, in which cells with 5 or more foci were considered positive, both bystander and irradiated cells were considered positive for foci formation in the constructs if they exhibited one or more foci due to the significant decrease in foci formation seen in the constructs. Figure 38 shows 53BP1 foci in AG01522 fibroblasts within the 3D tissue constructs in both control constructs and in constructs irradiated with 2 Gy protons, and Figure 39 shows 53BP1 foci induction in AG01522 fibroblasts within the control and bystander constructs at 12 h following proton irradiation.

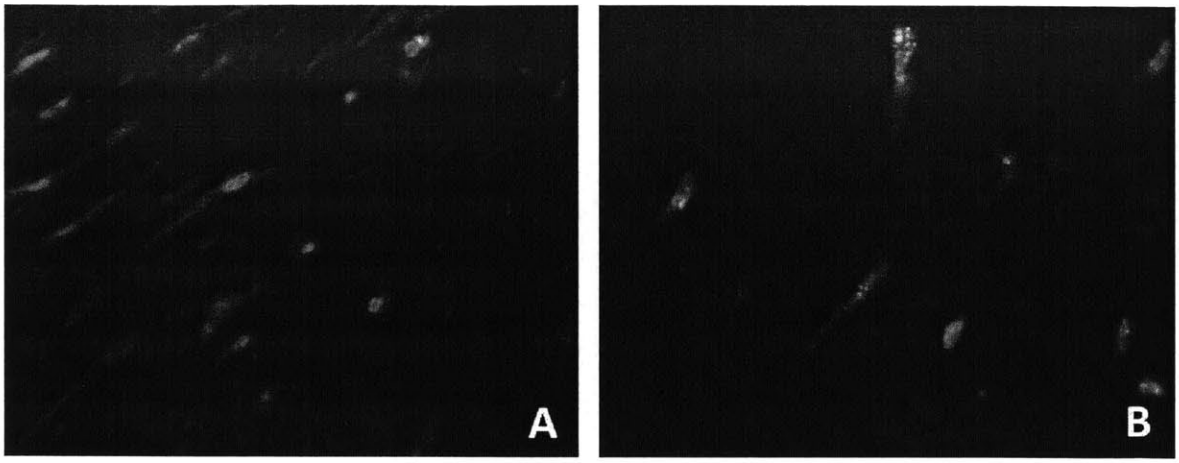

Figure 38: Immunofluorescence detection of 53BP1 foci in AG01522 fibroblasts within the 3D tissue constructs 1 h after proton irradiation: (A) unirradiated controls; (B) cells from constructs irradiated with 2 Gy of protons.

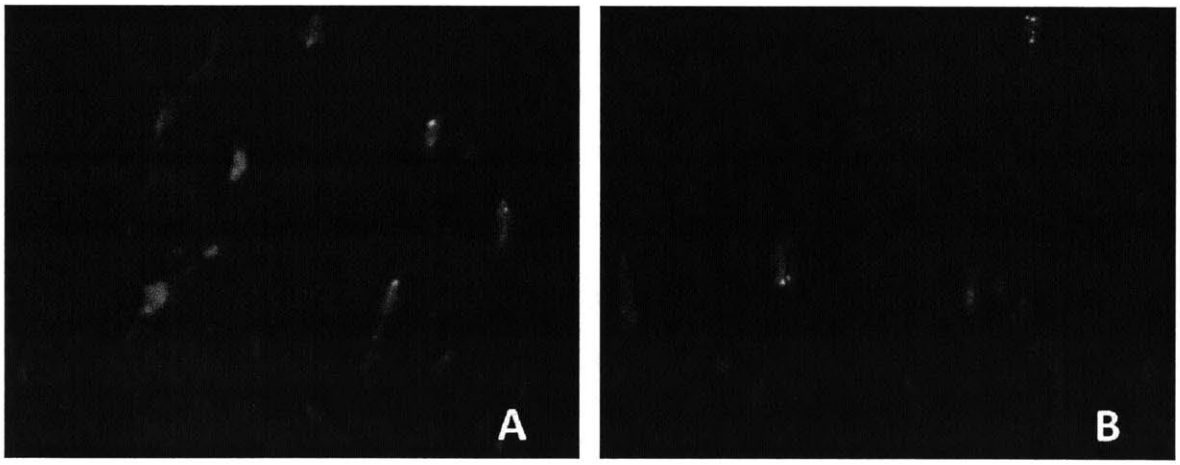

Figure 39: Immunofluorescence detection of 53BP1 foci in AG01522 fibroblasts within the bystander tissues 12 h after proton irradiation: (A) unirradiated controls; (B) bystander cells from constructs in proximity to those irradiated with 2 Gy of protons.

Experiments were carried out by irradiating constructs with either 0.1 and 1 Gy of iron ions or 0.1 and 2 Gy of protons and then placing them in co-culture with unirradiated bystander construct halves for 1, 5, 12, 24, 48, and 72 h. Both the keratinocytes and fibroblasts were assayed from the same constructs in both the irradiated and unirradiated halves. Figure 40 shows the magnitude of foci induction in fibroblasts irradiated with either protons or iron ions. It can be

seen that the kinetics of DNA double strand break repair in these cells are similar to those of cells in the 2D studies; namely, foci formation is greatest at the earliest time point (1 h) and gradually decreases in a non-linear fashion to background levels by either 12 or 48 h (following 2-Gy proton or 1-Gy iron ion irradiation, respectively). After a dose of 0.1 Gy, the fraction of cells with foci returned to control levels at 5 h following both proton and iron ion irradiation. Furthermore, the peak foci formation at 1 h is slightly greater following proton rather than iron ion irradiation (at 0.1 Gy), although this difference is not significant.

Figure 41 shows the magnitude of foci induction in keratinocytes irradiated with either protons or iron ions. It is interesting to note that the basal layer of keratinocytes (i.e., cells at the boundary between the dermal layer and the differentiated keratinocyte layers) showed efficient 53BP1 foci formation, whereas foci formation was virtually undetectable in keratinocyte layers above the basal layer; therefore, only keratinocytes in the basal cell layer were analyzed. Similar to the abovementioned fibroblast data, foci formation in the irradiated keratinocytes is greatest at the earliest time point (1 h) and gradually decreases to background levels by either 48 or 12 h (following 2-Gy proton or 1-Gy iron ion irradiation, respectively). After a dose of 0.1 Gy, the fraction of cells with foci returned to control levels by either 24 or 5 h (following proton or iron ion irradiation, respectively).

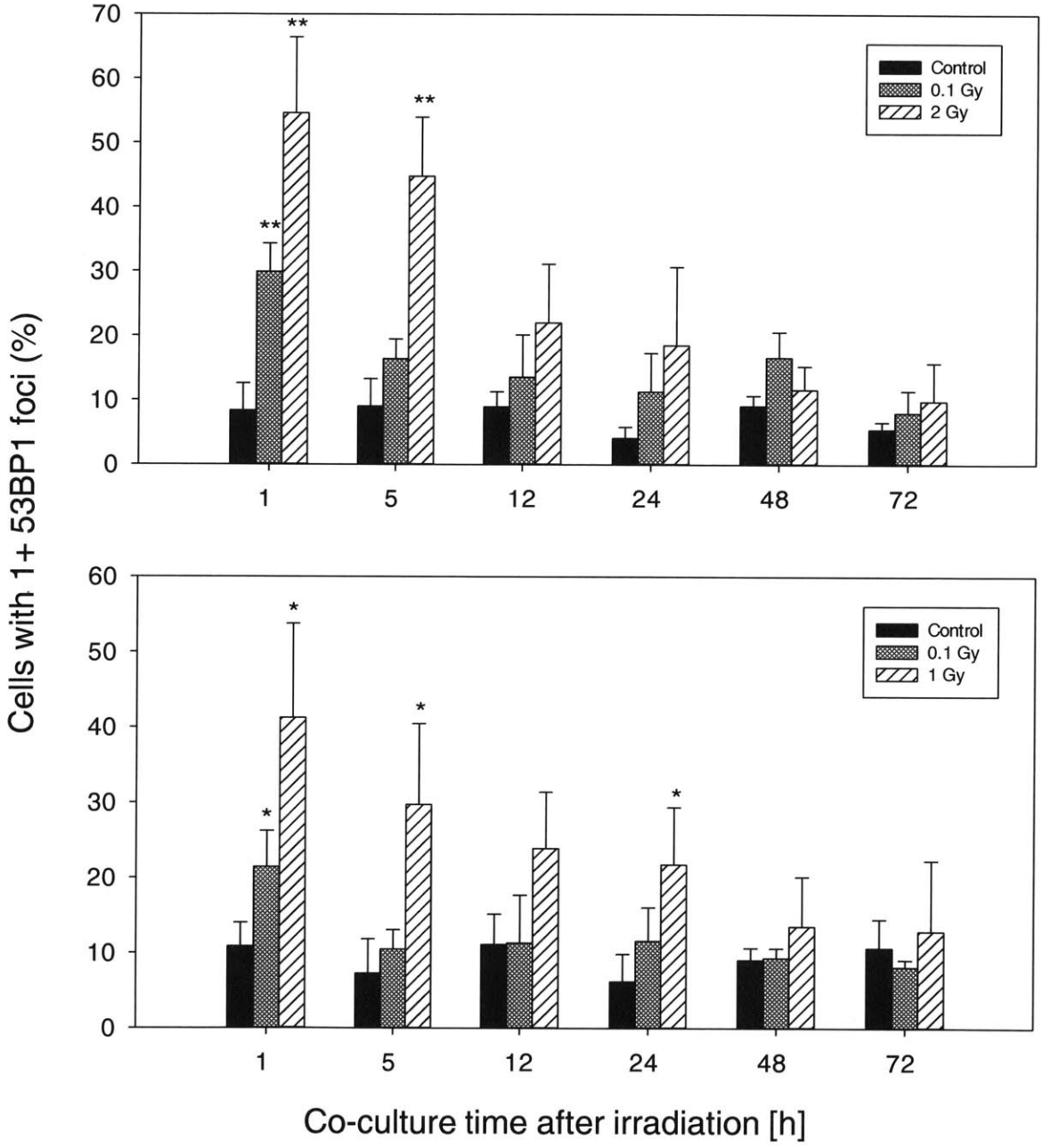

Figure 40: 53BP1 foci induction in proton (top)- and iron (bottom)-irradiated fibroblasts as a function of time that irradiated and unirradiated construct halves were in co-culture (*, $P < 0.05$; **, $P < 0.01$ vs. unirradiated control).

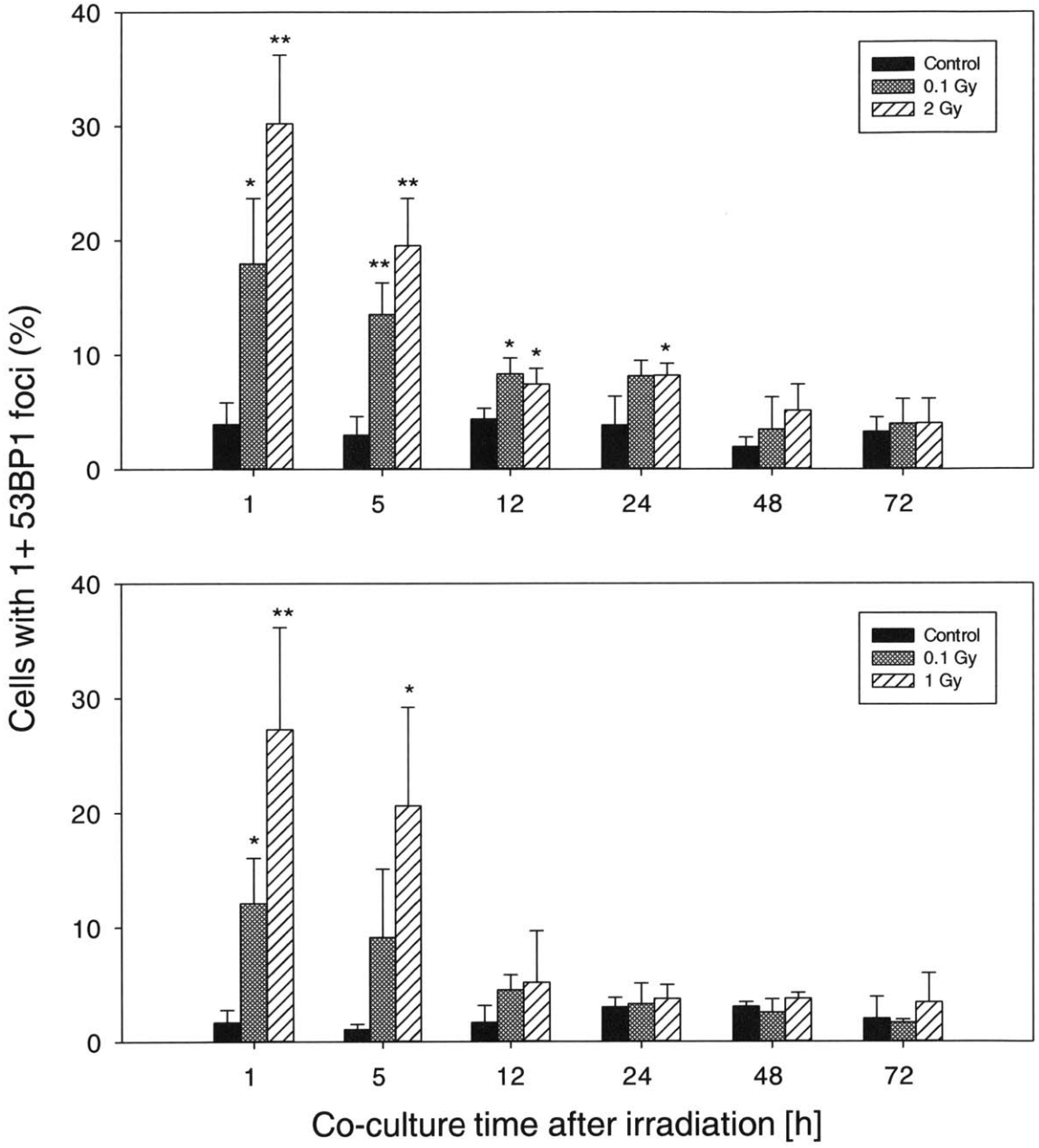

Figure 41: 53BP1 foci induction in proton (top)- and iron (bottom)-irradiated keratinocytes as a function of time that irradiated and unirradiated construct halves were in co-culture (*, $P < 0.05$; **, $P < 0.01$ vs. unirradiated control).

Foci formation in bystander fibroblasts and keratinocytes following either proton or iron ion irradiation is shown in Figure 42 and Figure 43. It can be seen in Figure 42 (top) that a

bystander response is present in fibroblasts within the constructs placed in co-culture with proton-irradiated constructs with a peak at 12 h, and the response is gone by 24 h; namely, a 1.9- and 2.6-fold increase in 53BP1 foci formation was present at doses of 0.1 and 2 Gy, respectively, at 12 h.

As shown in the lower panel of Figure 42, a bystander response is also present in fibroblasts within tissues placed in co-culture with iron-irradiated tissues when assayed between 24-48 h after irradiation. For example, at 24 h, there was a 3.6- and 2.5-fold increase in the number of cells positive for 53BP1 foci induction at doses of 0.1 and 1 Gy, respectively. Thus, for subsequent low fluence and scavenger experiments, co-culture times of 12 and 24 h were used for proton and iron irradiations, respectively.

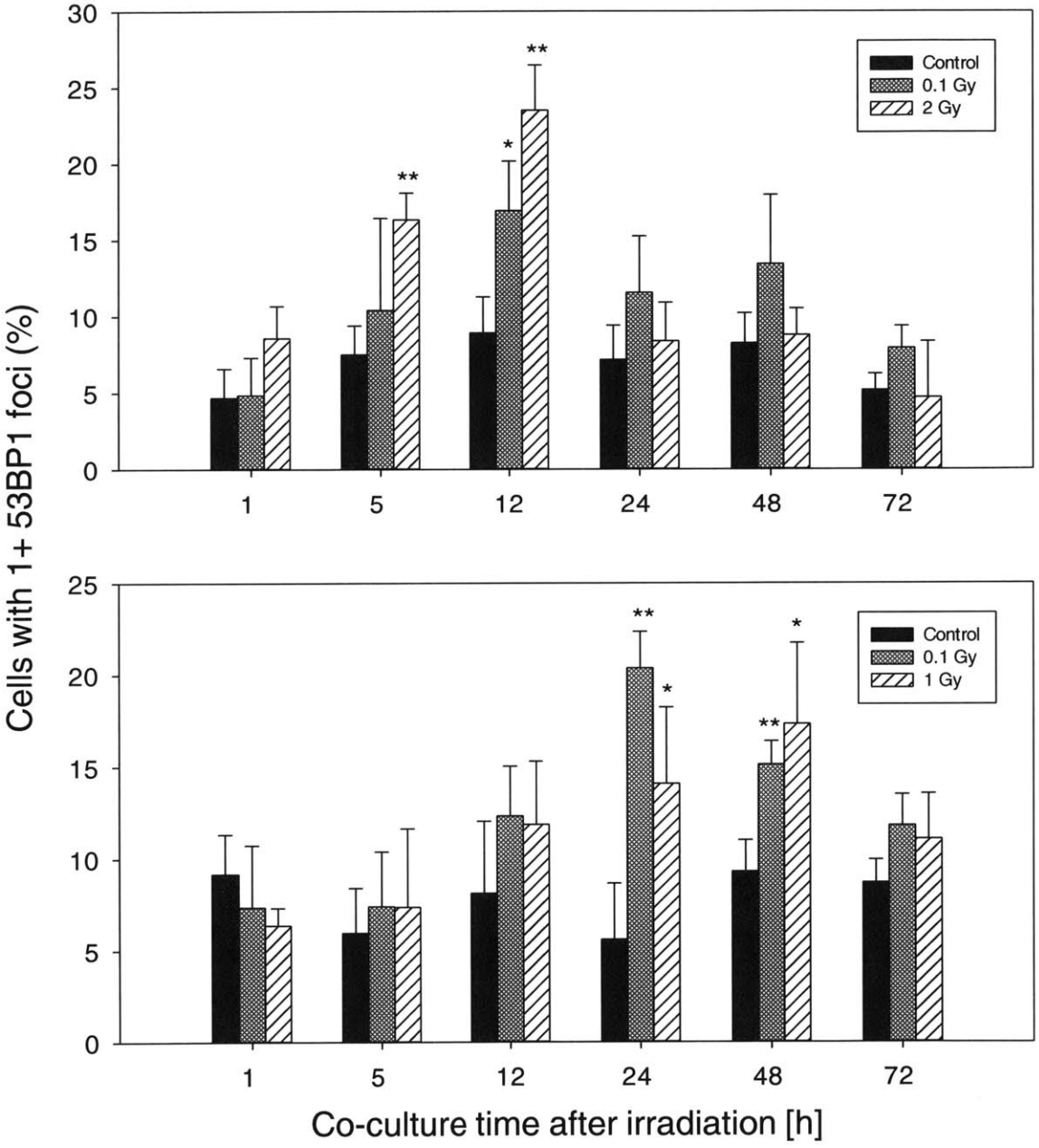

Figure 42: 53BP1 foci induction in bystander fibroblasts as a function of time that proton-irradiated (top) or iron-irradiated (bottom) and unirradiated construct halves were in co-culture (*, $P < 0.05$; **, $P < 0.01$ vs. unirradiated control).

Figure 43 (top) shows that a bystander response also exists in keratinocytes within tissues placed in co-culture with proton-irradiated tissues. Namely, a 2.7-fold increase in the number of keratinocytes positive for 53BP1 foci was found at doses of both 0.1 and 2 Gy after 12 h in co-culture. This response had disappeared by 24 h. In contrast, no bystander response was seen in keratinocytes within tissues placed in co-culture with iron-irradiated tissues (Figure 43, bottom) at any of the time points studied.

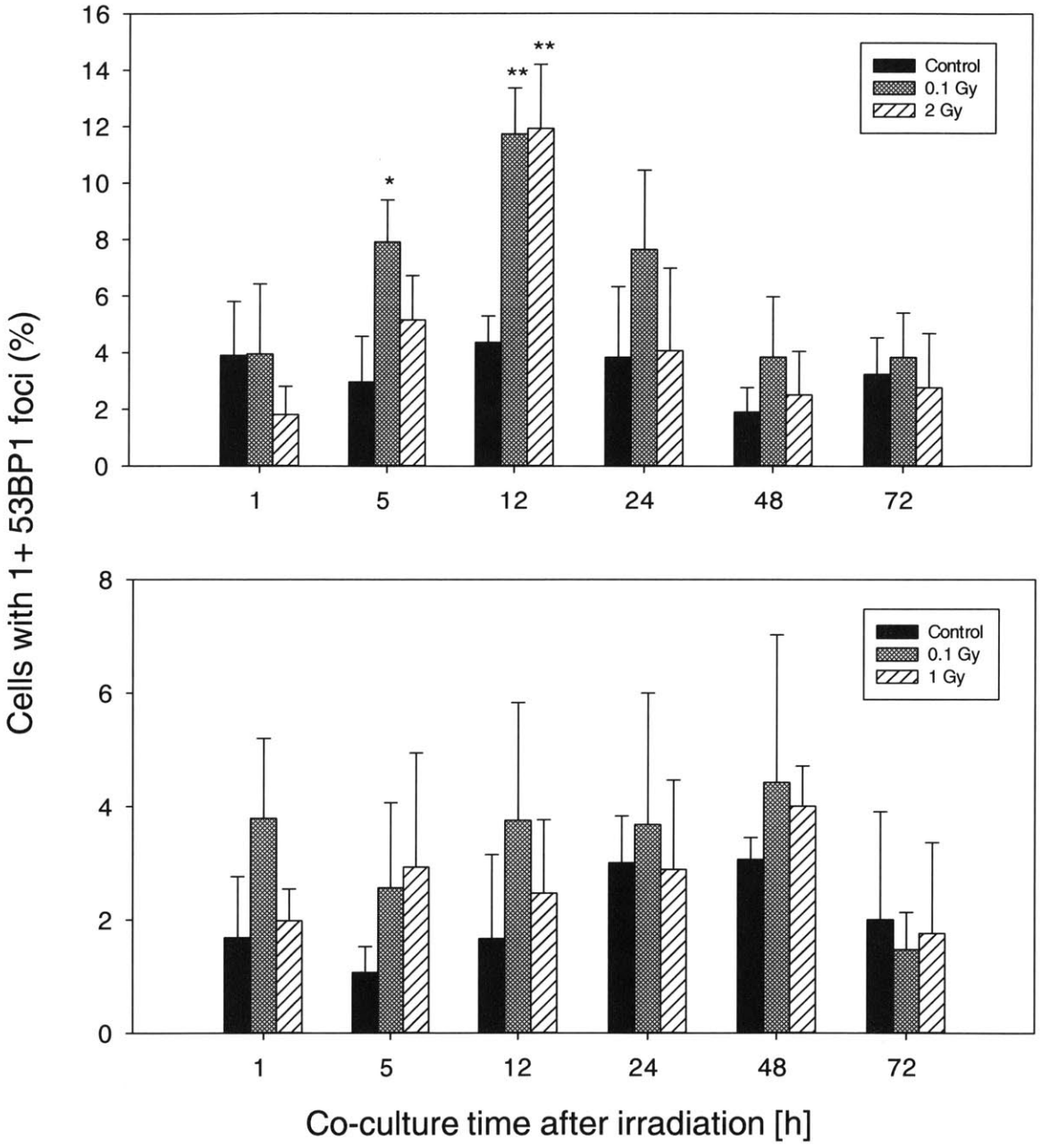

Figure 43: 53BP1 foci induction in bystander keratinocytes as a function of time that proton-irradiated (top) or iron-irradiated (bottom) and unirradiated construct halves were in co-culture (*, P<0.05; **, P < 0.01 vs. unirradiated control).

4.1.2 Low Fluence Analysis

To determine whether a bystander response is present in tissues under the more relevant doses found in the space radiation field, a set of experiments was conducted in which bystander tissues were placed in co-culture with tissues irradiated with low fluences of protons and iron ions.

The dose response for the induction of 53BP1 foci in AG01522 fibroblasts within the tissue constructs following proton irradiation is shown in Figure 44. In the irradiated population, the percentage of cells exhibiting foci is the same as control levels at fluences of $2x10^7$ protons/cm^2 (200 protons/cells or 8 mGy) and below. The level of foci induction then increases at fluences of $2.5x10^8$ protons/cm^2 ($2.5x10^3$ protons/cell or 0.1 Gy) and above. However, beginning at a fluence of $2x10^5$ protons/cm^2 (2 protons/cell or $8x10^{-5}$Gy), there is a significant increase in the percentage of cells exhibiting 53BP1 foci in the bystander population. This response plateaus out to a dose of 2 Gy ($5x10^4$ protons/cell or $5x10^9$ protons/cm^2).

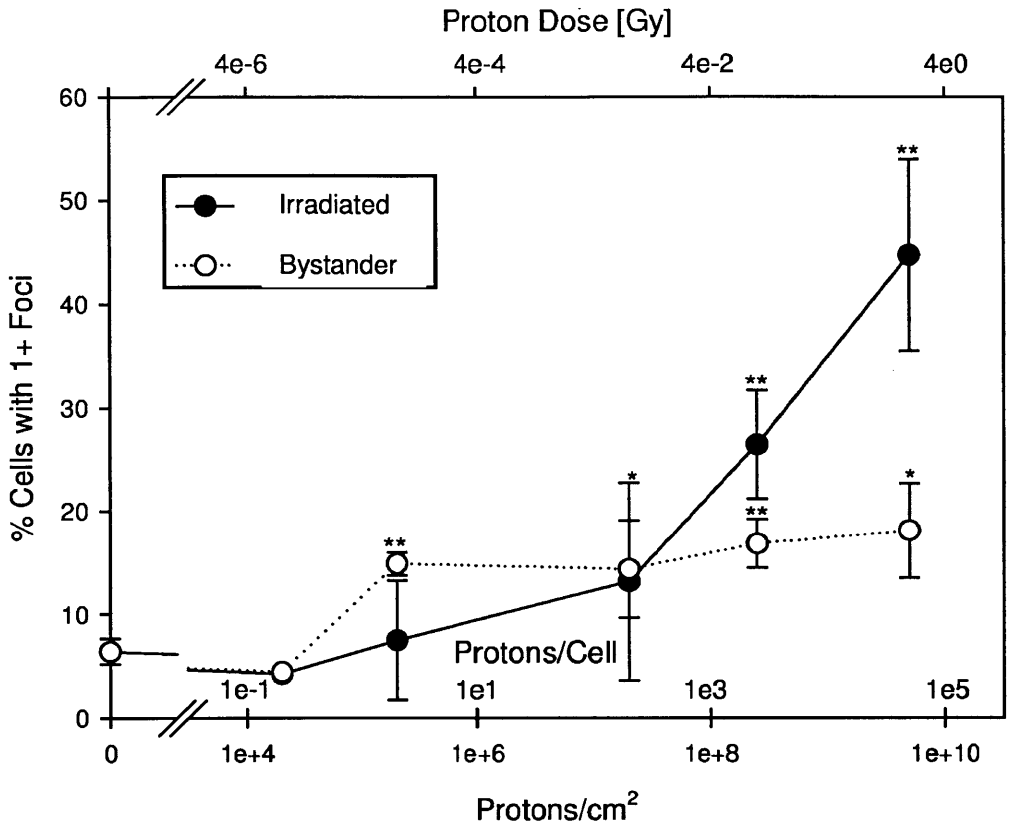

Figure 44: Dose responses for the induction of 53BP1 foci in AG01522 cells in constructs irradiated with low fluences of protons and in AG01522 cells in unirradiated construct halves (*, P < 0.05; **, P < 0.01 vs. unirradiated control).

In contrast, Figure 45 shows that at fluences of 2.25×10^5 Fe ions/cm^2 (2.25 Fe ions/cell or 0.054 Gy) or less, the fraction of cells positive for 53BP1 foci formation in the irradiated and bystander populations is the same as in the unirradiated control cells. However, significant increases in the percentage of cells positive for 53BP1 foci occurred in both irradiated and bystander populations at a fluence of 4.14×10^5 Fe ions/cm^2 (0.1 Gy or 4.14 Fe ions/cell) and above. Furthermore, the irradiated cell population showed an increase in foci induction with increasing dose above 0.1 Gy, whereas the induction of 53BP1 foci in the bystander population did not change with increasing dose above 0.1 Gy.

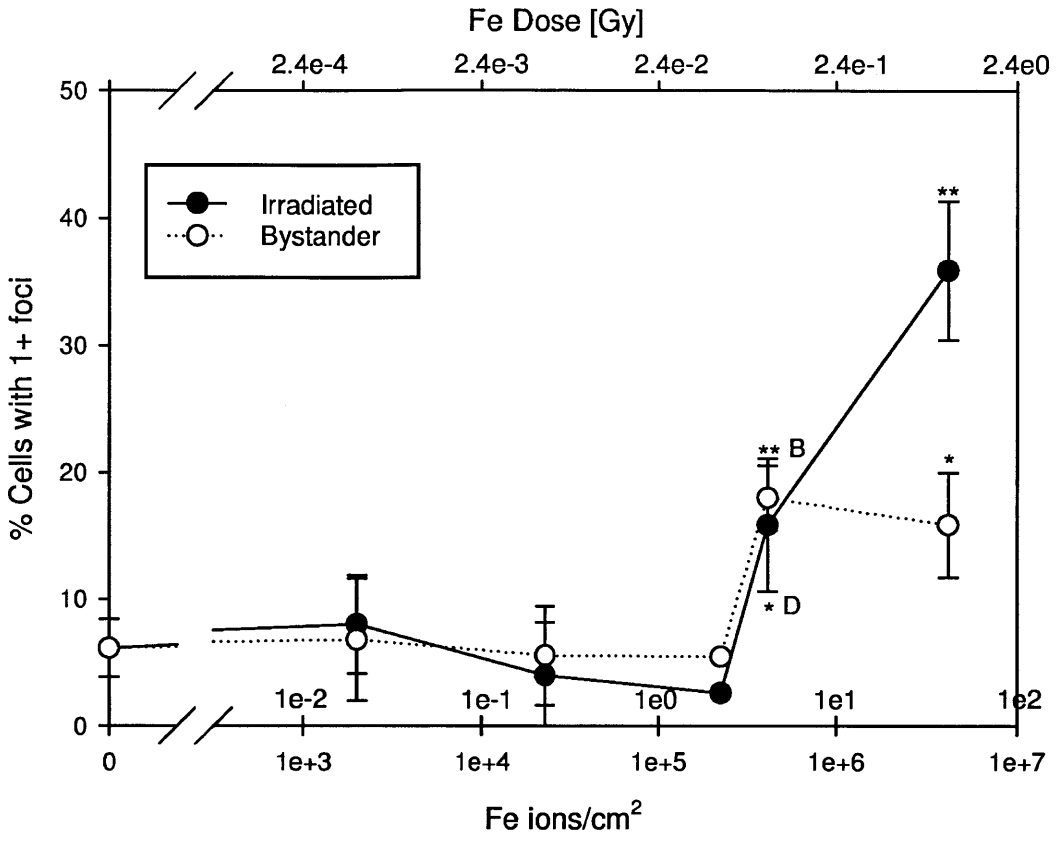

Figure 45: Dose responses for the induction of 53BP1 foci in AG01522 cells in constructs irradiated with low fluences of iron ions and in bystander AG01522 cells (*, P < 0.05; **, P < 0.01 vs. unirradiated control).

4.1.3 Modulation by Scavengers

Similar to the 2D scavenger experiments, the 3D scavenger experiments consisted of the introduction of either catalase, superoxide dismutase, or PTIO into the medium of constructs in co-culture following the irradiation of 1 piece with either 0.1 and 2 Gy of protons or 0.1 and 1 Gy of iron ions.

Figure 46 shows the response of AG01522 fibroblasts within constructs irradiated with

either 1 GeV protons or 1 GeV/n iron ions to the addition of scavengers to the medium. It can be seen that the scavengers do not cause any significant modulation of the percentage of cells exhibiting 53BP1 foci, suggesting that ROS/RNS are not significant contributors to the formation of DNA damage in irradiated cells within this system.

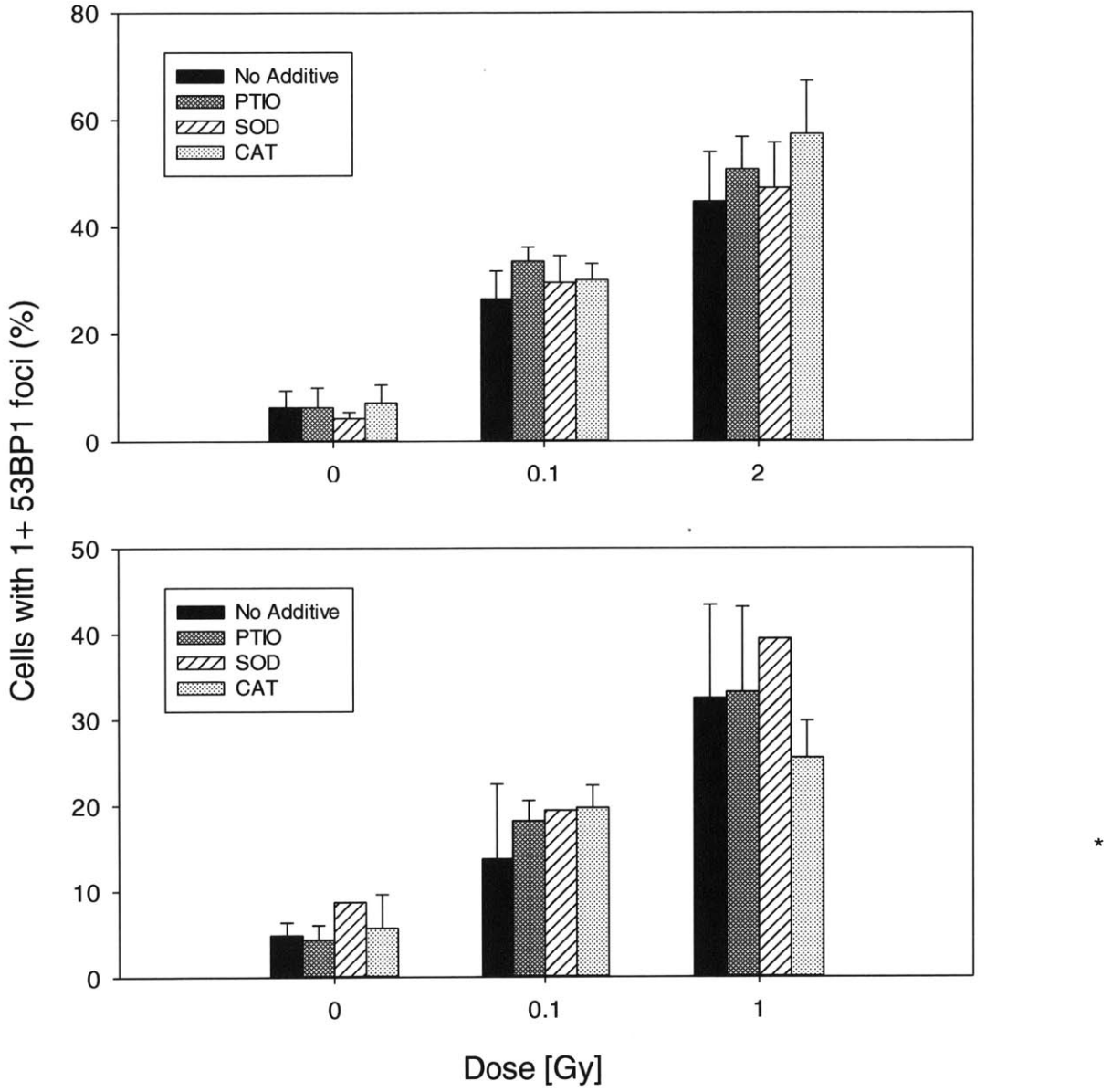

Figure 46: Dose responses for the induction of 53BP1 foci in AG01522 cells in constructs following the addition of ROS/RNS scavengers to the medium after irradiation with either 1 GeV protons (top) or 1 GeV/n iron ions (bottom). Data points are the averages ± SD obtained from 3 independent experiments with the exception of the iron SOD data, which are the result of 1 experiment.

Figure 47 shows the response of bystander AG01522 fibroblasts in co-culture with constructs irradiated with either 1 GeV protons or 1 GeV/n iron ions. Following proton irradiation, it can be seen that the addition of all three ROS/RNS scavengers resulted in a significant reduction of the bystander response ($P < 0.05$) compared to the corresponding response at the same dose (either 0.1 or 2 Gy) in the absence of scavengers, indicating the role of ROS/RNS in the induction of DNA damage in bystander cells.

Following iron irradiation, it can be seen that the addition of catalase resulted in a significant reduction of the bystander response ($P < 0.05$) compared to the corresponding response at the same dose (either 0.1 or 1 Gy) in the absence of scavengers. The addition of SOD into the medium also appears to have reduced the bystander effect, although the data are the result of a single experiment. However, although the percentage of bystander cells exhibiting 53BP1 foci following the addition of PTIO into the medium was reduced at doses of both 0.1 and 1 Gy, this effect was not significant.

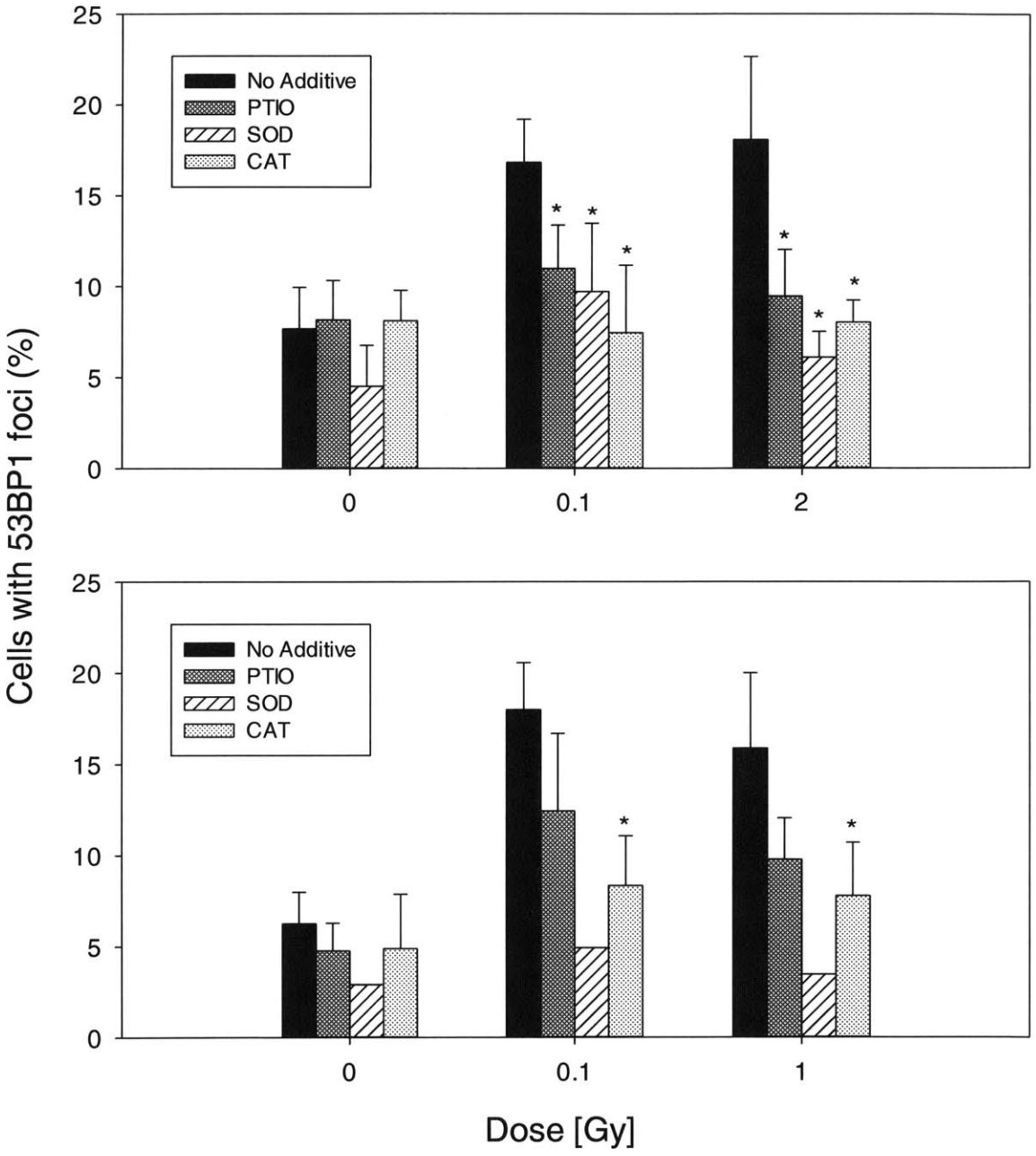

Figure 47: Dose responses for the induction of 53BP1 foci in AG01522 cells in bystander tissues following the addition of ROS/RNS scavengers to the medium after either 1 GeV proton (top) or 1 GeV/n iron irradiation (bottom) (*, $P < 0.05$ compared to foci formation in the corresponding bystander cells at the same dose in the absence of scavengers).

4.2 Discussion

The experiments in this chapter have demonstrated the occurrence of bystander effects in 3D skin tissue constructs in proximity to constructs irradiated with either 1 GeV/n protons or iron ions. Bystander effects were also demonstrated at low fluences of both protons and iron ions, and the effects were found to be modulated by the introduction of ROS/RNS scavengers into the medium of the tissues in co-culture following irradiation. Furthermore, direct evidence of LET-dependent differences was seen in both the kinetics of DNA damage formation and repair and in the magnitude of damage.

4.2.1 LET Dependence

The work presented in this chapter demonstrates several LET-dependent differences in the responses of unirradiated populations of fibroblasts and keratinocytes within the tissue constructs to the signals emitted by the cells within the constructs irradiated by either protons or iron ions. Using the endpoint of 53BP1 foci formation, it was found that there was a delay in the bystander effect from a peak at 12 h following proton irradiation to a peak at 24 h following iron ion irradiation in the fibroblasts within the bystander tissues. Interestingly, a similar peak at 12 h following proton irradiation was seen in the keratinocytes of the bystander tissue, but no bystander effect was detected in the keratinocytes following iron ion irradiation. This demonstrates that, regardless of the nature of the bystander signal(s) generated in this experimental system, there are obvious cell-dependent differences in the response of cells to the same signal(s). The fact that a bystander response was observed in the unirradiated keratinocytes following proton irradiation of the neighboring tissue demonstrates that the bystander signal(s) could be propagated over large distances to ultimately trigger a response in the keratinocytes. Therefore, it can be assumed that the lack of an observed bystander response in the keratinocytes

following iron ion irradiation of the neighboring tissue was not due to the failure of the signal to penetrate through the construct to the keratinocyte layer, but rather to the failure of the keratinocytes to respond to the generated signal. In this case, further experiments are warranted to determine if a bystander effect can be detected at perhaps different time points than those studied or using different endpoints.

The lack of an observed bystander response in the keratinocytes following iron ion irradiation is in agreement with results from Belyakov et al., who used a charged particle microbeam (delivering 7.2-MeV α-particles) to irradiate 400-800 cells in either the dermal or epidermal layer of a "full-thickness" skin model (EFT-300) corresponding to the dermis and epidermis of normal human skin [3]. At 72 h post-irradiation, apoptosis and MN induction were assessed in unirradiated cells in tissue sections parallel to the irradiated section. When the epidermal layer was irradiated, a clear bystander response in unirradiated keratinocytes was seen that extended out to a distance of 1.1 mm. However, when only the dermal region containing fibroblasts was irradiated, no bystander response was seen in the keratinocytes using either endpoint. This result provides further evidence that there is an LET-dependence of the bystander effect in keratinocytes within 3D skin constructs.

The finding that foci were only observed in the basal cell layer of keratinocytes might be explained by the finding that differentiated keratinocytes (above the basal cell layer) contain excessive amounts of keratin and that some of these cells may not be viable [129]. The finding by Suzuki et al. that differentiated two-dimensionally cultured normal human keratinocytes also showed a diminished response in terms of foci formation following X-ray irradiation provides further evidence that the reduced response may be related to differentiation [130]. Differentiation is known to be coupled with the termination of cell proliferation, which results in

the stimulation of heterochromatinization [131-133]. Due to the diminished DNA damage response in the heterochromatin regions [134-137], it is possible that differentiation-related chromatin structure hinders focus formation.

4.2.2 Low Fluence Effects

In the low fluence experiments described in this chapter, the data suggest that the lowest doses (fluences) that induce statistically significant effects in bystander cells within the tissue constructs are 80 μGy ($2x10^5$ protons/cm^2or 2 protons/cell) of protons or 0.1 Gy (4.14 Fe ions/cm^2 or 4.14 Fe ions/cell) of iron ions. With both ion species, the level of damage (expressed as 53BP1 foci formation) does not increase with increasing dose or fluence, thereby demonstrating the saturation or plateauing effect that is commonly seen in bystander studies (reviewed in [125]), including the 2D study presented in Chapter 3. Therefore, these data provide potentially important evidence that the magnitude of the bystander response is independent of radiation type and dose beyond a certain threshold that is dependent on radiation quality. Future studies should probe these low fluence bystander effects in more depth by, for example, expanding the number of time points used to assess DNA damage in the bystander cells to determine whether the kinetics of damage as assessed by 53BP1 foci formation are altered at low fluences.

4.2.3 Modulation by Scavengers

In an effort to elucidate potential signaling molecules responsible for eliciting the bystander responses described in this section, the scavenging molecules catalase, superoxide

dismutase, and PTIO were introduced into the medium of the irradiated and bystander tissue constructs in co-culture immediately following irradiation. Catalase and superoxide dismutase scavenge the reactive oxygen species hydrogen peroxide and superoxide, respectively, while PTIO scavenges the reactive nitrogen species nitric oxide. Although it was found that these ROS/RNS scavengers reduced the fraction of cells exhibiting 53BP1 foci to background levels in the 2D model described in Chapter 3, it was expected that their effect would be attenuated in the 3D model due to the more complex extracellular environment of the tissue constructs. However, it was found in the scavenger experiments presented in this section that the addition of either SOD, catalase, or PTIO was successful in reducing the fraction of cells exhibiting 53BP1 foci to background levels following both proton and iron ion irradiation, with only a few exceptions. Overall, these data suggest that hydrogen peroxide, superoxide, and nitric oxide are all involved in medium-mediated bystander signaling irrespective of radiation quality, dose, or tissue architecture. For a more detailed explanation of proposed signaling pathways involved in the propagation of the bystander effect by the ROS/RNS species investigated in this thesis, see Section 3.2.4.

CHAPTER 5

Comparison of 2D and 3D Bystander Responses

Studies directly comparing bystander responses between 2D and 3D cellular systems are lacking in the literature but are important in determining the relevance of the numerous 2D bystander studies in existence to *in vivo* cancer risk estimation. This chapter presents data from both the 2D and 3D irradiated and bystander cells using the same y-axis scale to allow a direct comparison of DNA damage between the experimental systems in terms of the induction of 53BP1 foci. It should be noted that all of the data from this chapter were presented in the previous two chapters, albeit in a different format and in some cases using different y-axis scales to allow better visualization of the data.

5.1 Results

The percentages of fibroblasts in the 2D and 3D models exhibiting 53BP1 foci following irradiation with 2 Gy of protons are shown in Figure 48. It can be seen that a significantly greater amount of DNA damage occurs in fibroblasts within a 2D vs. 3D tissue architecture. For example, at 1 h following irradiation, there was a 3.7-fold decrease in the percentage of fibroblasts exhibiting foci in the 3D constructs compared to 2D cell monolayers. This decrease existed throughout the entire time course investigated, namely from 1 to 72 h.

The corresponding comparison of DNA damage in 2D and 3D bystander fibroblasts in co-culture with cells or tissues irradiated with 2 Gy of protons is shown in Figure 49. At 1 h in co-culture, there is a 20-fold decrease in the average number of foci per cell in the 3D compared to 2D fibroblasts. (It should be noted here that the y-axis of this figure was changed from the

percentage of cells exhibiting foci to the average number of foci per cell due to the significant decrease in the magnitude of foci-positive cells, which could not be seen clearly when the magnitude was expressed in terms of a percentage). As discussed previously, the bystander response peaked for cells in both architectures at a co-culture time of 12 h, with the 3D fibroblasts exhibiting a 15-fold decrease in the average number of foci per cell compared to 2D fibroblasts. From 24-72 h in co-culture, the magnitude of cell damage dropped in both cell populations back to control levels. Thus, the kinetics of DNA damage appearance and removal, in terms of 53BP1 foci, are similar in bystander cells in both 2D and 3D experimental systems, but the magnitude of damage is dramatically decreased in the 3D system. This trend was also present following iron ion irradiation in that both the 2D and 3D cell populations exhibited a peak in the bystander effect at 24 h but the magnitude of damage was significantly decreased in the 3D system.

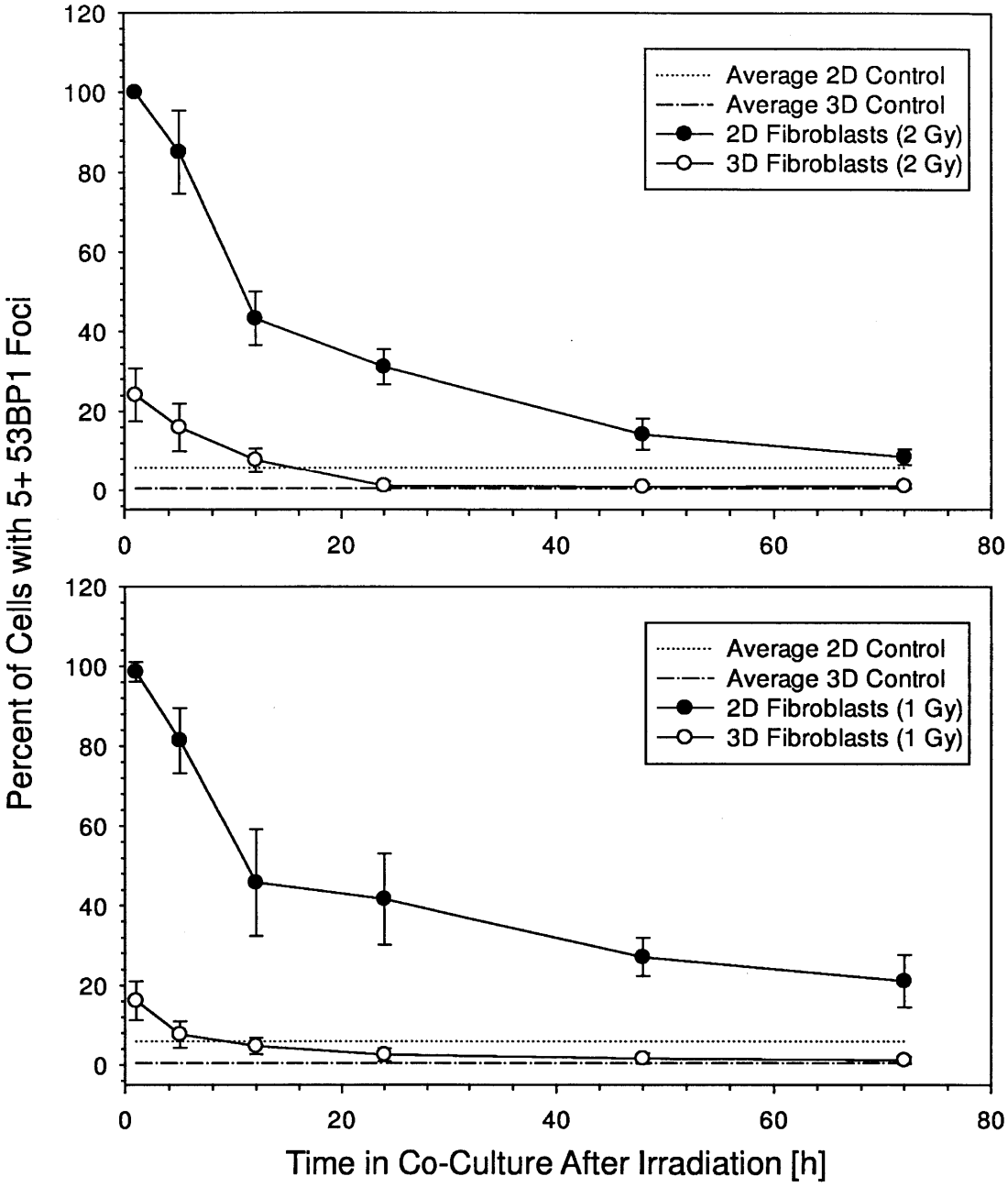

Figure 48: Comparison of DNA damage (in terms of the percentage of cells expressing 53BP1 foci) in irradiated fibroblasts in 2D and 3D following 2 Gy of protons (top) or 1 Gy of iron ions (bottom).

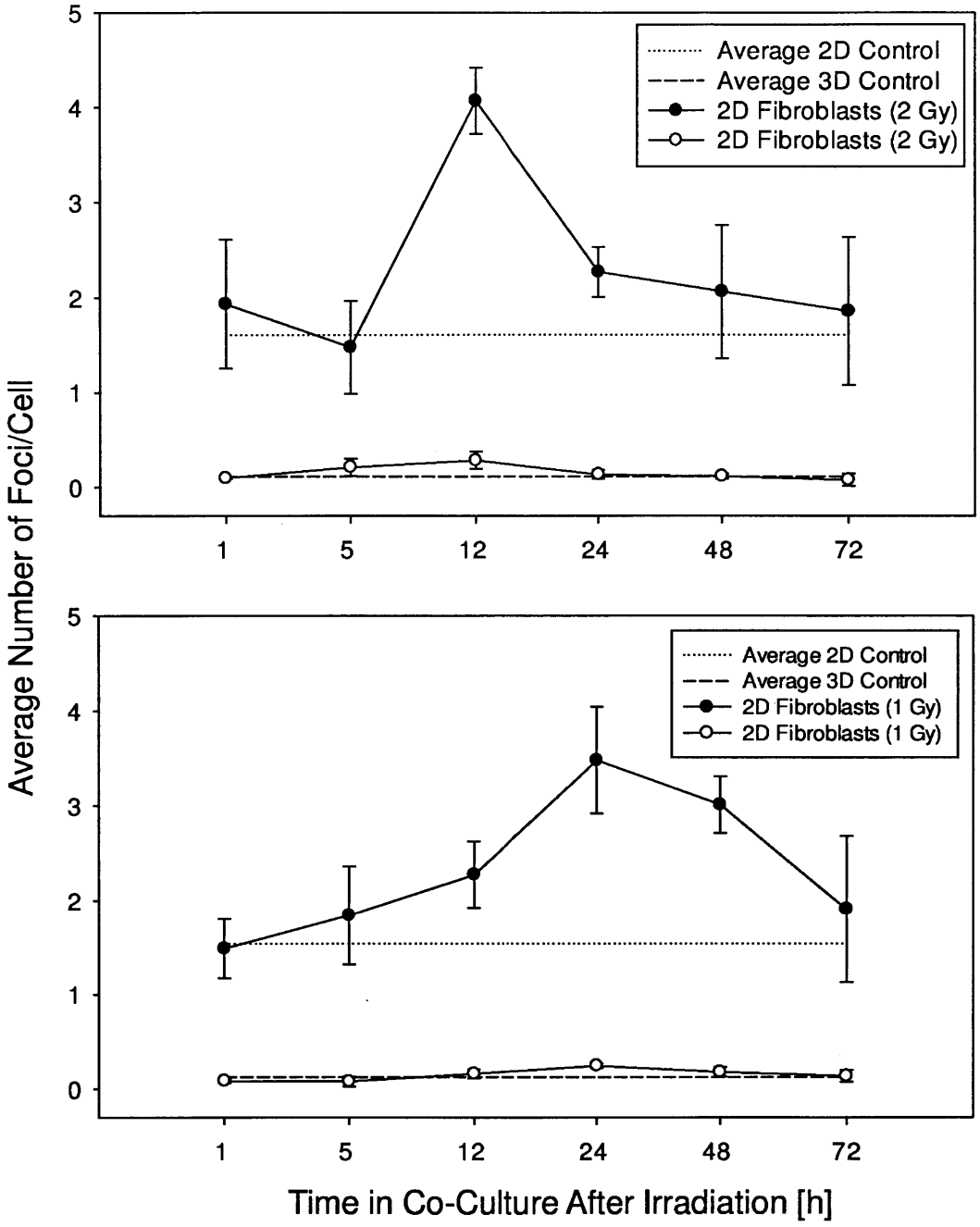

Figure 49: Comparison of DNA damage (in terms of the average number of 53BP1 foci per cell) in bystander fibroblasts in 2D and 3D in co-culture with cells or constructs irradiated with either 2 Gy of protons (top) or 1 Gy of iron ions (bottom).

5.2 Discussion

Knowledge of DNA damage responses in cells arranged within a 3D tissue architecture is extremely limited, and to our knowledge, there have been no studies to date that have compared bystander responses between 2D and 3D experimental systems. Such studies are critical to enabling accurate predictions of radiation-induced health risks in humans. In this chapter, radiation responses were compared for AG01522 fibroblasts cultured in 2D monolayers and those cultured in 3D skin constructs in terms of the formation and dissolution of 53BP1 foci over a time course of 1 to 72 h following irradiation.

Perhaps the most significant finding from this work is that the fraction of cells showing foci in unirradiated, irradiated, and bystander populations is reduced in 3D compared to 2D skin model systems. For example, a four-fold increase in the percentage of fibroblasts with foci in the 2D vs. 3D system was found following 2-Gy proton irradiation in the irradiated cells/tissues. This difference was even greater in the bystander cell populations, where a decrease of between 10- and 20-fold was found in bystander cells within the 3D constructs compared to those cultured as 2D cell monolayers. This decrease in the magnitude of radiation-induced damage in 3D compared to 2D tissues is in accordance with some other studies that have also found cells in 3D systems to be more resistant to DNA damage than cells in 2D systems. For example, studies on spheroids have shown that such cell clusters are generally more resistant to damage from ionizing radiation than cell monolayers [138], and a study by Su et al. demonstrated that EpiDerm tissue constructs displayed fewer 53BP1 and ATM foci than observed for 2D human fibroblasts following irradiation with different doses of γ-rays (0.1-5 Gy) [129].

Several potential mechanisms for this possible protective effect afforded by the 3D microenvironment have been suggested, including cell shape-mediated changes in (repair-

related) gene expression and alterations in chromatin packaging, which influence DNA repair. Cells in a 3D environment exhibit a round morphology resulting from interactions between cell-extracellular matrix-mediating focal adhesions and the actin cytoskeleton [139]. Through physical forces between the actin cytoskeleton, nuclear matrix, and cell membrane, cell morphology is thought to contribute to gene expression and chromatin reorganization. For example, Storch et al. showed that 3D A549, UTSCC15, and HP1α-EGFP cell cultures exhibited diminished levels of histone H3 acetylation and induced HP1α expression compared to the same cells grown in 2D cell monolayers [140]. These results indicate that cells grown in 3D contain a greater amount of heterochromatin than euchromatin compared to cells grown in 2D culture. Furthermore, they showed that both A549 and UTSCC15 cells exhibited significantly less damage under 3D compared to 2D conditions based on a diminished number of γH2AX/p53BP1-positive foci at 24 hours after irradiation with 2 to 6 Gy of 200-kV X-rays, as well as on a significant decrease in the number of chromosomal fragments in 3D compared to 2D cell clusters [140]. Thus, they showed that the increased radiation survival of cells grown in 3D compared to 2D results from a larger amount of heterochromatin, a lower number of lethal chromosome aberrations, and a differential dissemination of euchromatin to heterochromatin-associated DSBs. It has also been proposed by Cowell et al. that the apparent differences in radiosensitivity between cells grown in 2D compared to 3D could be due to differences in the free radical scavenging capacity between chromatin compartments [141]. For example, Warters and Lyons showed that the decondensation of chromatin in isolated nuclei following hypotonic treatment resulted in a 4.5-fold increase in the sensitivity of DNA to DSB induction as estimated by gel electrophoresis [142]. This result was likely due to the reduced protection of DNA from radical damage in decondensed chromatin associated with a decrease in the local concentration of

histones and other proteins and molecules that scavenge free radicals.

In contrast to the present work and the aforementioned studies that have provided evidence of cells in 3D systems being more resistant to radiation-induced DNA damage than cells in 2D monolayers, other studies do not corroborate these findings. For example, in a study by Lin et al. that compared radiation effects in human MCF10A mammary epithelial cells cultured as 2D monolayers or 3D structures in Matrigel, no significant differences in levels of reproductive cell death, chromosomal aberrations, and γ-H2AX foci were found following γ irradiation [143]. Alternatively, a study by Roig et al. found that HZE-particle-induced damage persisted longer in 3D organotypic cultures compared to 2D cultures in a colon epithelial cell model [144]. Therefore, these results highlight not only the importance of tissue architecture when evaluating responses to DNA damage, but also the importance of investigating these responses in different tissue and cellular systems. Further studies are needed to elucidate the mechanisms that cause differential responses of cells in 2D and 3D systems to ionizing radiation.

CHAPTER 6

Conclusions

6.1 Summary

Since the initial experiments demonstrating bystander effects, substantial progress has been made to understand and characterize these effects. Numerous laboratories have launched investigations into this phenomenon using a variety of cell types, radiation qualities, doses, and endpoints. However, despite the vast array of effects that have been demonstrated in unirradiated cells in communication with irradiated cells, there still does not exist a cohesive framework within which to address some of the fundamental questions regarding bystander effects, such as the nature of the bystander signal and its relevance to the risk of human radiation exposures. This problem is due in part to a lack of a diagnostic endpoint that can be used to characterize bystander responses, as it has been shown in this thesis and in other studies that the bystander response is modulated by many factors, such as cell type, radiation quality, and endpoint used.

Another fundamental aspect of the bystander phenomenon that is not known is whether it is a biological protective mechanism or a damaging mechanism. Although a bystander signal that results in cell death may seem like an adverse response, this may actually serve as a protective mechanism by removing damaged cells, such as neoplastic cells that may lead to cancer, from the population. Because many cell populations carry damaged cells without being exposed to radiation (so-called "background damage"), it is possible that radiation exposures may cause the removal of cells damaged by agents other than the radiation [145]. Alternatively, it is possible that the bystander signal itself is toxic and, rather than serving as a protective mechanism, it initiates further damage by randomly removing healthy unirradiated cells. An example of the

discrepant nature of the bystander signal is the finding by many groups of an enhanced degree of apoptosis in bystander cells, which can either be beneficial or detrimental. It can be viewed as beneficial if it serves to remove abnormal or irreparably damaged irradiated and bystander cells from a tissue population for the purpose of preventing pre-malignant responses. However, if the degree of apoptosis is excessive to the point where too many additional cells are undergoing cell death due to bystander effects, there could be a breakdown in tissue function.

Despite the many unknowns that still remain regarding the bystander effect, an important characteristic effect of all bystander studies is that the effect is triggered by low radiation doses, regardless of radiation quality, and then saturates with increasing dose, usually by 10-30 cGy [45, 119]. Therefore, bystander effects are thought to be of particular importance at low doses or low particle fluences and could have important consequences for astronauts on long-duration missions to the moon, Mars, or beyond since the space radiation field is characterized by such low particle fluences. However, generalizations can not yet be made regarding the potential risk of such radiation exposure to astronauts due to the aforementioned difficulties in combining the existing bystander studies into a cohesive framework and uncertainties in extrapolating data from *in vitro* studies to predict human cancer risk.

6.2 Thesis Contributions

In an effort to provide a more cohesive framework regarding bystander signaling under conditions relevant for the eventual assessment of space radiation risk, this thesis investigated bystander signaling under a comprehensive set of experimental conditions using both 2D and 3D models. Specifically, the contributions of this thesis are three-fold:

- ***Utilized a transwell insert system to investigate bystander signaling in a 2D skin model of mixed cell types.*** Bystander signaling was assessed according to three different cell signaling combinations (namely, keratinocytes to fibroblasts, fibroblasts to keratinocytes, and keratinocytes to keratinocytes) using a wide range of particle fluences with both low- and high-LET radiation types (protons and iron ions, respectively) and two different endpoints (MN and 53BP1 foci formation). Although bystander responses were seen in most of the cell populations cultured in both the 2D and 3D systems and were of similar magnitude, these studies demonstrated that the bystander response is dependent on radiation quality, cell type, and endpoint studied. Specifically, it was found that keratinocytes and fibroblasts exhibit different bystander effects in response to the same signal (i.e., from irradiated keratinocytes) and that there is an LET-dependent difference in the signal emitted from irradiated keratinocytes as evidenced by the expression of MN in bystander fibroblasts following proton irradiation of keratinocytes but not iron irradiation. Furthermore, no dose dependence in the bystander effect was found beyond a threshold at low fluences that was modulated by radiation quality.

- ***Developed a 3D skin model to test the hypothesis that bystander signaling differs between 2D and 3D systems.*** A 3D skin tissue construct was developed that has a morphology (as demonstrated by H&E staining) resembling that of native skin. Constructs were subjected to the same radiation qualities and doses as those used in the 2D bystander signaling investigation to allow a more direct comparison of how signaling is modulated by tissue architecture than has been done previously in bystander investigations. Interestingly, the kinetics of the bystander response were found to be

similar in the 2D and 3D systems, with bystander responses peaking at the same time points, but the magnitude of DNA damage as measured using the endpoint of 53BP1 foci induction was significantly less in the 3D compared to the 2D system. Furthermore, in the 3D system, irradiation with low particle fluences yielded a bystander response at lower fluences of protons than of iron ions, whereas the response occurred at approximately the same fluences in the 2D system (although these responses were modulated slightly by cell type).

- ***Tested the hypothesis that the bystander effect is mediated by ROS/RNS in both the 2D and 3D models.*** SOD, catalase, and PTIO were introduced into the medium immediately following irradiation of both the 2D cell monolayers and 3D tissue constructs to investigate the roles of superoxide, hydrogen peroxide, and nitric oxide, respectively, in bystander signaling. All three scavengers were found to reduce the bystander effect, as measured by 53BP1 foci formation, indicating that the roles of these reactive oxygen/nitrogen species are similar in both 2D and 3D cellular architectures.

6.3 Future Work

This thesis has contributed to the bystander literature by providing a comprehensive characterization study of bystander signaling in both 2D and 3D cellular architectures using consistent experimental conditions to allow a more direct comparison of results than has been conducted to date. In future work, there are many potential modifications to the 3D tissue system that could be made to better investigate the effects of charged particles and bystander signaling on the induction of carcinogenesis.

One potential modification to the 3D tissue constructs could be the introduction of

additional cell types into the constructs to mimic real skin even more closely. One cell type to consider is dendritic cells (DCs), as these cells play a critical role in immune surveillance and triggering innate and adaptive responses to precancerous and neoplastic cells [146]. Although it is known that ionizing radiation can activate DCs [147], the dependence of this activation on radiation quality and dose is not known. Furthermore, it is not clear how ionizing radiation modulates the important role of DCs in cancer development.

The 3D tissue model could also be modified to investigate the role of ionizing radiation and bystander signaling in the induction of basal cell carcinoma (BCC), which is the most commonly diagnosed human cancer and thus could be highly relevant to the prediction of radiation risk to astronauts. BCCs are derived from keratinocytes, and genetic alterations in oncogenes or tumor suppressor genes in keratinocytes may contribute to carcinogenesis. The role of such genetic alterations, such as mutations in TP53 that appear to play a role in skin cancer [148], has not been widely studied. Thus, genetically altered pre-neoplastic keratinocytes could be incorporated into the constructs with normal keratinocytes and fibroblasts, and endpoints relevant to carcinogenesis such as apoptosis, differentiation, and proliferation in the pre-neoplastic cells could be measured after irradiation with a wide range of particle LETs.

Another potential study could be to investigate bystander signaling in the 3D model developed in this thesis within a broader range of particle LETs. For example, in addition to using low-LET protons and high-LET iron ions, future studies could utilize low fluences of particles with intermediate LETs, such as carbon ions. In addition to these studies, it will be important to better characterize the dose distribution received by cells in the irradiated population. For example, at the low fluences found in space, cells may either be traversed directly by an ionizing particle, traversed by the low-energy delta rays emitted by that particle, or

they may not receive any amount of dose. The latter cell population would then be considered a bystander population even though it may be localized within an irradiated tissue region. As an example of the potential large differences in dose distribution due to the low fluences of particles found in space, it was estimated in a study by Brooks et al. that, for every cell traversed by a primary 1 GeV/n iron particle in a tissue, 32 cells were hit by delta rays [149]. Thus, better detection methods are needed to identify DNA damage in these various cell populations to better characterize the role of bystander signaling in overall cancer risk due to the low-fluence radiation field in space.

Ultimately, to extrapolate the bystander responses found in this thesis and in other studies to cancer risk estimation, in vivo animal models that correlate cancer induction with the end points used in in vitro studies need to be established. Such studies could include the irradiation of mice with a variety of particle LETs and doses (including the low fluences used in this thesis) and the assessment of cancer induction in various organ systems. In parallel, tissue sections should be taken from the corresponding organs and analyzed for various endpoints, such as MN, foci formation, and apoptosis. Only after correlations are made between such DNA damage endpoints and cancer induction will advancements be made in the formulation of a more accurate model for assessing the health effects of low doses of low- and high-LET ionizing radiation in the general population, and in the particular realm of this thesis, in estimating cancer risk for astronauts on long-duration missions to the moon, Mars, and beyond.

Bibliography

1. Goodhead DT. Initial events in the cellular effects of ionizing radiations: Clustered damage in DNA. Int J Radiat Biol. 1994 Jan;65(1):7-17.

2. Brenner DJ, Elliston CD. The potential impact of bystander effects on radiation risks in a mars mission. Radiat Res. 2001 Nov;156(5 Pt 2):612-7.

3. Belyakov OV, Mitchell SA, Parikh D, Randers-Pehrson G, Marino SA, Amundson SA, et al. Biological effects in unirradiated human tissue induced by radiation damage up to 1 mm away. Proc Natl Acad Sci U S A. 2005 Oct 4;102(40):14203-8.

4. Sedelnikova OA, Nakamura A, Kovalchuk O, Koturbash I, Mitchell SA, Marino SA, et al. DNA double-strand breaks form in bystander cells after microbeam irradiation of three-dimensional human tissue models. Cancer Res. 2007 May 1;67(9):4295-302.

5. Yang H, Magpayo N, Rusek A, Chiang IH, Sivertz M, Held KD. Effects of very low fluences of high-energy protons or iron ions on irradiated and bystander cells. Radiat Res. 2011 Dec;176(6):695-705.

6. Anzenberg V, Massachusetts Institute of Technology. Dept. of Nuclear Engineering. Do heavy ions induce the bystander effect? : Study to determine the induction of the bystander effect from fe ion beam compared to X-rays in human keratinocytes. ; 2005.

7. Hellweg CE, Baumstark-Khan C. Getting ready for the manned mission to mars: The astronauts' risk from space radiation. Naturwissenschaften. 2007 Jul;94(7):517-26.

8. Schimmerling W. Overview of NASA's space radiation research program. Gravit Space Biol Bull. 2003 Jun;16(2):5-10.

9. Setlow R, Dicello J, Fry RJ, Little J, Preston RJ, Smathers JB, et al. Radiation hazards to crews of interplanetary missions: Biological issues and research strategies. National Academy Press; 1996.

10. Wilson JW, Townsend LW, Nealy JE, Chun SY, Hong BS, Buck WW, et al. BRYNTRN: A baryon transport model. 1989. Report No.: N-89-17562; NASA-TP--2887; L--16512; NAS--1.60:2887.

11. Simonsen LC, Cucinotta FA, Atwell W, Nealy JE. Temporal analysis of the october 1989 proton flare using computerized anatomical models. Radiat Res. 1993 Jan;133(1):1-11.

12. Luna gaia: A closed loop habitat for the moon. 2006.

13. Kiefer J. Radiation risk in manned space flights. Mutat Res. 1999 Dec 6;430(2):307-13.

14. Curtis SB, Letaw JR. Galactic cosmic rays and cell-hit frequencies outside the magnetosphere. Adv Space Res. 1989;9(10):293-8.

15. Health risks from exposure to low levels of ionizing radiation : BEIR VII. National Academy of Sciences; 2006.

16. Hoel DG, Li P. Threshold models in radiation carcinogenesis. Health Phys. 1998 Sep;75(3):241-50.

17. Little MP, Wakeford R, Tawn EJ, Bouffler SD, Berrington de Gonzalez A. Risks associated with low doses and low dose rates of ionizing radiation: Why linearity may be (almost) the best we can do. Radiology. 2009 Apr;251(1):6-12.

18. U.S. National Academy of Sciences, National Researach Council, Committee to Assess Health Risks from Exposure to Low Levels of Ionizing Radiation. Health risks from exposure to low levels of ionizing radiation. Washington, DC: National Academies Press; 2006. Report No.: BEIR VII Phase 2.

19. Rapp D. Radiation effects and shielding requirements in human missions to the moon and mars. MARS. 2006;2:46-71.

20. Stanford M, Jones JA. Space radiation concerns for manned exploration. Acta Astronaut. 1999 Jul;45(1):39-47.

21. Recommendations of dose limits for low earth orbit. National Council on Radiation Protection; 2000. Report No.: 132.

22. Human research roadmap: A risk reduction strategy for human space exploration. National Aeronautics and Space Administration; 2010.

23. Tsuchida Y, Tsuboi K, Ohyama H, Ohno T, Nose T, Ando K. Cell death induced by high-linear-energy transfer carbon beams in human glioblastoma cell lines. Brain Tumor Pathol. 1998;15(2):71-6.

24. Worgul BV, Medvedovsky C, Powers-Risius P, Alpen E. Accelerated heavy ions and the lens. IV. biomicroscopic and cytopathological analyses of the lenses of mice irradiated with 600 MeV/amu 56Fe ions. Radiat Res. 1989 Nov;120(2):280-93.

25. Scholz M, Kraft-Weyrather W, Ritter S, Kraft G. Cell cycle delays induced by heavy ion irradiation of synchronous mammalian cells. Int J Radiat Biol. 1994 Jul;66(1):59-75.

26. Goodhead DT. Molecular and cell models of biological effects of heavy ion radiation. Radiat Environ Biophys. 1995 Jun;34(2):67-72.

27. Chatterjee A, Schaefer HJ. Microdosimetric structure of heavy ion tracks in tissue. Radiat Environ Biophys. 1976 Oct 7;13(3):215-27.

28. Yousif AA, Bahari IB, Yasir MS. Physical parameters that influence the effectiveness of ionizing radiation at low
doses. Aust J Basic Appl Sci. 2011;5(3):369.

29. Watt DE. A unified system of radiation bio-effectiveness and its consequences in practical application. Radiat Prot Dosimetry. 1997;70(1-4):529.

30. Hall EJ, Giaccia AJ. Radiobiology for the radiologist. Philadelphia: Lippincott Williams & Wilkins; 2006.

31. Durante M, George K, Wu H, Cucinotta FA. Karyotypes of human lymphocytes exposed to high-energy iron ions. Radiat Res. 2002 Nov;158(5):581-90.

32. George K, Durante M, Willingham V, Wu H, Yang TC, Cucinotta FA. Biological effectiveness of accelerated particles for the induction of chromosome damage measured in metaphase and interphase human lymphocytes. Radiat Res. 2003 Oct;160(4):425-35.

33. Johannes C, Horstmann M, Durante M, Chudoba I, Obe G. Chromosome intrachanges and interchanges detected by multicolor banding in lymphocytes: Searching for clastogen signatures in the human genome. Radiat Res. 2004 May;161(5):540-8.

34. Hada M, Cucinotta FA, Gonda SR, Wu H. mBAND analysis of chromosomal aberrations in human epithelial cells exposed to low- and high-LET radiation. Radiat Res. 2007 Jul;168(1):98-105.

35. Lobrich M, Cooper PK, Rydberg B. Non-random distribution of DNA double-strand breaks induced by particle irradiation. Int J Radiat Biol. 1996 Nov;70(5):493-503.

36. Prise KM, Pinto M, Newman HC, Michael BD. A review of studies of ionizing radiation-induced double-strand break clustering. Radiat Res. 2001 Nov;156(5 Pt 2):572-6.

37. Rydberg B, Heilbronn L, Holley WR, Lobrich M, Zeitlin C, Chatterjee A, et al. Spatial distribution and yield of DNA double-strand breaks induced by 3-7 MeV helium ions in human fibroblasts. Radiat Res. 2002 Jul;158(1):32-42.

38. Belli M, Cherubini R, Dalla Vecchia M, Dini V, Esposito G, Moschini G, et al. DNA fragmentation in V79 cells irradiated with light ions as measured by pulsed-field gel electrophoresis. I. experimental results. Int J Radiat Biol. 2002 Jun;78(6):475-82.

39. Hada M, Sutherland BM. Spectrum of complex DNA damages depends on the incident radiation. Radiat Res. 2006 Feb;165(2):223-30.

40. Valentin J, International Commission on Radiological Protection. The 2007 recommendations of the international commission on radiological protection. Oxford, England: Published for the International Commission on Radiological Protection by Elsevier; 2007.

41. Hall EJ. The bystander effect. Health Phys. 2003 Jul;85(1):31-5.

42. Little JB. Cellular radiation effects and the bystander response. Mutat Res. 2006 May 11;597(1-2):113-8.

43. Nagasawa H, Little JB. Induction of sister chromatid exchanges by extremely low doses of alpha-particles. Cancer Res. 1992 Nov 15;52(22):6394-6.

44. Mothersill C, Seymour CB. Cell-cell contact during gamma irradiation is not required to induce a bystander effect in normal human keratinocytes: Evidence for release during irradiation of a signal controlling survival into the medium. Radiat Res. 1998 Mar;149(3):256-62.

45. Yang H, Asaad N, Held KD. Medium-mediated intercellular communication is involved in bystander responses of X-ray-irradiated normal human fibroblasts. Oncogene. 2005 Mar 17;24(12):2096-103.

46. Yang H, Anzenberg V, Held KD. Effects of heavy ions and energetic protons on normal human fibroblasts. Radiats Biol Radioecol. 2007 May-Jun;47(3):302-6.

47. Yang H, Anzenberg V, Held KD. The time dependence of bystander responses induced by iron-ion radiation in normal human skin fibroblasts. Radiat Res. 2007 Sep;168(3):292-8.

48. Shao C, Furusawa Y, Kobayashi Y, Funayama T, Wada S. Bystander effect induced by counted high-LET particles in confluent human fibroblasts: A mechanistic study. FASEB J. 2003 Aug;17(11):1422-7.

49. Mothersill C, Seymour C. Medium from irradiated human epithelial cells but not human fibroblasts reduces the clonogenic survival of unirradiated cells. Int J Radiat Biol. 1997 Apr;71(4):421-7.

50. Lorimore SA, Kadhim MA, Pocock DA, Papworth D, Stevens DL, Goodhead DT, et al. Chromosomal instability in the descendants of unirradiated surviving cells after alpha-particle irradiation. Proc Natl Acad Sci U S A. 1998 May 12;95(10):5730-3.

51. Wu LJ, Randers-Pehrson G, Xu A, Waldren CA, Geard CR, Yu Z, et al. Targeted cytoplasmic irradiation with alpha particles induces mutations in mammalian cells. Proc Natl Acad Sci U S A. 1999 Apr 27;96(9):4959-64.

52. Lyng FM, Seymour CB, Mothersill C. Production of a signal by irradiated cells which leads to a response in unirradiated cells characteristic of initiation of apoptosis. Br J Cancer. 2000 Nov;83(9):1223-30.

53. Mothersill C, Rea D, Wright EG, Lorimore SA, Murphy D, Seymour CB, et al. Individual variation in the production of a 'bystander signal' following irradiation of primary cultures of normal human urothelium. Carcinogenesis. 2001 Sep;22(9):1465-71.

54. Azzam EI, de Toledo SM, Gooding T, Little JB. Intercellular communication is involved in the bystander regulation of gene expression in human cells exposed to very low fluences of alpha particles. Radiat Res. 1998 Nov;150(5):497-504.

55. Nelson GA. Fundamental space radiobiology. Gravit Space Biol Bull. 2003 Jun;16(2):29-36.

56. Narayanan PK, Goodwin EH, Lehnert BE. Alpha particles initiate biological production of superoxide anions and hydrogen peroxide in human cells. Cancer Res. 1997 Sep 15;57(18):3963-71.

57. Narayanan PK, LaRue KE, Goodwin EH, Lehnert BE. Alpha particles induce the production of interleukin-8 by human cells. Radiat Res. 1999 Jul;152(1):57-63.

58. Shao C, Folkard M, Prise KM. Role of TGF-beta1 and nitric oxide in the bystander response of irradiated glioma cells. Oncogene. 2008 Jan 17;27(4):434-40.

59. Lyng FM, Maguire P, McClean B, Seymour C, Mothersill C. The involvement of calcium and MAP kinase signaling pathways in the production of radiation-induced bystander effects. Radiat Res. 2006 Apr;165(4):400-9.

60. Zhou H, Ivanov VN, Gillespie J, Geard CR, Amundson SA, Brenner DJ, et al. Mechanism of radiation-induced bystander effect: Role of the cyclooxygenase-2 signaling pathway. Proc Natl Acad Sci U S A. 2005 Oct 11;102(41):14641-6.

61. Azzam EI, De Toledo SM, Spitz DR, Little JB. Oxidative metabolism modulates signal transduction and micronucleus formation in bystander cells from alpha-particle-irradiated normal human fibroblast cultures. Cancer Res. 2002 Oct 1;62(19):5436-42.

62. Azzam EI, de Toledo SM, Little JB. Expression of CONNEXIN43 is highly sensitive to ionizing radiation and other environmental stresses. Cancer Res. 2003 Nov 1;63(21):7128-35.

63. Glover D, Little JB, Lavin MF, Gueven N. Low dose ionizing radiation-induced activation of connexin 43 expression. Int J Radiat Biol. 2003 Dec;79(12):955-64.

64. Azzam EI, de Toledo SM, Little JB. Direct evidence for the participation of gap junction-mediated intercellular communication in the transmission of damage signals from alpha - particle irradiated to nonirradiated cells. Proc Natl Acad Sci U S A. 2001 Jan 16;98(2):473-8.

65. Nagar S, Smith LE, Morgan WF. Characterization of a novel epigenetic effect of ionizing radiation: The death-inducing effect. Cancer Res. 2003 Jan 15;63(2):324-8.

66. Lewis DA, Mayhugh BM, Qin Y, Trott K, Mendonca MS. Production of delayed death and neoplastic transformation in CGL1 cells by radiation-induced bystander effects. Radiat Res. 2001 Sep;156(3):251-8.

67. Zhou H, Suzuki M, Geard CR, Hei TK. Effects of irradiated medium with or without cells on bystander cell responses. Mutat Res. 2002 Feb 20;499(2):135-41.

68. Suzuki M, Zhou H, Hei TK, Tsuruoka C, Fujitaka K. Effects of irradiated medium on chromatid aberrations in mammalian cells using double mylar dishes. Biol Sci Space. 2004 Nov;18(3):110-1.

69. Zhou H, Suzuki M, Randers-Pehrson G, Vannais D, Chen G, Trosko JE, et al. Radiation risk to low fluences of alpha particles may be greater than we thought. Proc Natl Acad Sci U S A. 2001 Dec 4;98(25):14410-5.

70. Hu B, Wu L, Han W, Zhang L, Chen S, Xu A, et al. The time and spatial effects of bystander response in mammalian cells induced by low dose radiation. Carcinogenesis. 2006 Feb;27(2):245-51.

71. Shao C, Lyng FM, Folkard M, Prise KM. Calcium fluxes modulate the radiation-induced bystander responses in targeted glioma and fibroblast cells. Radiat Res. 2006 Sep;166(3):479-87.

72. Turesson I, Carlsson J, Brahme A, Glimelius B, Zackrisson B, Stenerlow B, et al. Biological response to radiation therapy. Acta Oncol. 2003;42(2):92-106.

73. Sjostedt S, Bezak E. Non-targeted effects of ionising radiation and radiotherapy. Australas Phys Eng Sci Med. 2010 Sep;33(3):219-31.

74. Ianzini F, Mackey MA. Delayed DNA damage associated with mitotic catastrophe following X-irradiation of HeLa S3 cells. Mutagenesis. 1998 Jul;13(4):337-44.

75. Ianzini F, Mackey MA. Spontaneous premature chromosome condensation and mitotic catastrophe following irradiation of HeLa S3 cells. Int J Radiat Biol. 1997 Oct;72(4):409-21.

76. Mackey MA, Ianzini F. Enhancement of radiation-induced mitotic catastrophe by moderate hyperthermia. Int J Radiat Biol. 2000 Feb;76(2):273-80.

77. Chu K, Teele N, Dewey MW, Albright N, Dewey WC. Computerized video time lapse study of cell cycle delay and arrest, mitotic catastrophe, apoptosis and clonogenic survival in irradiated 14-3-3sigma and CDKN1A (p21) knockout cell lines. Radiat Res. 2004 Sep;162(3):270-86.

78. Nitta M, Kobayashi O, Honda S, Hirota T, Kuninaka S, Marumoto T, et al. Spindle checkpoint function is required for mitotic catastrophe induced by DNA-damaging agents. Oncogene. 2004 Aug 26;23(39):6548-58.

79. Vakifahmetoglu H, Olsson M, Zhivotovsky B. Death through a tragedy: Mitotic catastrophe. Cell Death Differ. 2008 Jul;15(7):1153-62.

80. Han J, Hendzel MJ, Allalunis-Turner J. Quantitative analysis reveals asynchronous and more than DSB-associated histone H2AX phosphorylation after exposure to ionizing radiation. Radiat Res. 2006 Mar;165(3):283-92.

81. Pilch DR, Sedelnikova OA, Redon C, Celeste A, Nussenzweig A, Bonner WM. Characteristics of gamma-H2AX foci at DNA double-strand breaks sites. Biochem Cell Biol. 2003 Jun;81(3):123-9.

82. Medvedeva NG, Panyutin IV, Panyutin IG, Neumann RD. Phosphorylation of histone H2AX in radiation-induced micronuclei. Radiat Res. 2007 Oct;168(4):493-8.

83. Asaithamby A, Uematsu N, Chatterjee A, Story MD, Burma S, Chen DJ. Repair of HZE-particle-induced DNA double-strand breaks in normal human fibroblasts. Radiat Res. 2008 Apr;169(4):437-46.

84. Smith GC, Jackson SP. The DNA-dependent protein kinase. Genes Dev. 1999 Apr 15;13(8):916-34.

85. Chen BP, Chan DW, Kobayashi J, Burma S, Asaithamby A, Morotomi-Yano K, et al. Cell cycle dependence of DNA-dependent protein kinase phosphorylation in response to DNA double strand breaks. J Biol Chem. 2005 Apr 15;280(15):14709-15.

86. Schultz LB, Chehab NH, Malikzay A, Halazonetis TD. p53 binding protein 1 (53BP1) is an early participant in the cellular response to DNA double-strand breaks. J Cell Biol. 2000 Dec 25;151(7):1381-90.

87. Little JB, Nagasawa H, Li GC, Chen DJ. Involvement of the nonhomologous end joining DNA repair pathway in the bystander effect for chromosomal aberrations. Radiat Res. 2003 Feb;159(2):262-7.

88. Frankenberg D, Greif KD, Giesen U. Radiation response of primary human skin fibroblasts and their bystander cells after exposure to counted particles at low and high LET. Int J Radiat Biol. 2006 Jan;82(1):59-67.

89. Boyd M, Ross SC, Dorrens J, Fullerton NE, Tan KW, Zalutsky MR, et al. Radiation-induced biologic bystander effect elicited in vitro by targeted radiopharmaceuticals labeled with alpha-, beta-, and auger electron-emitting radionuclides. J Nucl Med. 2006 Jun;47(6):1007-15.

90. Gow MD, Seymour CB, Ryan LA, Mothersill CE. Induction of bystander response in human glioma cells using high-energy electrons: A role for TGF-beta1. Radiat Res. 2010 Jun;173(6):769-78.

91. Liu Z, Mothersill CE, McNeill FE, Lyng FM, Byun SH, Seymour CB, et al. A dose threshold for a medium transfer bystander effect for a human skin cell line. Radiat Res. 2006 Jul;166(1 Pt 1):19-23.

92. Fournier C, Becker D, Winter M, Barberet P, Heiss M, Fischer B, et al. Cell cycle-related bystander responses are not increased with LET after heavy-ion irradiation. Radiat Res. 2007 Feb;167(2):194-206.

93. Fournier C, Barberet P, Pouthier T, Ritter S, Fischer B, Voss KO, et al. No evidence for DNA and early cytogenetic damage in bystander cells after heavy-ion microirradiation at two facilities. Radiat Res. 2009 May;171(5):530-40.

94. Groesser T, Cooper B, Rydberg B. Lack of bystander effects from high-LET radiation for early cytogenetic end points. Radiat Res. 2008 Dec;170(6):794-802.

95. Kanasugi Y, Hamada N, Wada S, Funayama T, Sakashita T, Kakizaki T, et al. Role of DNA-PKcs in the bystander effect after low- or high-LET irradiation. Int J Radiat Biol. 2007 Feb;83(2):73-80.

96. Baskar R, Balajee AS, Geard CR. Effects of low and high LET radiations on bystander human lung fibroblast cell survival. Int J Radiat Biol. 2007 Aug;83(8):551-9.

97. Shao C, Furusawa Y, Aoki M, Matsumoto H, Ando K. Nitric oxide-mediated bystander effect induced by heavy-ions in human salivary gland tumour cells. Int J Radiat Biol. 2002 Sep;78(9):837-44.

98. Anzenberg V, Massachusetts Institute of Technology. Dept. of Nuclear Science and Engineering. LET dependence of radiation-induced bystander effects using human prostate tumor cells. ; 2008.

99. Bishayee A, Hill HZ, Stein D, Rao DV, Howell RW. Free radical-initiated and gap junction-mediated bystander effect due to nonuniform distribution of incorporated radioactivity in a three-dimensional tissue culture model. Radiat Res. 2001 Feb;155(2):335-44.

100. Persaud R, Zhou H, Baker SE, Hei TK, Hall EJ. Assessment of low linear energy transfer radiation-induced bystander mutagenesis in a three-dimensional culture model. Cancer Res. 2005 Nov 1;65(21):9876-82.

101. Persaud R, Zhou H, Hei TK, Hall EJ. Demonstration of a radiation-induced bystander effect for low dose low LET beta-particles. Radiat Environ Biophys. 2007 Nov;46(4):395-400.

102. Koturbash I, Rugo RE, Hendricks CA, Loree J, Thibault B, Kutanzi K, et al. Irradiation induces DNA damage and modulates epigenetic effectors in distant bystander tissue in vivo. Oncogene. 2006 Jul 20;25(31):4267-75.

103. Mancuso M, Pasquali E, Leonardi S, Tanori M, Rebessi S, Di Majo V, et al. Oncogenic bystander radiation effects in patched heterozygous mouse cerebellum. Proc Natl Acad Sci U S A. 2008 Aug 26;105(34):12445-50.

104. Dormann S, Schwieger A, Hanusch J, Haufel T, Engelmann I, Bauer G. Intercellular induction of apoptosis through modulation of endogenous survival factor concentration: A review. Anticancer Res. 1999 Jan-Feb;19(1A):87-103.

105. Dickson MA, Hahn WC, Ino Y, Ronfard V, Wu JY, Weinberg RA, et al. Human keratinocytes that express hTERT and also bypass a p16(INK4a)-enforced mechanism that limits life span become immortal yet retain normal growth and differentiation characteristics. Mol Cell Biol. 2000 Feb;20(4):1436-47.

106. Walsh KM, Belford M. NASA space radiobiology research takes off at new brookhaven facility. *Discover Brookhaven: a U.S. Department of Energy National Laboratory.* 2003; **1**(3).

107. Fenech M, Morley AA. Cytokinesis-block micronucleus method in human lymphocytes: Effect of in vivo ageing and low dose X-irradiation. Mutat Res. 1986 Jul;161(2):193-8.

108. Berking C, Herlyn M. Human skin reconstruct models: A new application for studies of melanocyte and melanoma biology. Histol Histopathol. 2001 Apr;16(2):669-74.

109. Meier F, Nesbit M, Hsu MY, Martin B, Van Belle P, Elder DE, et al. Human melanoma progression in skin reconstructs : Biological significance of bFGF. Am J Pathol. 2000 Jan;156(1):193-200.

110. Cucinotta FA, Durante M. Cancer risk from exposure to galactic cosmic rays: Implications for space exploration by human beings. Lancet Oncol. 2006 May;7(5):431-5.

111. Blakely EA. Biological effects of cosmic radiation: Deterministic and stochastic. Health Phys. 2000 Nov;79(5):495-506.

112. Held KD. Effects of low fluences of radiations found in space on cellular systems. Int J Radiat Biol. 2009 May;85(5):379-90.

113. Han W, Wu L, Hu B, Zhang L, Chen S, Bao L, et al. The early and initiation processes of radiation-induced bystander effects involved in the induction of DNA double strand breaks in non-irradiated cultures. Br J Radiol. 2007 Sep;80 Spec No 1:S7-12.

114. Belyakov OV, Folkard M, Mothersill C, Prise KM, Michael BD. A proliferation-dependent bystander effect in primary porcine and human urothelial explants in response to targeted irradiation. Br J Cancer. 2003 Mar 10;88(5):767-74.

115. Suzuki M, Zhou H, Geard CR, Hei TK. Effect of medium on chromatin damage in bystander mammalian cells. Radiat Res. 2004 Sep;162(3):264-9.

116. Belyakov OV, Folkard M, Mothersill C, Prise KM, Michael BD. Bystander-induced apoptosis and premature differentiation in primary urothelial explants after charged particle microbeam irradiation. Radiat Prot Dosimetry. 2002;99(1-4):249-51.

117. Buchanan C. Micronuclei induction in AGO1522 cells is independent of temperature and linear energy transfer [dissertation]. Massachusetts Institute of Technology; 2008.

118. Buonanno M, de Toledo SM, Pain D, Azzam EI. Long-term consequences of radiation-induced bystander effects depend on radiation quality and dose and correlate with oxidative stress. Radiat Res. 2011 Apr;175(4):405-15.

119. Schettino G, Folkard M, Michael BD, Prise KM. Low-dose binary behavior of bystander cell killing after microbeam irradiation of a single cell with focused c(k) x rays. Radiat Res. 2005 Mar;163(3):332-6.

120. Belyakov OV, Malcolmson AM, Folkard M, Prise KM, Michael BD. Direct evidence for a bystander effect of ionizing radiation in primary human fibroblasts. Br J Cancer. 2001 Mar 2;84(5):674-9.

121. Wang R, Coderre JA. A bystander effect in alpha-particle irradiations of human prostate tumor cells. Radiat Res. 2005 Dec;164(6):711-22.

122. Ponnaiya B, Jenkins-Baker G, Brenner DJ, Hall EJ, Randers-Pehrson G, Geard CR. Biological responses in known bystander cells relative to known microbeam-irradiated cells. Radiat Res. 2004 Oct;162(4):426-32.

123. Smilenov LB, Hall EJ, Bonner WM, Sedelnikova OA. A microbeam study of DNA double-strand breaks in bystander primary human fibroblasts. Radiat Prot Dosimetry. 2006;122(1-4):256-9.

124. Tomita M, Maeda M, Maezawa H, Usami N, Kobayashi K. Bystander cell killing in normal human fibroblasts is induced by synchrotron X-ray microbeams. Radiat Res. 2010 Mar;173(3):380-5.

125. Blyth BJ, Sykes PJ. Radiation-induced bystander effects: What are they, and how relevant are they to human radiation exposures? Radiat Res. 2011 Aug;176(2):139-57.

126. Hei TK, Zhou H, Ivanov VN, Hong M, Lieberman HB, Brenner DJ, et al. Mechanism of radiation-induced bystander effects: A unifying model. J Pharm Pharmacol. 2008 Aug;60(8):943-50.

127. Koyama S, Kodama S, Suzuki K, Matsumoto T, Miyazaki T, Watanabe M. Radiation-induced long-lived radicals which cause mutation and transformation. Mutat Res. 1998 Oct 12;421(1):45-54.

128. Han W, Wu L, Chen S, Bao L, Zhang L, Jiang E, et al. Constitutive nitric oxide acting as a possible intercellular signaling molecule in the initiation of radiation-induced DNA double strand breaks in non-irradiated bystander cells. Oncogene. 2007 Apr 5;26(16):2330-9.

129. Su Y, Meador JA, Geard CR, Balajee AS. Analysis of ionizing radiation-induced DNA damage and repair in three-dimensional human skin model system. Exp Dermatol. 2010 Aug;19(8):e16-22.

130. Suzuki K, Nakashima M, Yamashita S. Dynamics of ionizing radiation-induced DNA damage response in reconstituted three-dimensional human skin tissue. Radiat Res. 2010 Oct;174(4):415-23.

131. Lanctot C, Cheutin T, Cremer M, Cavalli G, Cremer T. Dynamic genome architecture in the nuclear space: Regulation of gene expression in three dimensions. Nat Rev Genet. 2007 Feb;8(2):104-15.

132. Schofer C, Weipoltshammer K. Gene dynamics and nuclear architecture during differentiation. Differentiation. 2008 Jan;76(1):41-56.

133. Brunmeir R, Lagger S, Seiser C. Histone deacetylase HDAC1/HDAC2-controlled embryonic development and cell differentiation. Int J Dev Biol. 2009;53(2-3):275-89.

134. Ayoub N, Jeyasekharan AD, Bernal JA, Venkitaraman AR. HP1-beta mobilization promotes chromatin changes that initiate the DNA damage response. Nature. 2008 May 29;453(7195):682-6.

135. Falk M, Lukasova E, Kozubek S. Chromatin structure influences the sensitivity of DNA to gamma-radiation. Biochim Biophys Acta. 2008 Dec;1783(12):2398-414.

136. Goodarzi AA, Noon AT, Deckbar D, Ziv Y, Shiloh Y, Lobrich M, et al. ATM signaling facilitates repair of DNA double-strand breaks associated with heterochromatin. Mol Cell. 2008 Jul 25;31(2):167-77.

137. Goodarzi AA, Noon AT, Jeggo PA. The impact of heterochromatin on DSB repair. Biochem Soc Trans. 2009 Jun;37(Pt 3):569-76.

138. Olive PL, Durand RE. Drug and radiation resistance in spheroids: Cell contact and kinetics. Cancer Metastasis Rev. 1994 Jun;13(2):121-38.

139. Yamada KM, Pankov R, Cukierman E. Dimensions and dynamics in integrin function. Braz J Med Biol Res. 2003 Aug;36(8):959-66.

140. Storch K, Eke I, Borgmann K, Krause M, Richter C, Becker K, et al. Three-dimensional cell growth confers radioresistance by chromatin density modification. Cancer Res. 2010 May 15;70(10):3925-34.

141. Cowell IG, Sunter NJ, Singh PB, Austin CA, Durkacz BW, Tilby MJ. gammaH2AX foci form preferentially in euchromatin after ionising-radiation. PLoS One. 2007 Oct 24;2(10):e1057.

142. Warters RL, Lyons BW. Variation in radiation-induced formation of DNA double-strand breaks as a function of chromatin structure. Radiat Res. 1992 Jun;130(3):309-18.

143. Lin YF, Nagasawa H, Peng Y, Chuang EY, Bedford JS. Comparison of several radiation effects in human MCF10A mammary epithelial cells cultured as 2D monolayers or 3D acinar stuctures in matrigel. Radiat Res. 2009 Jun;171(6):708-15.

144. Roig AI, Hight SK, Shay JW. Two- and three-dimensional models for risk assessment of radiation-enhanced colorectal tumorigenesis. Radiat Res. 2009 Jan;171(1):33-40.

145. Mothersill C, Seymour C. Radiation-induced bystander effects: Are they good, bad or both? Med Confl Surviv. 2005 Apr-Jun;21(2):101-10.

146. Banchereau J, Briere F, Caux C, Davoust J, Lebecque S, Liu YJ, et al. Immunobiology of dendritic cells. Annu Rev Immunol. 2000;18:767-811.

147. Cummings RJ, Mitra S, Foster TH, Lord EM. Migration of skin dendritic cells in response to ionizing radiation exposure. Radiat Res. 2009 Jun;171(6):687-97.

148. de Zwaan SE, Haass NK. Genetics of basal cell carcinoma. Australas J Dermatol. 2010 May;51(2):81,92; quiz 93-4.

149. Brooks A, Bao S, Rithidech K, Couch LA, Braby LA. Relative effectiveness of HZE iron-56 particles for the induction of cytogenetic damage in vivo. Radiat Res. 2001 Feb;155(2):353-9.